Effects of Interactions between Particles on Nonequilibrium Steady States in Colloidal Dispersion Systems

井上, 雅郎

https://doi.org/10.15017/1928614

出版情報：九州大学, 2017, 博士（理学）, 課程博士
バージョン：
権利関係：

A Thesis Submitted to Kyushu University for the Degree of Doctor of Science

Effects of Interactions between Particles on Nonequilibrium Steady States in Colloidal Dispersion Systems

Masao Inoue

Department of Physics, Graduate School of Science, Kyushu University, Japan

Abstract

In this thesis, I clarify effects of interactions between colloidal particles on nonequilibrium steady states in colloidal dispersion systems. I consider a probe particle fixed in a flowing colloidal suspension comprised of hard-sphere colloidal particles and a solvent. Particularly, in the field of microrheology, mechanical properties of a suspension are determined from the relation between the force on probe particles and the flux velocity. In order to examine the effects of interactions between the colloidal particles, I calculate the force exerted by the colloidal particles on the probe particle via numerical calculations using two theoretical methods. The methods are the time-dependent density functional theory (TDDFT) and the combination of the density functional theory (DFT) with the two-fluid model.

In the first method, assuming that the solvent velocity field is uniform in the whole system, I calculate the force exerted by the colloidal particles on the probe particle via numerical calculations using the TDDFT. By solving numerically the equation of the density field derived from the TDDFT, I obtain the density field of colloidal particles around the probe particle. From the numerical integration of the density field, I calculate the force exerted by the colloidal particles on the hard-sphere probe particle. In order to examine the effects of interactions between the colloidal particles, I compare the results for interacting colloidal particles and those for noninteracting colloidal particles. For small flux velocity, the calculated results show that the force decreases due to the interactions between the colloidal particles. In contrast, for large flux velocity and the large volume fraction of colloids, the force increases due to the interactions.

In the second method, considering the nonuniformity of the solvent velocity field, I examine the modification of the effect of the interactions obtained in the first method by this nonuniformity. In order to consider the nonuniform solvent velocity field disturbed by the colloidal particles, I derive the equations of motion for the colloidal particles and for the solvent by combining the DFT with the two-fluid model. Here, I assume that the probe particle is a soft-core particle and the solvent velocity field is disturbed only by the colloidal particles. Using the expansion in powers of the volume fraction, I solve the second-order equations numerically and obtain the density field of the colloidal particles and the nonuniform solvent velocity field for small volume fractions. The calculated results of the force show qualitatively the same effect of the interactions between the colloidal particles as that obtained in the first study using the TDDFT. This means that for small volume fractions, the effect of the interactions on the force is qualitatively not modified by the nonuniformity of the solvent velocity field.

Contents

Chapter 1

Introduction

Physical properties of many-particle systems are under the influence of interactions between the constituting particles. Even a simple repulsive interaction has a great influence on the arrangement of the particles (in other words, the structure of the many-particle systems). The effects of interactions between particles are caused not only by atoms or molecules in a liquid system, but also by large particles, such as colloidal particles, in a soft-matter system. Therefore, interactions between particles are an important factor in determining properties of soft matter.

Microrheology is the field of study for determining mechanical properties of complex fluids (e.g., colloids, polymer solutions, and gels) using microsize probe particles [1–10]. In microrheology, mechanical properties of complex fluids are determined from the analysis of motion of the probe particles which are embedded into the fluids. Experiments of microrheology are classified into two types: passive microrheology and active microrheology. In experiments of passive microrheology, the Brownian motion of probe particles in complex fluids is observed. In contrast, in experiments of active microrheology, motion of probe particles driven by external force (e.g., magnetic and optical tweezers) is observed.

Squires and Brady considered a simple model for the active microrheology and obtained effective viscosity of a colloidal suspension by numerical calculation [7]. They considered a hard-sphere probe particle pulled at a constant velocity through a colloidal suspension comprised of hard-sphere colloidal particles and a solvent. Although complex fluids had been considered as the continuity in the majority of theoretical studies of microrheology [1, 2], Squires and Brady focused on the microscopic distribution of the colloidal particles. They obtained the distribution of the colloidal particles around the probe particle by numerically solving the Smoluchowski equation of the distribution. As a result, they obtained the dependence of the effective viscosity on the velocity of the probe particle.

The results obtained by Squires and Brady have not been verified by experimental studies. The verification is considered difficult because assumptions in their study are difficult to be satisfied in experimental studies. One of the assumptions is the neglect of interactions between colloidal particles. It has not been well understood how the neglect of interactions between colloidal particles affects the motion of the probe particle. Although this assumption is satisfied when the colloidal suspension is in the dilute limit, experimental studies for extremely dilute

suspensions have not been conducted.

Additionally, Squires and Brady assumed that the solvent velocity is constant in the whole system. However, the solvent velocity field should be nonuniform particularly in the vicinity of the probe particle because the solvent flows around the probe particle. In solving the Smoluchowski equation, they assumed the uniform solvent velocity field around the probe particle. It has not been well understood how the neglect of the nonuniform solvent velocity field affects the distribution of the colloidal particles.

In this study, considering a simple model similar to that studied by Squires and Brady, I examine effects of interactions between colloidal particles. To examine the effects of the interactions, I calculate the distribution of colloidal particles numerically by employing the time-dependent density functional theory (TDDFT) [11,12]. This theory gives the equation of the temporal development of the distribution which includes the term of interactions between particles. Next, to examine how the effects of the interactions are modified by the nonuniform solvent velocity field, I calculate the distribution of the colloidal particles and the solvent velocity field numerically by combining the density functional theory (DFT) with the two-fluid model. The application of the two-fluid model to a colloidal suspension gives two equations of motion: one for the colloidal particles and for the solvent.

This thesis is organized as follows. In Sect. 2, I introduce studies of microrheology: mainly, the theoretical study by Squires and Brady [7] and the experimental study by Wilson *et al.* [4] Next, I derive the equations of motion of the two-fluid model, referring to the theoretical study by Doi and Onuki [13] (Sect. 3). In Sect. 4, I explain the method and results of my numerical study based on the TDDFT. Then, I explain the method of combining the DFT with the two-fluid model (Sect. 5) and apply this method to a system comprised of a soft-core probe particle, hard-sphere colloidal particles, and a solvent (Sect. 6).

Chapter 2

Microrheology

Microrheology is the field of study of complex fluids (e.g., colloids, polymer solutions, and gels), where microsize probe particles are used [1–10]. In experiments of microrheology, researchers embed probe particles into complex fluids and observe motion of the probe particles. From the analysis of the motion of the probe particles, mechanical properties of the complex fluids are determined. Microrheology has been promoted by modern developments of devices of photographing and controlling probe particles. To control probe particles, magnetic and optical tweezers are often used in experiments of microrheology.

There are two methods of experiments of microrheology. One is the observation of the Brownian motion of probe particles in complex fluids, which is called passive microrheology. From the passive microrheology, the diffusion coefficients of the complex fluid are obtained. The other method is the observation of probe particles driven by magnetic and optical tweezers, which is called active microrheology. From the active microrheology, the friction coefficients of the complex fluids are obtained.

2.1 Theoretical study of microrheology

For the passive microrheology, the measured diffusion coefficients are generally related to the mechanical properties of the complex fluids via the generalized Stokes-Einstein (GSE) relation [1, 2]. The GSE relation is based on the assumption that the local mechanical properties around the probe particles equal the macroscopic mechanical properties of the complex fluids. For the active microrheology, the measured friction coefficients are generally related to the viscosity of the complex fluids via the Stokes law [3, 4]. Here, the Stokes law is also employed on the assumption that the local viscosity around the probe particles equals the macroscopic viscosity of the complex fluids. However, the validity of these assumptions has not been verified adequately.

In principle, the local mechanical properties around the probe particles should be different from the macroscopic mechanical properties because the structure of the complex fluids is disturbed by the probe particles. The complex fluids include microsize constituting particles (e.g., colloidal particles and polymer chains)

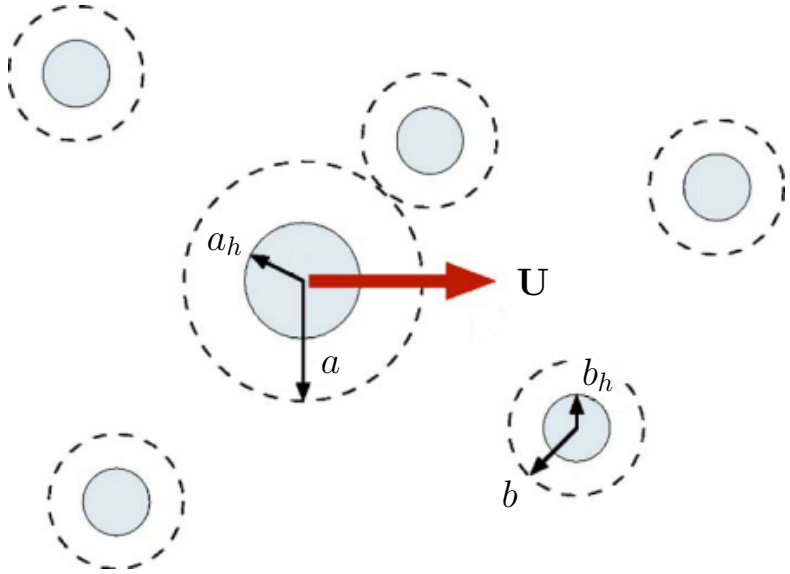

Figure 2.1: Model system for active microrheology. This figure is from Squires and Brady [7]. A probe particle is pulled at a constant velocity **U** through a colloidal suspension. a_h and b_h are hydrodynamic radii of the probe and colloidal particles, respectively. Long-range repulsive interactions are modeled with a hard-sphere potential at effective radii of a for the probe particle and b for the colloidal particles.

which have comparable sizes to those of the probe particles. The distribution of the constituting particles around the probe particles depends on the motion of the probe particles and interactions among the probe and constituting particles. If the distribution around the probe particles is different from the average distribution over the whole system, the local mechanical properties should be different from the macroscopic mechanical properties. However, it has not been understood adequately how the constituting particles are distributed around the probe particles.

Some theoretical studies of microrheology have intended to obtain the distribution of constituting particles of complex fluids around probe particles [7–10]. In particular, Squires and Brady calculated the distribution of colloidal particles around a probe particle by using a simple model for active microrheology [7]. From the calculated distribution, they determined the force exerted by the colloidal particles on the probe particle. The result of their study was compared with the results of some experimental studies of microrheology [3, 4]. In this section, I introduce the method and results of their study [7].

2.1.1 Model system for active microrheology

Squires and Brady considered a probe particle pulled at a constant velocity **U** through a colloidal suspension comprised of hard spheres and a solvent (Fig. 2.1). As the interaction between the probe and colloidal particles, they adopted the

hard-sphere potential,

$$V(r) = \begin{cases} \infty, & \text{at} \quad r < a + b, \\ 0, & \text{at} \quad r \geq a + b, \end{cases} \tag{2.1}$$

where a and b are the hard-sphere radii of the probe and colloidal particles, respectively, and r is the distance between the probe and colloidal particles. Here, they assumed that the probe and colloidal particles have the hydrodynamic radii a_h and b_h, respectively, which are defined by

$$a_h = \frac{k_{\mathrm{B}}T}{6\pi\eta D_a} \quad \text{and} \quad b_h = \frac{k_{\mathrm{B}}T}{6\pi\eta D}, \tag{2.2}$$

where D_a and D are the diffusion coefficients of the probe and colloidal particles, respectively, and η is the viscosity of the solvent.

For simplicity, Squires and Brady neglected hydrodynamic interactions among particles. The hydrodynamic interactions are negligible when the hard-sphere radii are much larger than the hydrodynamic radii ($a \gg a_h$ and $b \gg b_h$). They stated that $a \gg a_h$ and $b \gg b_h$ are satisfied, for example, when the particles have large ionic screening lengths or when long polymer hairs are grafted on the surfaces of the particles. Although the neglect of the hydrodynamic interactions may seem to be a poor approximation, they stated that their simple model captured and illustrated the significant physics of the active microrheology. When the hydrodynamic interactions are negligible, the solvent is not disturbed by the probe and colloidal particles so that the solvent velocity is constant in the whole system.

Additionally, Squires and Brady also neglected the hard-sphere interactions among the colloidal particles. Effects of these interactions are negligible when the colloidal suspension is in the dilute limit $\phi \ll 1$, where ϕ is the volume fraction of the colloidal particles defined by

$$\phi = \frac{4}{3}\pi b^3 \rho_0, \tag{2.3}$$

where ρ_0 is the homogeneous number density of the colloidal particles far from the probe particle. In the dilute limit, the colloidal particles hardly collide with each other so that the neglect of the interactions among them is valid.

2.1.2 Motion of probe particle

In the system represented by Fig. 2.1, the probe particle is subject to the forces exerted by the solvent and colloidal particles. They assumed that the force exerted by the solvent is obtained from the Stokes law and expressed by

$$\mathbf{F}_{\mathrm{sol}} = -6\pi\eta a_h \mathbf{U}. \tag{2.4}$$

The force exerted by the colloidal particles is expressed by

$$\mathbf{F}_{\mathrm{col}} = -k_{\mathrm{B}}T \oint_S \rho(\mathbf{r})\mathbf{n}\mathrm{d}S, \tag{2.5}$$

where $\rho(\mathbf{r})$ is the density field of the colloidal particles at steady states, S is the spherical surface satisfying $|\mathbf{r}| = a + b$, and $\mathbf{n}$ is the normal vector of S. Equation (2.5) is accurate when the velocity distribution of the colloidal particles is given by the Maxwell–Boltzmann distribution. The derivation of Eq. (2.5) is described in Append. A.

From Eqs. (2.4) and (2.5), the force on the probe particle $\mathbf{F}$ is given by

$$\mathbf{F} = -6\pi\eta a_h \mathbf{U} - k_\mathrm{B}T \oint_S \rho(\mathbf{r})\mathbf{n}\mathrm{d}S. \tag{2.6}$$

Employing the simple Stokes drag, Squires and Brady defined the effective viscosity of the colloidal suspension η_eff as

$$\mathbf{F} = -6\pi\eta_\mathrm{eff} a_h \mathbf{U}. \tag{2.7}$$

From Eqs. (2.6) and (2.7), the effective viscosity η_eff is given by

$$\frac{\eta_\mathrm{eff}}{\eta} = 1 + \frac{k_\mathrm{B}T}{6\pi\eta a_h |\mathbf{U}|} \oint_S \rho(\mathbf{r}) n_z \mathrm{d}S, \tag{2.8}$$

where n_z is the z-component of the normal vector $\mathbf{n}$ (z-axis is parallel to $\mathbf{U}$). Additionally, Squires and Brady defined the viscosity increment $\Delta\eta \equiv \eta_\mathrm{eff} - \eta$. From Eq. (2.8), the viscosity increment is given by

$$\frac{\Delta\eta}{\eta} = \frac{k_\mathrm{B}T}{6\pi\eta a_h |\mathbf{U}|} \oint_S \rho(\mathbf{r}) n_z \mathrm{d}S. \tag{2.9}$$

2.1.3 Density field of colloidal particles

To determine the viscosity increment [Eq. (2.9)], Squires and Brady calculated the density field of the colloidal particles $\rho(\mathbf{r})$ by using the Smoluchowski equation. They considered the system of Fig. 2.1 in a frame fixed on the probe particle so that the colloidal particles are advected with the constant velocity $-\mathbf{U}$. In the dilute limit ($\phi \ll 1$), the density flux of the colloidal particles includes the diffusive and advective terms,

$$\mathbf{j}(\mathbf{r}) = -D\nabla\rho(\mathbf{r}) - \mathbf{U}\rho(\mathbf{r}). \tag{2.10}$$

At steady states, since the continuity of the colloidal particles requires $\nabla\cdot\mathbf{j}(\mathbf{r}) = 0$, the Smoluchowski equation is given by

$$D\nabla^2\rho(\mathbf{r}) + \mathbf{U}\cdot\nabla\rho(\mathbf{r}) = 0. \tag{2.11}$$

The boundary condition for Eq. (2.11) is that the density flux is zero across the surface of the probe particle,

$$\mathbf{n}\cdot\mathbf{j}(\mathbf{r}) = D\mathbf{n}\cdot\nabla\rho(\mathbf{r}) + \mathbf{n}\cdot\mathbf{U}\rho(\mathbf{r}) = 0, \quad \text{at} \quad |\mathbf{r}| = a + b. \tag{2.12}$$

Another boundary condition is that the density field equals the homogeneous density ρ_0 far from the probe particle,

$$\rho(\mathbf{r}) = \rho_0, \quad \text{as} \quad |\mathbf{r}| \to \infty. \tag{2.13}$$

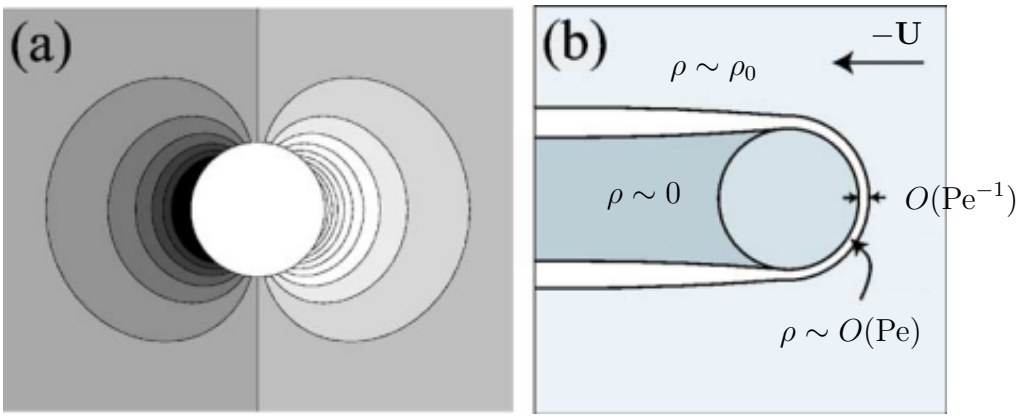

Figure 2.2: Low- and high-Pe density fields. These figures are from Squires and Brady [7]. (a) The density field in the low-Pe limit. It forms a symmetric diffusive dipole. The circle at the center represents the probe particle. A darker region corresponds to a lower particle density. The direction of the flux $-\mathbf{U}$ is leftward. (b) The density field in the high-Pe limit. It forms a thin convection-diffusion boundary layer. On the upstream side outside of the boundary layer, the density field equals the homogeneous density ($\rho \sim \rho_0$). On the downstream side outside of the boundary layer, the density field equals zero ($\rho \sim 0$).

Squires and Brady solved Eq. (2.11) approximately in the limits of the low Péclet number $\mathrm{Pe} \ll 1$ and the high Péclet number $\mathrm{Pe} \gg 1$, where the Péclet number Pe is defined by

$$\mathrm{Pe} = \frac{a+b}{D}|\mathbf{U}|. \tag{2.14}$$

In the low-Pe limit, they expanded $\rho(\mathbf{r})$ in Pe and neglected the second- and higher-order terms of Pe,

$$\rho(\mathbf{r}) \approx \rho^{(0)}(\mathbf{r}) + \rho^{(1)}(\mathbf{r})\mathrm{Pe}. \tag{2.15}$$

Here, $\rho^{(0)}(\mathbf{r})$ is the density field at equilibrium states ($\mathrm{Pe} = 0$),

$$\rho^{(0)}(\mathbf{r}) = \begin{cases} 0, & \text{at} \quad |\mathbf{r}| < a+b, \\ \rho_0, & \text{at} \quad |\mathbf{r}| \geq a+b. \end{cases} \tag{2.16}$$

Neglecting the second- and higher-order terms of Pe, the Smoluchowski equation [Eq. (2.11)] and the boundary conditions [Eqs. (2.12) and (2.13)] are reduced to

$$\nabla^2 \rho^{(1)}(\mathbf{r}) = 0, \tag{2.17}$$

$$(a+b)\frac{\partial \rho^{(1)}(\mathbf{r})}{\partial r} = -\rho_0 \cos\theta, \quad \text{at} \quad r = a+b, \tag{2.18}$$

$$\rho^{(1)}(\mathbf{r}) = 0, \quad \text{as} \quad r \to \infty, \tag{2.19}$$

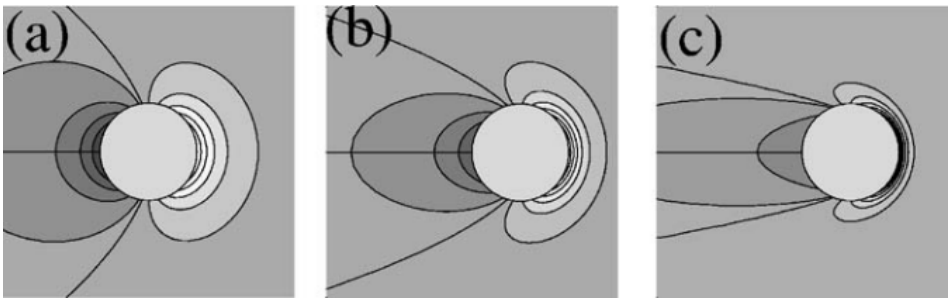

Figure 2.3: Density fields for intermediate Pe. These figures are from Squires and Brady [7]. (a) The density field for Pe = 0.15. The circle at the center represents the probe particle. A darker region corresponds to a lower particle density. The direction of the flux $-\mathbf{U}$ is leftward. (b) The density field for Pe = 0.5. (c) The density field for Pe = 1.5.

where r is the radial distance of the spherical coordinates and θ is the polar angle to the vector $\mathbf{U}$. From these equations, the density field in the low-Pe limit is obtained analytically,

$$\rho(r \geq a+b, \theta\,; \mathrm{Pe} \ll 1) = \left[1 + \mathrm{Pe}\frac{(a+b)^2 \cos\theta}{2r^2} \right] \rho_0, \tag{2.20}$$

while the density field at $r < a+b$ equals zero. The density field at $r \geq a+b$ is the simple diffusive dipole [Fig. 2.2 (a)].

In contrast, in the high-Pe limit, a thin convection-diffusion boundary layer is formed at the front of the probe particle [Fig. 2.2 (b)]. Here, gradients of the density field along this boundary layer are smaller than those across this layer. Neglecting the gradients along the boundary layer, the Smoluchowski equation [Eq. (2.11)] is reduced to

$$(a+b)\frac{\partial^2 \rho(\mathbf{r})}{\partial \zeta^2} + \mathrm{Pe}\frac{\partial \rho(\mathbf{r})}{\partial \zeta}\cos\theta = 0, \tag{2.21}$$

where ζ is a coordinate perpendicular to the local surface of the boundary layer ($\zeta = r - a - b$ at $\theta < \pi/2$). Squires and Brady determined the coefficient of the solution to Eq. (2.21) from the flux balance through the boundary layer and obtained the density field in the high-Pe limit,

$$\rho\left(r \geq a+b, \theta < \frac{\pi}{2}; \mathrm{Pe} \gg 1 \right) \sim \left[1 + \frac{\mathrm{Pe}}{2} e^{-\mathrm{Pe}\,\zeta\cos\theta/(a+b)} \cos\theta \right] \rho_0, \tag{2.22}$$

while the density field at $r < a+b$ or $\pi/2 < \theta < \pi$ equals zero. Note that Eq. (2.22) does not satisfy the boundary condition defined by Eq. (2.12).

Furthermore, Squires and Brady also solved Eq. (2.11) for arbitrary Pe. Expressing the density field by

$$\rho(\mathbf{r}) = \rho_0 (1 + \mathrm{Pe}\, f(\mathbf{r}) e^{-\mathrm{Pe}\, z/2}), \tag{2.23}$$

they transformed the Smoluchowski equation [Eq. (2.11)] to the Helmholtz equation,

$$\nabla^2 f(\mathbf{r}) = \kappa^2 f(\mathbf{r}), \tag{2.24}$$

$$\kappa = \frac{\mathrm{Pe}}{2}. \tag{2.25}$$

Here, $f(\mathbf{r})$ satisfies the boundary conditions,

$$\frac{\partial f(\mathbf{r})}{\partial r} + \kappa f(\mathbf{r}) \cos\theta = -e^{\kappa \cos\theta} \cos\theta, \quad \text{at} \quad r = a + b, \tag{2.26}$$

$$f(\mathbf{r}) = 0, \quad \text{as} \quad r \to \infty. \tag{2.27}$$

The general solution to the Helmholtz equation [Eq. (2.24)] is given by

$$f(r, \theta) = \sum_{n=0}^{\infty} C_n h_n(\kappa r) P_n(\cos\theta), \tag{2.28}$$

where C_n is the undetermined constant, $h_n(x)$ is the modified spherical Bessel function of the second kind, and $P_n(x)$ is the Legendre polynomials. From the boundary conditions, Squires and Brady determined C_n for $0 \leq n \leq 18$ via numerical calculations. The density fields for some intermediate Pe are shown in Fig. 2.3.

2.1.4 Results of viscosity increment

Using Eqs. (2.9), (2.20), and (2.22), Squires and Brady obtained the viscosity increment in the limit of the low Pe and high Pe. From Eqs. (2.14) and (2.9), the viscosity increment is given by

$$\frac{\Delta\eta}{\eta} = \frac{D_a}{D} \frac{a+b}{\mathrm{Pe}} \oint_S \rho(\mathbf{r}; \mathrm{Pe}) n_z \mathrm{d}S. \tag{2.29}$$

In the low-Pe limit, the viscosity increment is obtained from Eqs. (2.20) and (2.29),

$$\begin{aligned} \frac{\Delta\eta(\mathrm{Pe} \ll 1)}{\eta} &= \frac{D_a}{D} \frac{(a+b)^3}{\mathrm{Pe}} 2\pi\rho_0 \int_0^{\pi} \left(1 + \frac{\mathrm{Pe}}{2} \cos\theta\right) \cos\theta \sin\theta \mathrm{d}\theta \\ &= \frac{D_a}{D} \frac{(1+\alpha)^3}{2} \phi, \end{aligned} \tag{2.30}$$

where $\alpha = a/b$ and Eq. (2.3) is used. In contrast, in the high-Pe limit, the viscosity increment is obtained from Eqs. (2.22) and (2.29),

$$\begin{aligned} \frac{\Delta\eta(\mathrm{Pe} \gg 1)}{\eta} &= \frac{D_a}{D} \frac{(a+b)^3}{\mathrm{Pe}} 2\pi\rho_0 \int_0^{\frac{\pi}{2}} \left(1 + \frac{\mathrm{Pe}}{2} \cos\theta\right) \cos\theta \sin\theta \mathrm{d}\theta \\ &= \frac{D_a}{D} \frac{(1+\alpha)^3}{4} \phi. \end{aligned} \tag{2.31}$$

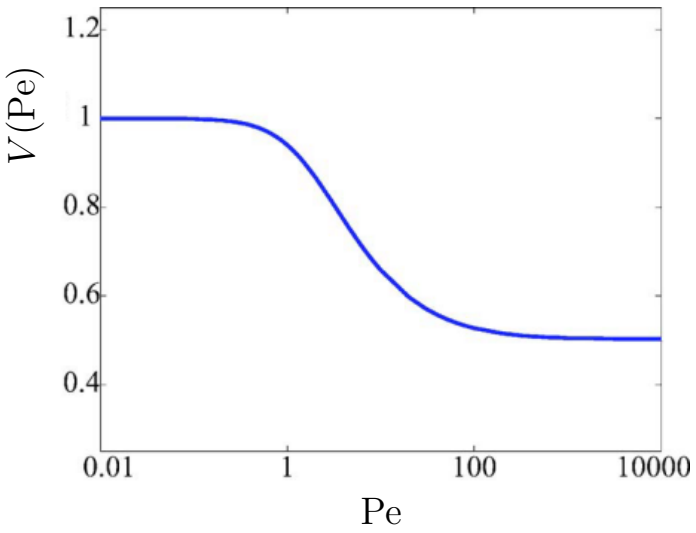

Figure 2.4: Péclet-number dependence of normalized viscosity increment. This figure is from Squires and Brady [7]. $V(\mathrm{Pe})$ is defined by Eq. (2.32) and Pe is defined by Eq. (2.14).

Note that the integration range in Eq. (2.31) is $0 \leq \theta \leq \pi/2$ because the density field at $\pi/2 < \theta < \pi$ equals zero [see Eq. (2.22)]. Equations (2.30) and (2.31) show that the viscosity increment becomes half from the low-Pe limit to the high-Pe limit.

Additionally, using the solution to the Helmholtz equation [Eq. (2.24)], Squires and Brady obtained the viscosity increment for arbitrary values of Pe. They defined the normalized viscosity increment as

$$V(\mathrm{Pe}) = \frac{2}{\phi(1+\alpha)^3}\frac{D}{D_a}\frac{\Delta\eta(\mathrm{Pe})}{\eta}, \tag{2.32}$$

where $V(\mathrm{Pe}) = 1$ in the low-Pe limit. C_n in Eq. (2.28) was numerically determined up to $n = 18$ so that $V(\mathrm{Pe})$ was expressed by the 19-term expansion in Pe. To obtain $V(\mathrm{Pe})$ for large values of Pe, Squires and Brady extrapolated $V(\mathrm{Pe})$ to the high-Pe limit by using the Padé approximation. The values of $V(\mathrm{Pe})$ for arbitrary Pe are plotted in Fig. 2.4. Figure 2.4 shows that the value of $V(\mathrm{Pe})$ decreases as Pe increases in the range of $1 \leq \mathrm{Pe} \leq 100$.

2.2 Experimental study of microrheology

Next, I introduce the experimental study by Wilson *et al.* [4] The purpose of their study is the verification of the result obtained by Squires and Brady [7]. In the experimental study, by using optical tweezers, the force exerted on probe particles is measured, which is the similar system to that studied by Squires and Brady.

2.2.1 Preparation

In the experimental study by Wilson *et al.*, they prepared the colloidal suspension comprised of PMMA particles and a mixture of mixed (cis- and trans-) decalin

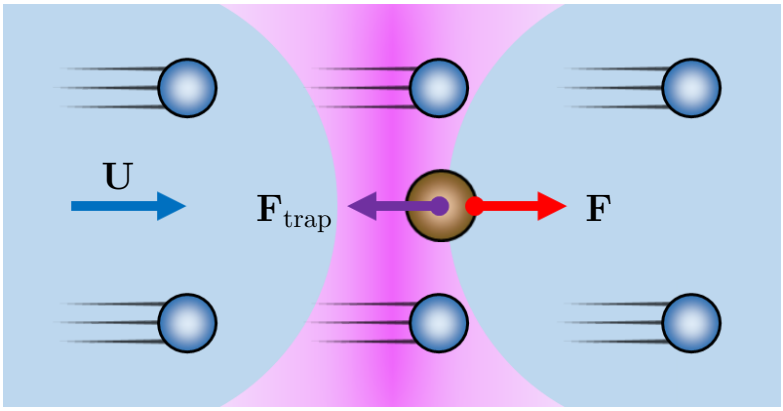

Figure 2.5: Schema of experimental system studied by Wilson *et al.* A probe particle is trapped by optical tweezers in a flowing colloidal suspension. Colloidal particles and a solvent flow at a constant velocity $\mathbf{U}$. The probe particle is subject to the drag force $\mathbf{F}$ exerted by the flowing suspension and the trapping force $\mathbf{F}_{\text{trap}}$ caused by the optical tweezers. At steady states, the magnitude of $\mathbf{F}$ balances with that of $\mathbf{F}_{\text{trap}}$.

and cycloheptylbromide (CHB). They grafted poly-12-hydroxystearic acid (PHSA) on the PMMA particles and added tetrabutylammonium chloride to the solvent mixture so that the PMMA particles behaved as hard spheres. The refractive index of the solvent matched that of the PMMA particles ($n = 1.49$). The viscosity of the solvent was $\eta_0 = 2.56$ mPa $\cdot$ s measured by rheometer. Although Wilson *et al.* prepared two batches of the PMMA particles with radii $b = 860$ and 960 nm (measured by light scattering), there was no systematic difference between the results of these batches.

To measure mechanical properties of this colloidal suspension, they used probe particles made of melamine resin. These probe particles were coated with PHSA so that the interaction between the probe and colloidal particles was given by hard spheres. The radius of the probe particles was $a = 1.04$ μm measured by light scattering. The refractive index of the probe particles was $n = 1.7$ different from that of the colloidal particles and the solvent. Because of the mismatching of the refractive indices, the probe particles are trapped by optical tweezers in the colloidal suspension.

2.2.2 Method

Wilson *et al.* fixed the probe particles spatially by optical tweezers. The optical tweezers trap microsize particles in the vicinity of a focus of a condensed laser beam. If the trapped particles deviate from the focus, the particles are subject to the restoring force directed to the focus. The magnitude of the restoring force is determined from the deviation from the focus. Since the restoring force of the optical tweezers is generated by refraction of a laser beam at the boundary between trapped particles and a medium, the optical tweezers trap only the probe particles with the refractive index different from that of the solvent.

Trapping the probe particles by the optical tweezers, Wilson *et al.* translated

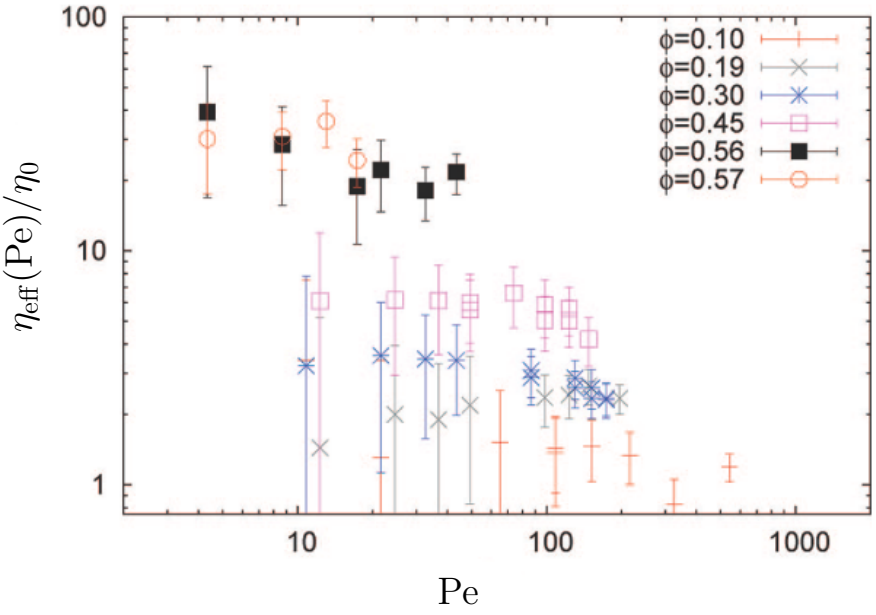

Figure 2.6: Péclet-number dependence of effective viscosity. This figure is from Wilson *et al.* [4]. $\eta_{\rm eff}({\rm Pe})$ and Pe are defined by Eq. (2.33) and (2.34), respectively. $\eta_{\rm eff}({\rm Pe})$ is scaled by the solvent viscosity $\eta_0 = 2.56$ mPa $\cdot$ s.

the sample stage at a constant velocity $\mathbf{U}$ relative to the laser trap (Fig 2.5). They measured positions of the trapped probe particles at steady states for various $\mathbf{U}$ and the volume fraction of the colloidal particles ϕ. In the experimental system, the trapped probe particles are subject to the drag force $\mathbf{F}$ exerted by the flowing colloidal suspension and the restoring force $\mathbf{F}_{\rm trap}$ caused by the optical tweezers. At steady states, the magnitude of $\mathbf{F}$ balances with that of $\mathbf{F}_{\rm trap}$. Since the magnitude of $\mathbf{F}_{\rm trap}$ is determined from the deviation from the focus of the condensed laser beam, $\mathbf{F}$ is obtained from the measurement of the positions of the probe particles.

2.2.3 Results

Wilson *et al.* determined the effective viscosity of the colloidal suspension $\eta_{\rm eff}({\rm Pe})$ defined by

$$\eta_{\rm eff}({\rm Pe}) = \frac{|\mathbf{F}|}{6\pi a|\mathbf{U}|}. \tag{2.33}$$

Figure 2.6 represents the Péclet-number dependence of $\eta_{\rm eff}({\rm Pe})$ for various values of the volume fraction ϕ. Assuming $a = b$, Wilson *et al.* defined Pe as

$${\rm Pe} = \frac{2a}{D_a}|\mathbf{U}|, \tag{2.34}$$

where D_a is the diffusion coefficient of the probe particles in the solvent. Note that Eq. (2.34) corresponds to Eq. (2.14) in the case of $a = b$. In Fig. 2.6, $\eta_{\rm eff}({\rm Pe})$

is scaled by η_0. Theoretically, from Eq. (2.32), $\eta_{\rm eff}({\rm Pe})/\eta_0$ is expected to satisfy the relation

$$\frac{\eta_{\rm eff}({\rm Pe})}{\eta_0} = \frac{\phi}{2}\left(\frac{a+b}{b}\right)^3 \frac{D_a}{D} V({\rm Pe}) + 1, \tag{2.35}$$

where D is the diffusion coefficient of the colloidal particles and $V({\rm Pe})$ is the normalized viscosity increment obtained by Squires and Brady (Fig. 2.4).

From Fig. 2.6, Wilson *et al.* stated that the results for $\phi = 0.3$ and 0.45 showed the decrease in the effective viscosity at large values of Pe but the results for the other values of ϕ did not represent the decrease. They considered that the decrease in the effective viscosity might be related with the decrease in the normalized viscosity increment shown in Fig. 2.4. Similar results showing the decrease in the effective viscosity had been obtained by Meyer *et al.* [3] However, Wilson *et al.* also stated that the decrease in the effective viscosity might be caused by the correction of the measurement at the edge of a condensed laser beam.

I consider that it is difficult to regard the experimental results obtained by Wilson *et al.* (Fig. 2.6) as the verification of the numerical result obtained by Squires and Brady (Fig. 2.4). First, the effective viscosity for $\phi = 0.3$ and 0.45 decreases at ${\rm Pe} > 100$ in Fig. 2.6, while the normalized viscosity increment in Fig. 2.4 decreases at $1 \leq {\rm Pe} \leq 100$. Next, although Fig. 2.4 was obtained by assuming the dilute limit, values of ϕ in Fig. 2.6 ($\phi = 0.3$ and 0.45) are so large that effects of interactions between the colloidal particles are not negligible. Furthermore, since error bars in Fig. 2.6 are large, it is difficult to see the Pe-dependence of the effective viscosity clearly. I consider that the differences between the numerical results (Fig. 2.4) and the experimental results (Fig. 2.6) are caused by excessive simplification in the study by Squires and Brady: neglect of the nonuniform solvent velocity field and interactions between colloidal particles.

2.3 Summary

Squires and Brady considered a simple model for active microrheology in a colloidal suspension (Fig. 2.1). They obtained the density field of colloidal particles around a probe particle by solving the Smoluchowski equation. In the limits of low Pe and high Pe, they obtained the approximate solutions to the Smoluchowski equation analytically. They also obtained the density field for arbitrary Pe by solving the Smoluchowski equation numerically. By using the obtained density field, they calculated the viscosity increment due to the colloidal particles [Eq. (2.29)]. The results (Fig. 2.4) show that the viscosity increment in the high-Pe limit is half of that in the low-Pe limit.

The results obtained by Squires and Brady have not been verified by experimental studies of microrheology. Wilson *et al.* obtained the effective viscosity of a hard-sphere colloidal suspension (Fig. 2.6) from the experiment of active microrheology using hard-sphere probe particles and the optical tweezers. Although some of their results shows the Pe-dependence similar to that shown in Fig. 2.4, the error bars in Fig. 2.6 are so large that it is difficult to see the Pe-dependence clearly. In

addition, the Pe- and ϕ-dependence shown in Fig. 2.6 is different from that shown in Fig. 2.4. I consider that the differences between these results are caused by excessive simplification in the theoretical study: neglect of the nonuniform solvent velocity field and interactions between colloidal particles. In my study, I examine effects of the nonuniform solvent velocity field and interactions between particles on probe particles in active microrheology.

Chapter 3

Two-fluid model

3.1 Introduction

In the theoretical study by Squires and Brady [7], the solvent velocity was assumed to be constant in the whole system (see Sect. 2.1). In fact, since motion of a solvent is disturbed by the probe and colloidal particles, the solvent velocity field should be nonuniform. However, the nonuniform solvent velocity field cannot be treated in the framework of the Smoluchowski equation used in their study. To consider the disturbance due to the particles, the solvent velocity field should be obtained simultaneously with the distribution of the particles. I consider that these difficulties can be resolved by use of the two-fluid model.

For the mixture of two types of fluids, the two-fluid model gives two equations of motion for the fluids [13–15]. This model has often been applied to polymer solutions and binary polymer blends by regarding an aggregation of polymers as a fluid. In my study, regarding colloidal particles and a solvent as two types of fluids, I apply the two-fluid model to a colloidal suspension (Chap. 5). Here, to treat interactions between the colloidal particles, I combine the density functional theory (DFT) with the two-fluid model (Chap. 5). In this chapter, referring to the study by Doi and Onuki [13], I derive the equations of motion of the two-fluid model as the preparation for my study.

3.2 Derivation of equations

3.2.1 Continuity equation and incompressibility condition

Here, I consider a complex fluid comprised of colloidal particles and a solvent, in which the velocity of the colloidal particles differs from that of the solvent velocity. The velocity fields of the colloidal particles and the solvent are represented by $\mathbf{v}_c(\mathbf{r}, t)$ and $\mathbf{v}_s(\mathbf{r}, t)$, respectively. The volume-fraction field of the colloidal particles is represented by $\phi(\mathbf{r}, t)$. I assume that the volume-fraction field of the solvent is represented by $1-\phi(\mathbf{r}, t)$. The continuity equation is derived from the conservation

law and expressed by

$$\frac{\partial \phi(\mathbf{r},t)}{\partial t} = -\nabla \cdot (\phi(\mathbf{r},t)\mathbf{v}_c(\mathbf{r},t)). \tag{3.1}$$

Additionally, the incompressibility condition is expressed by

$$0 = \nabla \cdot [\phi(\mathbf{r},t)\mathbf{v}_c(\mathbf{r},t) + (1-\phi(\mathbf{r},t))\mathbf{v}_s(\mathbf{r},t)]. \tag{3.2}$$

3.2.2 Rayleigh's variational method

To obtain the equations of motion for the colloidal particles and for the solvent, I employ the Rayleigh's variational method [16, 17]. The equations of motion are derived from the condition that $\phi(\mathbf{r},t)$, $\mathbf{v}_c(\mathbf{r},t)$, and $\mathbf{v}_s(\mathbf{r},t)$ change with the lapse of time, minimizing the sum of the energy dissipation per unit time and the time derivative of the free energy of the complex fluid. I define the Rayleighian as

$$R = \frac{W}{2} + \dot{F}, \tag{3.3}$$

where W is the energy dissipation per unit time and F is the free energy of the complex fluid. By use of the Rayleigh's variational method, the equations of motion at steady states are obtained from the condition that the derivatives of R equal zero. The obtained equations do not include the terms of acceleration, which are derived from the Lagrangian formalism.

To obtain the equations of motion under the incompressibility condition [Eq. (3.2)], I add the term of the constraint condition to the Rayleighian defined by Eq. (3.3). The modified Rayleighian including the constraint condition is given by

$$R' = \frac{W}{2} + \dot{F} - \int p(\mathbf{r},t)\nabla \cdot [\phi(\mathbf{r},t)\mathbf{v}_c(\mathbf{r},t) + (1-\phi(\mathbf{r},t))\mathbf{v}_s(\mathbf{r},t)]\mathrm{d}\mathbf{r}, \tag{3.4}$$

where $p(\mathbf{r},t)$ is the undetermined multiplier of the Lagrange multiplier method. From the obtained equations, $p(\mathbf{r},t)$ turns out to be the pressure field of the complex fluids. To determine the pressure field $p(\mathbf{r},t)$ satisfying the incompressibility condition [Eq. (3.2)], I derive the equations of motion from the modified Rayleighian given by Eq. (3.4).

3.2.3 Energy dissipation

The energy dissipation W is the sum of the dissipation due to relative motion between the colloidal particles and the solvent W_f and that due to the solvent viscosity W_{visc}. Here, W_f is given by

$$W_f = \int \Gamma(\phi(\mathbf{r},t))(\mathbf{v}_c(\mathbf{r},t) - \mathbf{v}_s(\mathbf{r},t))^2\mathrm{d}\mathbf{r}, \tag{3.5}$$

where $\Gamma(\phi(\mathbf{r},t))$ is the friction coefficient between the colloidal particles and the solvent. In the Rayleigh's variational method, W_{visc} is defined as the function including only the second-order terms of $\mathbf{v}_s(\mathbf{r},t)$. Additionally, to determine W_{visc}, I make the following assumptions,

1. $W_{\rm visc}$ has the translational symmetry, so that it includes only the terms of the gradient of $\mathbf{v}_s(\mathbf{r},t)$;

2. $W_{\rm visc}$ does not include the second- or higher-order differential terms of $\mathbf{v}_s(\mathbf{r},t)$.

Under these assumptions, $W_{\rm visc}$ is given by

$$W_{\rm visc} = \int \sum_{\alpha,\beta} \left[\mu \frac{\partial v_s^\alpha}{\partial x^\beta} \frac{\partial v_s^\alpha}{\partial x^\beta} + (\mu+\lambda) \frac{\partial v_s^\alpha}{\partial x^\alpha} \frac{\partial v_s^\beta}{\partial x^\beta} \right] \mathrm{d}\mathbf{r}, \tag{3.6}$$

$$\mathbf{v}_s(\mathbf{r},t) = (v_s^x, v_s^y, v_s^z), \tag{3.7}$$

where μ and λ are the shear viscosity and volume viscosity of the solvent, respectively, and α and β represent either of three components of the vector $\mathbf{r}$.

3.2.4 Time derivative of free energy

The free energy F consists of the mixing free energy $F_{\rm mix}$ and the elastic free energy $F_{\rm el}$. The mixing free energy $F_{\rm mix}$ is generated by mixing the colloidal particles with the solvent. The elastic free energy $F_{\rm el}$ is associated with the conformation of the constituting particles such as polymer chains. For simplicity, I assume that the conformation of the colloidal particles is in equilibrium so that $F_{\rm el}$ is negligible. Additionally, I neglect the terms of $\nabla\phi(\mathbf{r},t)$ in $F_{\rm mix}$, which arises from the inhomogeneity of $\phi(\mathbf{r},t)$. Here, $F_{\rm mix}$ depends on $\phi(\mathbf{r},t)$ only.

When $F_{\rm mix}$ is the functional of $\phi(\mathbf{r},t)$, $F_{\rm mix}$ is given by

$$F_{\rm mix} = \int f(\phi(\mathbf{r},t))\mathrm{d}\mathbf{r}, \tag{3.8}$$

where $f(\phi(\mathbf{r},t))$ is the mixing free energy per unit volume with the volume-fraction field $\phi(\mathbf{r},t)$. From the continuity equation [Eq. (3.1)], the time derivative of $F_{\rm mix}$ is given by

$$\begin{aligned} \dot{F}_{\rm mix} &= \int \frac{\partial f(\phi(\mathbf{r},t))}{\partial \phi(\mathbf{r},t)} \dot{\phi}(\mathbf{r},t) \mathrm{d}\mathbf{r} \\ &= -\int \frac{\partial f(\phi(\mathbf{r},t))}{\partial \phi(\mathbf{r},t)} \nabla \cdot (\phi(\mathbf{r},t)\mathbf{v}_c(\mathbf{r},t)) \mathrm{d}\mathbf{r}. \end{aligned} \tag{3.9}$$

Since $F_{\rm el}$ has been assumed to be negligible, the total free energy F corresponds to $F_{\rm mix}$. Therefore, the time derivative of F is given by Eq. (3.9).

3.2.5 Motion equations at steady states

Eventually, the modified Rayleighian is given by

$$\begin{aligned} R' = \int \Bigg\{ & \frac{1}{2}\Gamma(\phi(\mathbf{r},t))(\mathbf{v}_c(\mathbf{r},t) - \mathbf{v}_s(\mathbf{r},t))^2 \\ & + \frac{1}{2}\sum_{\alpha,\beta}\left[\mu \frac{\partial v_s^\alpha}{\partial x^\beta}\frac{\partial v_s^\alpha}{\partial x^\beta} + (\mu+\lambda)\frac{\partial v_s^\alpha}{\partial x^\alpha}\frac{\partial v_s^\beta}{\partial x^\beta}\right] \\ & - \frac{\partial f(\phi(\mathbf{r},t))}{\partial \phi(\mathbf{r},t)}\nabla\cdot(\phi(\mathbf{r},t)\mathbf{v}_c(\mathbf{r},t)) \\ & - p(\mathbf{r},t)\nabla\cdot[\phi(\mathbf{r},t)\mathbf{v}_c(\mathbf{r},t) + (1-\phi(\mathbf{r},t))\mathbf{v}_s(\mathbf{r},t)]\Bigg\}\mathrm{d}\mathbf{r}. \end{aligned} \tag{3.10}$$

The equation of motion for the colloidal particles at steady states is obtained from the condition that the functional derivative of R' by $\mathbf{v}_c(\mathbf{r},t)$ equals zero. The obtained equation for the colloidal particles is given by

$$\begin{aligned} \mathbf{0} = & \Gamma(\phi(\mathbf{r},t))(\mathbf{v}_c(\mathbf{r},t) - \mathbf{v}_s(\mathbf{r},t)) + \phi(\mathbf{r},t)\nabla\frac{\partial f(\phi(\mathbf{r},t))}{\partial\phi(\mathbf{r},t)} \\ & + \phi(\mathbf{r},t)\nabla p(\mathbf{r},t). \end{aligned} \tag{3.11}$$

In the same way, the equation of motion for the solvent is obtained from the functional derivative of R' by $\mathbf{v}_s(\mathbf{r},t)$. The obtained equation for the solvent is given by

$$\begin{aligned} \mathbf{0} = & \Gamma(\phi(\mathbf{r},t))(\mathbf{v}_s(\mathbf{r},t) - \mathbf{v}_c(\mathbf{r},t)) + (1-\phi(\mathbf{r},t))\nabla p(\mathbf{r},t) \\ & - \mu\nabla^2\mathbf{v}_s(\mathbf{r},t) - (\mu+\lambda)\nabla(\nabla\cdot\mathbf{v}_s(\mathbf{r},t)). \end{aligned} \tag{3.12}$$

3.2.6 Approximate incompressibility condition

In addition to the incompressibility condition given by Eq. (3.2), I consider the approximate incompressibility condition defined by

$$0 = \nabla\cdot\mathbf{v}_s(\mathbf{r},t). \tag{3.13}$$

This is the standard incompressibility condition for a simple fluid composed of a solvent. The approximate incompressibility condition is accurate in the dilute limit because the incompressibility of the colloidal particles is neglected in Eq. (3.13). Under this incompressibility condition, the energy dissipation due to the solvent viscosity W_{visc} is given by

$$W_{\mathrm{visc}} = \mu\int \mathrm{d}\mathbf{r}\sum_{\alpha,\beta}\frac{\partial v_s^\alpha}{\partial x^\beta}\frac{\partial v_s^\alpha}{\partial x^\beta}. \tag{3.14}$$

From Eqs. (3.13) and (3.14), the modified Rayleighian is given by

$$\begin{aligned} R' = \int \Bigg\{ & \frac{1}{2}\Gamma(\phi(\mathbf{r},t))(\mathbf{v}_c(\mathbf{r},t) - \mathbf{v}_s(\mathbf{r},t))^2 + \frac{1}{2}\sum_{\alpha,\beta}\mu\frac{\partial v_s^\alpha}{\partial x^\beta}\frac{\partial v_s^\alpha}{\partial x^\beta} \\ & - \frac{\partial f(\phi(\mathbf{r},t))}{\partial\phi(\mathbf{r},t)}\nabla\cdot(\phi(\mathbf{r},t)\mathbf{v}_c(\mathbf{r},t)) - p(\mathbf{r},t)\nabla\cdot\mathbf{v}_s(\mathbf{r},t)\Bigg\}\mathrm{d}\mathbf{r}. \end{aligned} \tag{3.15}$$

From the condition that the functional derivative of R' by $\mathbf{v}_c(\mathbf{r},t)$ equals zero, the equation of motion for the colloidal particles at steady states is obtained,

$$\mathbf{0} = \Gamma(\phi(\mathbf{r},t))(\mathbf{v}_c(\mathbf{r},t) - \mathbf{v}_s(\mathbf{r},t)) + \phi(\mathbf{r},t)\nabla\frac{\partial f(\phi(\mathbf{r},t))}{\partial\phi(\mathbf{r},t)}. \tag{3.16}$$

In the same way, the equation of motion for the solvent is obtained from the functional derivative of R' by $\mathbf{v}_s(\mathbf{r},t)$,

$$\mathbf{0} = \Gamma(\phi(\mathbf{r},t))(\mathbf{v}_s(\mathbf{r},t) - \mathbf{v}_c(\mathbf{r},t)) + \nabla p(\mathbf{r},t) - \mu\nabla^2\mathbf{v}_s(\mathbf{r},t). \tag{3.17}$$

These equations are simpler than Eqs. (3.11) and (3.12). However, note that Eqs. (3.16) and (3.17) are accurate only in the dilute limit.

Chapter 4

Application of time-dependent density functional theory to numerical study of microrheology

4.1 Introduction

Squires and Brady considered a simple model for active microrheology in a colloidal suspension and obtained the force exerted by colloidal particles on a probe particle (see Sect. 2.1). In their study, they assumed the dilute limit and neglected effects of interactions between colloidal particles. In this chapter, I examine effects of interactions between colloidal particles on the force acting on a probe particle via numerical calculations. Here, I consider a simple model for active microrheology in a colloidal suspension similar to that studied by Squires and Brady. To examine effects of interactions between colloidal particles, I employ the time-dependent density functional theory (TDDFT).

The TDDFT is a powerful tool for studying effects of interactions between particles [18–38]. In particular, this theory has been successful in describing the dynamics of simple liquids [18–33]. For instance, the application of the TDDFT has allowed one to examine effects of interactions between solvent particles on the dynamics of them around a solute [18–26]. The TDDFT has also been applied to systems of large particles constituting soft matter because the application of the TDDFT is not restricted by particle size [34–38]. Applying the TDDFT to a system of active microrheology in a colloidal suspension, I examine effects of interactions between colloidal particles via numerical calculations [11, 12].

4.2 Model and method

4.2.1 Model system

A probe particle is fixed at the origin in a colloidal suspension flowing at a constant velocity $\mathbf{U}$ (Fig. 4.1). Here, I focus on the force $\mathbf{F}$ exerted by the colloidal particles on the probe particle. I assume that the probe and colloidal particles are hard

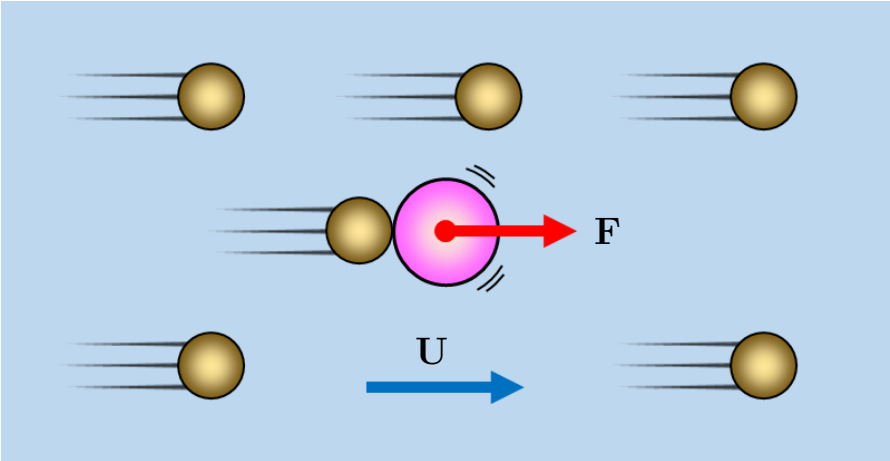

Figure 4.1: Model system for active microrheology in colloidal suspension. A probe particle is fixed spatially in a colloidal suspension. The colloidal suspension flows at a constant velocity $\mathbf{U}$. The probe particle is subject to the force $\mathbf{F}$ exerted by the colloidal particles. The probe and colloidal particles are hard spheres with radii a and b, respectively.

spheres with radii a and b, respectively. The colloidal particles interact with each other as well as with the probe particle. To examine effects of the hard-sphere interactions between the colloidal particles on $\mathbf{F}$, I calculate the density field of the colloidal particles at steady states.

This system (Fig. 4.1) is similar to the system studied by Squires and Brady (Fig. 2.1) [7]. In the same way as their study, I assume that the solvent velocity is constant in the whole system. However, unlike their study, the colloidal particles interact with each other in the system shown in Fig. 4.1. To study effects of interactions between the colloidal particles, I employ the time-dependent density functional theory (TDDFT).

4.2.2 Time-dependent density functional theory

Applying the TDDFT to the system shown in Fig. 4.1, I calculate the temporal development of the density field of the colloidal particles $\rho(\mathbf{r})$ by the basic equation [18, 34, 35, 39],

$$\frac{\partial \rho(\mathbf{r},t)}{\partial t} + \mathbf{U}\cdot\nabla\rho(\mathbf{r},t) = D\nabla\cdot\left(\rho(\mathbf{r},t)\nabla\frac{\delta\beta F[\rho(\mathbf{r},t)]}{\delta\rho(\mathbf{r},t)}\right). \tag{4.1}$$

Here, D is the diffusion coefficient of the colloidal particles, $\beta = 1/k_{\mathrm{B}}T$, and $F[\rho(\mathbf{r},t)]$ is the free-energy functional of $\rho(\mathbf{r},t)$. In Eq. (4.1), the second term on the left-hand side is the advective term arising from the flux of the colloidal suspension. Because of the advective term with constant $\mathbf{U}$, $\rho(\mathbf{r},t)$ is in a nonequilibrium steady state even in the $t\to\infty$ limit. The boundary condition for Eq. (4.1) is that $\rho(\mathbf{r},t)$ equals the homogeneous density ρ_0 far from the probe particle.

In order to obtain the free-energy functional $F[\rho(\mathbf{r},t)]$ in Eq. (4.1), I employ the density functional theory (DFT). In the DFT, $F[\rho(\mathbf{r},t)]$ is defined through

the Legendre transformation; $F[\rho(\mathbf{r},t)]$ is obtained from the Legendre transformation of the thermodynamic potential which is defined by the virtual external field that the intensive variable paired with $\rho(\mathbf{r},t)$. The derivation of the equation of $F[\rho(\mathbf{r},t)]$ is explained in detail in Append. B. When the density field $\rho(\mathbf{r},t)$ is close to the homogeneous density ρ_0, $F[\rho(\mathbf{r},t)]$ is given by [18, 21, 39]

$$\begin{aligned}\beta F[\rho(\mathbf{r},t)] &= \beta F_{\text{ideal}}[\rho(\mathbf{r},t)] - \beta\Psi[\rho_0] \\ &\quad - \sum_{n=1}^{\infty}\frac{1}{n!}\int c_n(\mathbf{r}_1,\cdots,\mathbf{r}_n)\Delta\rho(\mathbf{r}_1,t)\cdots\Delta\rho(\mathbf{r}_n,t)\mathrm{d}\mathbf{r}_1\cdots\mathrm{d}\mathbf{r}_n, \end{aligned} \tag{4.2}$$

where

$$\Psi[\rho(\mathbf{r},t)] = F_{\text{ideal}}[\rho(\mathbf{r},t)] - F[\rho(\mathbf{r},t)], \tag{4.3}$$

$$\Delta\rho(\mathbf{r},t) = \rho(\mathbf{r},t) - \rho_0. \tag{4.4}$$

The n-particle direct correlation function $c_n(\mathbf{r}_1,\cdots,\mathbf{r}_n)$ is defined in the homogeneous system which is in the absence of the probe particle,

$$c_n(\mathbf{r}_1,\cdots,\mathbf{r}_n) = \left.\frac{\beta\delta^n\Psi[\rho(\mathbf{r},t)]}{\delta\rho(\mathbf{r}_1,t)\cdots\delta\rho(\mathbf{r}_n,t)}\right|_{\rho(\mathbf{r},t)=\rho_0}, \tag{4.5}$$

and $F_{\text{ideal}}[\rho(\mathbf{r},t)]$ is the free-energy functional for ideal gas,

$$\beta F_{\text{ideal}}[\rho(\mathbf{r},t)] = \int \rho(\mathbf{r},t)[\,\ln\rho(\mathbf{r},t) + \beta V(\mathbf{r}) + \ln\Lambda^3 - 1\,]\mathrm{d}\mathbf{r}. \tag{4.6}$$

Here, V($\mathbf{r}$) denotes the interaction between the probe and colloidal particles and Λ is the thermal de Broglie wave length given by

$$\Lambda = \left(\frac{h^2}{2\pi m k_{\mathrm{B}}T}\right)^{1/2}, \tag{4.7}$$

where h is the Planck's constant and m is the mass of a colloidal particle.

To obtain a computable expression of Eq. (4.2), I neglect the three- and more-particle direct correlation functions. Hence, I obtain the free-energy functional $F[\rho(\mathbf{r},t)]$,

$$\begin{aligned}\beta F[\rho(\mathbf{r},t)] &= \beta F_{\text{ideal}}[\rho(\mathbf{r},t)] - \beta\Psi[\rho_0] - c_1\int\Delta\rho(\mathbf{r},t)\mathrm{d}\mathbf{r} \\ &\quad - \frac{1}{2}\int c_2(\mathbf{r}_1-\mathbf{r}_2)\Delta\rho(\mathbf{r}_1,t)\Delta\rho(\mathbf{r}_2,t)\mathrm{d}\mathbf{r}_1\mathrm{d}\mathbf{r}_2. \end{aligned} \tag{4.8}$$

The neglect of the three- and more-particle direct correlation corresponds to the hypernetted-chain (HNC) approximation [40]. In the interest of consistency, the

HNC approximation should be employed in the calculation of $c_2(\mathbf{r})$. By substituting Eq. (4.8) into Eq. (4.1), I obtain

$$\frac{\partial \rho(\mathbf{r},t)}{\partial t} + \mathbf{U}\cdot\nabla\rho(\mathbf{r},t) = D\nabla\cdot\Bigg[\nabla\rho(\mathbf{r},t) + \beta\rho(\mathbf{r},t)\nabla V(\mathbf{r}) - \rho(\mathbf{r},t)\nabla\int c_2(\mathbf{r}-\mathbf{r}')\Delta\rho(\mathbf{r}',t)\mathrm{d}\mathbf{r}'\Bigg], \tag{4.9}$$

where the convolution-integral term of $c_2(\mathbf{r}-\mathbf{r}')$ is related to the interactions between the colloidal particles.

In order to examine effects of the interactions between the colloidal particles, I also calculate the density field of noninteracting colloidal particles. The noninteracting colloidal particles do not interact with each other, but they interact with the probe particle through the potential $V(\mathbf{r})$. Thus, the noninteracting colloidal particles are the same as the colloidal particles in the studied by Squires and Brady [7]. By removing the term of $c_2(\mathbf{r})$ from Eq. (4.9), I obtain the equation of the TDDFT for the noninteracting colloidal particles [7, 9, 10],

$$\frac{\partial \rho_{\mathrm{id}}(\mathbf{r},t)}{\partial t} + \mathbf{U}\cdot\nabla\rho_{\mathrm{id}}(\mathbf{r},t) = D\nabla\cdot[\nabla\rho_{\mathrm{id}}(\mathbf{r},t) + \beta\rho_{\mathrm{id}}(\mathbf{r},t)\nabla V(\mathbf{r})]. \tag{4.10}$$

I calculate the density field at steady states $\rho_{\mathrm{id}}(\mathbf{r},\infty)$ by solving Eq. (4.10), and determine the effects of the interactions from the difference between its value and $\rho(\mathbf{r},\infty)$.

4.2.3 Application to system of hard-sphere particles

Applying the TDDFT to the system comprised of hard-sphere particles (Fig. 4.1), I calculate density fields of the colloidal particles at steady states. In this system, I define $V(\mathbf{r})$, the interaction between the probe and colloidal particles, as

$$V(\mathbf{r}) = \begin{cases} \infty, & \text{at} \quad |\mathbf{r}| < a+b, \\ 0, & \text{at} \quad |\mathbf{r}| \geq a+b, \end{cases} \tag{4.11}$$

where a and b are the radii of the probe and colloidal particles, respectively. Here, the origin of the vector $\mathbf{r}$ is placed at the center of the probe particle. The interaction between the colloidal particles is also given by the hard sphere with the diameter $2b$. By substituting Eq. (4.11) into Eqs. (4.9) and (4.10), I obtain the equations of the TDDFT for $|\mathbf{r}| \geq a+b$,

$$\frac{\partial \rho(\mathbf{r},t)}{\partial t} = D\nabla^2\rho(\mathbf{r},t) - \mathbf{U}\cdot\nabla\rho(\mathbf{r},t) - D\nabla\cdot\left[\rho(\mathbf{r},t)\nabla\int c_2(\mathbf{r}-\mathbf{r}')\Delta\rho(\mathbf{r}',t)\mathrm{d}\mathbf{r}'\right], \tag{4.12}$$

$$\frac{\partial \rho_{\mathrm{id}}(\mathbf{r},t)}{\partial t} = D\nabla^2\rho_{\mathrm{id}}(\mathbf{r},t) - \mathbf{U}\cdot\nabla\rho_{\mathrm{id}}(\mathbf{r},t), \tag{4.13}$$

while $\rho(\mathbf{r},t)=0$ and $\rho_{\rm id}(\mathbf{r},t)=0$ at $|\mathbf{r}|<a+b$, independently of t.

To consider the hard-sphere interaction between the probe and colloidal particles, I impose a boundary condition on the spherical surface satisfying $|\mathbf{r}|=a+b$. This condition stipulates that the density flux equals zero across the surface,

$$\mathbf{n}\cdot\mathbf{j}(\mathbf{r},t)|_{|\mathbf{r}|=a+b}=0, \tag{4.14}$$

where $\mathbf{n}$ is the normal vector of the surface at $|\mathbf{r}|=a+b$. In Eq. (4.14), $\mathbf{j}(\mathbf{r},t)$ is the density flux of the interacting colloidal particles [Eq. (4.12)], which is given by

$$\begin{aligned}\mathbf{j}(\mathbf{r},t)=&D\nabla\rho(\mathbf{r},t)-\mathbf{U}\rho(\mathbf{r},t)\\&-D\rho(\mathbf{r},t)\nabla\int c_2(\mathbf{r}-\mathbf{r}')\Delta\rho(\mathbf{r}',t)\mathrm{d}\mathbf{r}'.\end{aligned} \tag{4.15}$$

Note that for the noninteracting colloidal particles [Eq. (4.13)], $\mathbf{j}(\mathbf{r},t)$ is defined in the same manner as Eq. (4.15) but for $c_2(\mathbf{r})=0$.

Using the density fields at steady states $\rho(\mathbf{r},\infty)$ and $\rho_{\rm id}(\mathbf{r},\infty)$, I calculate the forces exerted by the colloidal particles on the probe particle. The equations of the forces are given by [7]

$$\mathbf{F}=-k_{\rm B}T\oint_S\rho(\mathbf{r},\infty)\mathbf{n}\mathrm{d}S, \tag{4.16}$$

$$\mathbf{F}_{\rm id}=-k_{\rm B}T\oint_S\rho_{\rm id}(\mathbf{r},\infty)\mathbf{n}\mathrm{d}S, \tag{4.17}$$

where, $\mathbf{F}$ and $\mathbf{F}_{\rm id}$ are the forces exerted by the interacting and noninteracting colloidal particles, respectively, S is the spherical surface satisfying $|\mathbf{r}|=a+b$, and $\mathbf{n}$ is the normal vector of S. The derivation of these equations is described in Append. A. Equations (4.16) and (4.17) show that the forces are generated by the anisotropies of the density fields around the probe particle. As the anisotropy of $\rho(\mathbf{r},\infty)$ differs from that of $\rho_{\rm id}(\mathbf{r},\infty)$, the value of $\mathbf{F}$ differs from that of $\mathbf{F}_{\rm id}$. The difference between $\mathbf{F}$ and $\mathbf{F}_{\rm id}$ gives the effects of interactions between the colloidal particles.

4.2.4 Numerical calculation

In numerical calculations of Eqs. (4.12) and (4.13), the parameters are the reduced velocity $\tilde{U}$, the probe/colloidal particles size ratio a/b, and the volume fraction of the colloidal particles ϕ. Here, $\tilde{U}$ and ϕ are defined by

$$\tilde{U}\equiv\frac{a+b}{D}|\mathbf{U}|, \tag{4.18}$$

$$\phi\equiv\frac{4}{3}\pi b^3\rho_0. \tag{4.19}$$

$\tilde{U}$ is related to the advective term in nondimensional forms of Eqs. (4.12) and (4.13) and a/b is related to the boundary condition given by Eq. (4.14). ϕ is related to $c_2(\mathbf{r})$ as well as to the boundary condition far from the probe particle.

In order to obtain $\rho(\mathbf{r}, \infty)$ and $\rho_{\rm id}(\mathbf{r}, \infty)$, I solve Eqs. (4.12) and (4.13) via iterative calculations, under the condition that the time derivative equals zero. Here, the spatial derivatives in Eqs. (4.12) and (4.13) are calculated via the finite difference method in the axially-symmetric cylindrical coordinate system (r, z). I calculate the convolution integral in Eq. (4.12) by using the fast Fourier transform [41] on the z-axis and the discrete Hankel transform on the r-axis. In the numerical calculation, the convolution-integral term is updated only at every 100 steps of the iterative calculation, so that the calculation cost is reduced. The details of the numerical method are described in Append. C.

To calculate the term of the interactions between the colloidal particles, I use the $c_2(\mathbf{r})$ defined in the homogeneous system which is in the absence of the probe particle. I calculate $c_2(\mathbf{r})$ by employing the Ornstein–Zernike relation and the hypernetted-chain (HNC) approximation [40]. In the homogeneous system, the Ornstein–Zernike relation is given by

$$h(\mathbf{r}) = c_2(\mathbf{r}) + \rho_0 \int c_2(|\mathbf{r} - \mathbf{r}'|) h(\mathbf{r}') \mathrm{d}\mathbf{r}', \tag{4.20}$$

where $h(\mathbf{r})$ is the pair correlation function in the homogeneous system. The HNC approximation is given by

$$c_2(\mathbf{r}) = h(\mathbf{r}) - \ln[h(\mathbf{r}) + 1] - \beta V_c(\mathbf{r}), \tag{4.21}$$

where $V_c(\mathbf{r})$ is the potential of the interaction between the colloidal particles (hard-sphere potential with diameter $2b$). From Eqs. (4.20) and (4.21), I obtain $c_2(\mathbf{r})$ and $h(\mathbf{r})$ numerically via the iterative calculation.

In the numerical calculation of Eqs. (4.12) and (4.13), the data points are placed on the z-axis at constant intervals of $b/50$ and $b/100$ for Eq. (4.12) and $(a+b)/100$ for Eq. (4.13). The data points on the r-axis are placed on the zeros of the order-zero Bessel function of the first kind $J_0(r)$ to ensure the orthogonality of the discrete Hankel transform [42, 43], so that the average values of the intervals equal those on the z-axis. The numerical calculation ranges are $0 < r/b \leq 16$ and $-20.48 \leq z/b \leq 20.48$ for Eq. (4.12) and $0 < r/(a+b) \leq 8$ and $-10.24 \leq z/(a+b) \leq 10.24$ for Eq. (4.13), where the origin is placed at the center of the probe particle. I have confirmed that the calculated results remain almost unchanged when a half values of the intervals are adopted. The convergence of the iterative calculation is determined by checking that $|\nabla \cdot \mathbf{j}(\mathbf{r}, t)| < 10^{-4} D\rho_0/b^2$ at all data points.

4.3 Results

4.3.1 Dependence of force on volume fraction

Calculating $\mathbf{F}$ and $\mathbf{F}_{\rm id}$ from Eqs. (4.16) and (4.17), I examine the dependence of $\mathbf{F}$ and $\mathbf{F}_{\rm id}$ on ϕ. In the calculation of Eq. (4.16), $\rho(\mathbf{r}, \infty)$ is scaled by ϕ, which is

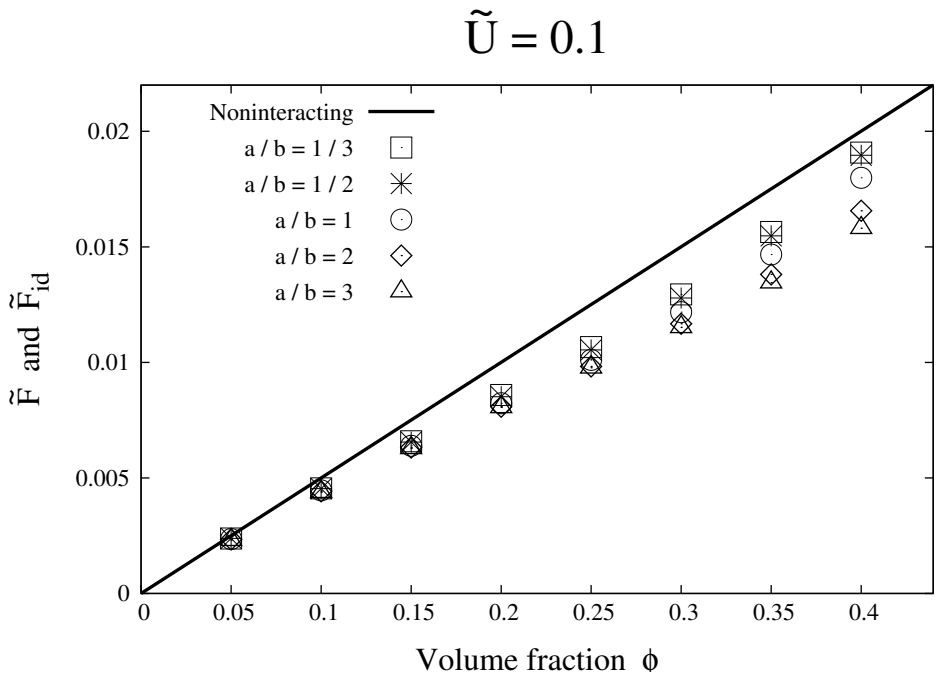

Figure 4.2: Volume fraction ϕ-dependence of calculated forces acting on probe particle $\mathbf{F}$ and $\mathbf{F}_{\rm id}$ for reduced velocity $\tilde{U} = 0.1$ and various probe/colloidal-particle size ratios a/b. The reduced force $\tilde{F}$ exerted by interacting colloidal particles (symbols) is defined by Eq. (4.24), while $\tilde{F}_{\rm id}$ (a solid line) exerted by noninteracting colloidal particles is defined by the same coefficient as Eq. (4.24). By using Eq. (4.18), the flux velocity is reduced to $\tilde{U}$. Five types of symbols represent the results of different a/b values (see the legend).

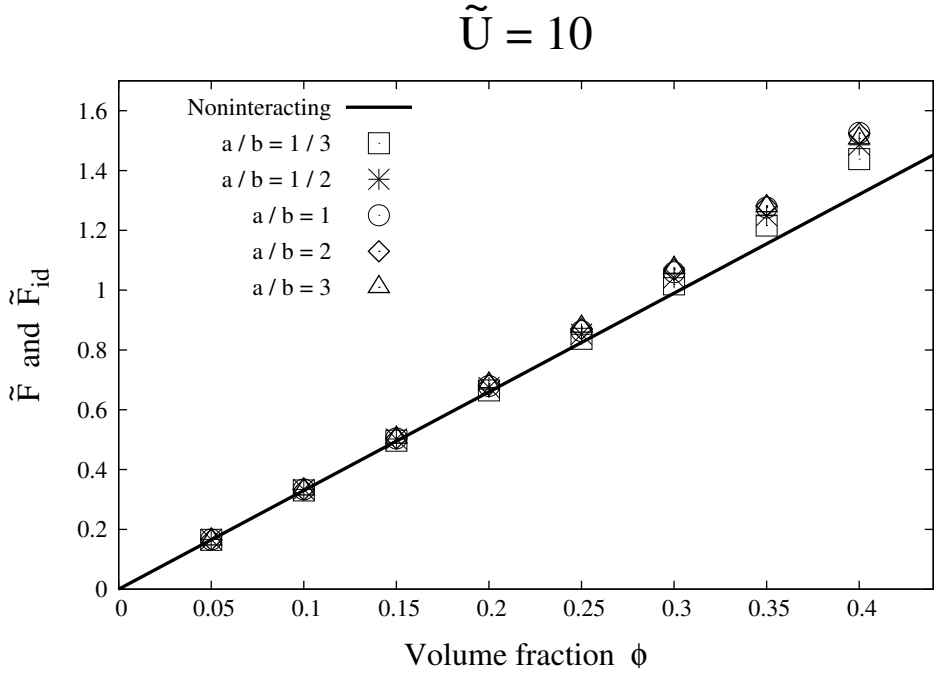

Figure 4.3: Identical to Fig. 4.2, but for $\tilde{U} = 10$.

expressed as

$$\tilde{\rho}(\mathbf{r},\infty) \equiv \frac{\rho(\mathbf{r},\infty)}{\rho_0} = \frac{4\pi b^3 \rho(\mathbf{r},\infty)}{3\phi}, \tag{4.22}$$

where Eq. (4.19) is employed. In this calculation, the surface S is scaled by $(a+b)^2$ so that Eq. (4.16) is expressed as

$$\mathbf{F} = -\frac{3(a+b)^2 k_{\mathrm{B}} T}{4\pi b^3} \oint_{|\tilde{\mathbf{r}}|=1} \tilde{\rho}(\tilde{\mathbf{r}},\infty) \mathrm{d}\tilde{S}, \tag{4.23}$$

where $\tilde{\mathbf{r}} \equiv \mathbf{r}/(a+b)$ and $\tilde{S}$ is the spherical surface satisfying $|\tilde{\mathbf{r}}| = 1$. In the calculation of Eq. (4.17), $\rho_{\mathrm{id}}(\mathbf{r},\infty)$ and S are scaled in the same manner as Eqs. (4.22) and (4.23), respectively. From Eqs. (4.22) and (4.23), I define the reduced force by

$$\tilde{F} \equiv \frac{b^3}{(a+b)^2 k_{\mathrm{B}} T} |\mathbf{F}|, \tag{4.24}$$

while I define the reduced force exerted by the noninteracting colloidal particles $\tilde{F}_{\mathrm{id}}$ by the same coefficient as Eq. (4.24).

I plot the dependence of the reduced forces $\tilde{F}$ and $\tilde{F}_{\mathrm{id}}$ on ϕ (Figs. 4.2 and 4.3). I calculate $\tilde{F}$ and $\tilde{F}_{\mathrm{id}}$ for two reduced velocity values, $\tilde{U} = 0.1$ (Fig. 4.2) and 10 (Fig. 4.3). Figures 4.2 and 4.3 show that $\tilde{F}$ and $\tilde{F}_{\mathrm{id}}$ increase with ϕ. Here, $\tilde{F}_{\mathrm{id}}$ is proportional to ϕ because $\rho_{\mathrm{id}}(\mathbf{r},\infty)$ is determined from a linear equation of the density field [Eq. (4.13)]. $\tilde{F}$ agrees with $\tilde{F}_{\mathrm{id}}$ at small values of ϕ for all probe/colloidal particles size ratios.

When $\tilde{U} = 0.1$ (Fig. 4.2), the values of $\tilde{F}$ (symbols) are smaller than those of $\tilde{F}_{\mathrm{id}}$ (a solid line) at all ϕ. The absolute value of the difference in the forces $|\tilde{F} - \tilde{F}_{\mathrm{id}}|$ is small at small ϕ, but grows with ϕ for $\phi < 0.3$. However, as the volume fraction increases from $\phi = 0.3$, $|\tilde{F} - \tilde{F}_{\mathrm{id}}|$ becomes small once more. This behavior of $|\tilde{F} - \tilde{F}_{\mathrm{id}}|$ is discussed in Sect. 4.4. $|\tilde{F} - \tilde{F}_{\mathrm{id}}|$ increases as the size of the colloidal particles becomes small. Note that $|\tilde{F} - \tilde{F}_{\mathrm{id}}|$ arises from the effect of the hard-sphere interactions between the colloidal particles.

In contrast to the case of $\tilde{U} = 0.1$, the results for $\tilde{U} = 10$ show that the effect of the interactions enhances the force values (Fig. 4.3). The values of $\tilde{F}$ are larger than those of $\tilde{F}_{\mathrm{id}}$ at large ϕ. Although $|\tilde{F} - \tilde{F}_{\mathrm{id}}|$ is small at small ϕ ($\phi < 0.2$), it increases with ϕ ($\phi > 0.3$). The values of $\tilde{F}$ are almost the same for all a/b values. In other words, the dependence of $\tilde{F}$ on the size of the colloidal particles is weaker than that for $\tilde{U} = 0.1$ (Fig. 4.2).

4.3.2 Velocity dependence of friction coefficient

Next, to examine the dependence of $\tilde{F}$ and $\tilde{F}_{\mathrm{id}}$ on $\tilde{U}$, I define the friction coefficients K and K_{id} by

$$K \equiv \frac{|\mathbf{F}|}{|\mathbf{U}|} \quad \text{and} \quad K_{\mathrm{id}} \equiv \frac{|\mathbf{F}_{\mathrm{id}}|}{|\mathbf{U}|}. \tag{4.25}$$

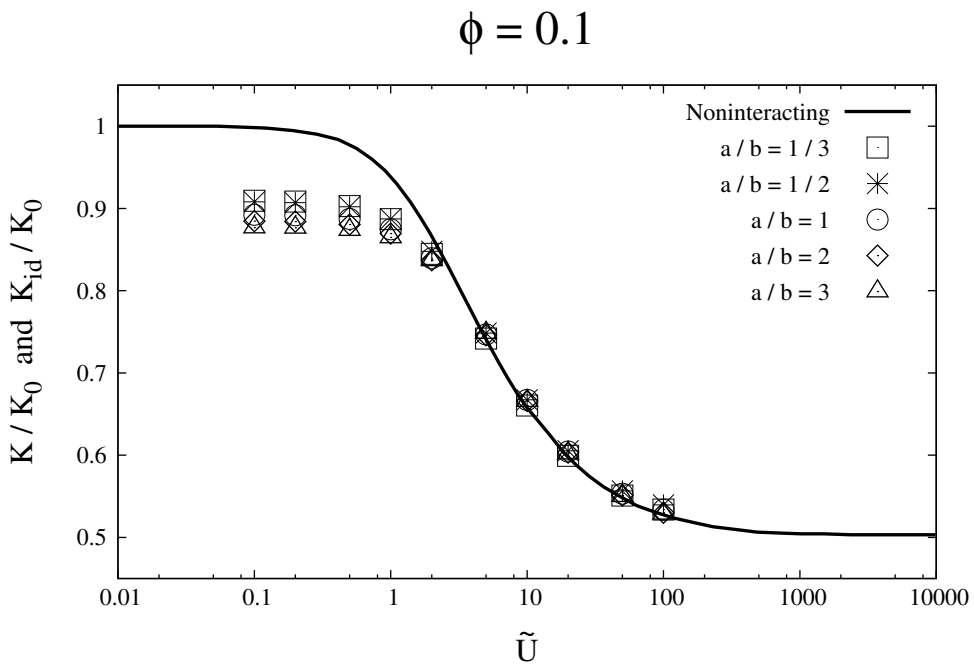

Figure 4.4: $\tilde{U}$-dependence of calculated friction coefficients K and $K_{\rm id}$ for $\phi = 0.1$ and various a/b. Here, K and $K_{\rm id}$ are defined by Eq. (4.25) for the interacting and noninteracting colloidal particles, respectively, and K_0 is $K_{\rm id}$ in the limit $\tilde{U} \to 0$. The solid curve represents $K_{\rm id}$ values obtained by Squires and Brady [7]. The reduced velocity $\tilde{U}$ is defined by Eq. (4.18). Five types of symbols represent the results of different a/b values (see the legend).

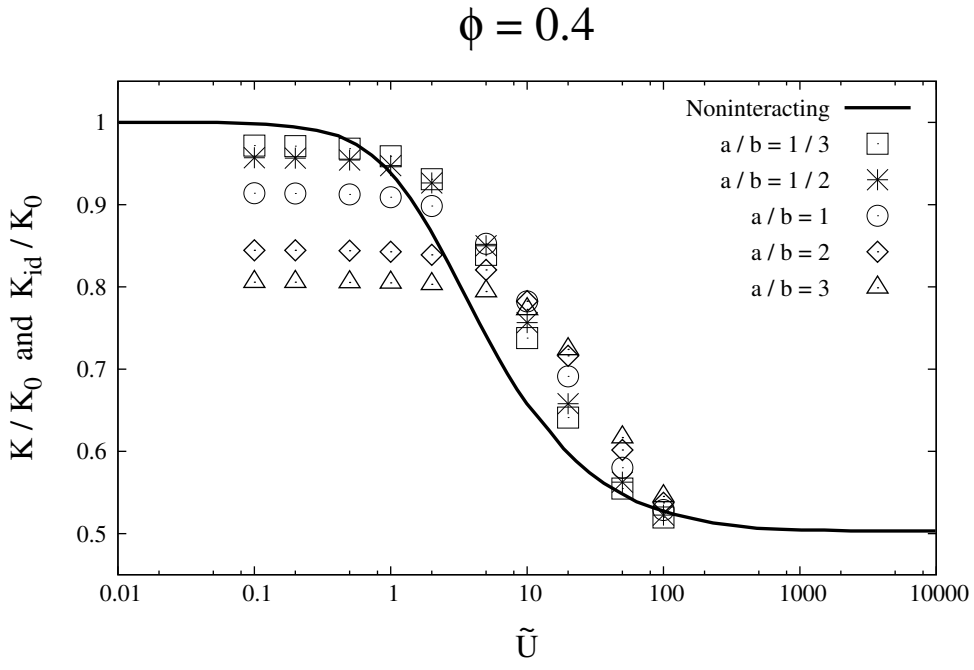

Figure 4.5: Identical to Fig. 4.4, but for $\phi = 0.4$.

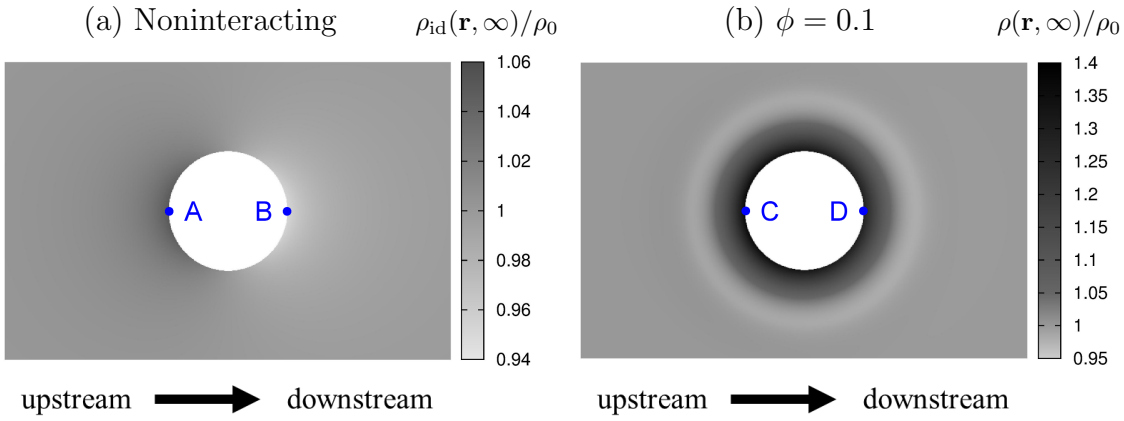

Figure 4.6: Calculated density fields at steady states for $\tilde{U} = 0.1$ in symmetric plane of probe particle. (a) $\rho_{\rm id}(\mathbf{r},\infty)$ is obtained by solving Eq. (4.13) for the noninteracting colloidal particles. (b) $\rho(\mathbf{r},\infty)$ is obtained by solving Eq. (4.12) for the interacting colloidal particles, with $\phi = 0.1$, where the size of the probe particle is the same as that of the colloidal particles. $\rho_{\rm id}(\mathbf{r},\infty)$ and $\rho(\mathbf{r},\infty)$ are scaled by the homogeneous density ρ_0, and darker areas represent higher density areas. The colloidal particles cannot enter the white areas, because of the excluded volume of the probe particle. The direction of $\mathbf{U}$ is rightward. At points A and B, the values of $\rho_{\rm id}(\mathbf{r},\infty)/\rho_0$ are 1.05 and 0.95, respectively. At points C and D, $\rho(\mathbf{r},\infty)/\rho_0$ are 1.38 and 1.29, respectively.

Note that K and $K_{\rm id}$ are defined not only in the linear region, where $\tilde{F}$ and $\tilde{F}_{\rm id}$ are proportional to $\tilde{U}$, but also in the nonlinear region for high $\tilde{U}$. I plot the calculated friction coefficients K and $K_{\rm id}$ for $\phi = 0.1$ (Fig. 4.4) and 0.4 (Fig. 4.5) in the $0.1 \le \tilde{U} \le 100$ range. Here, K and $K_{\rm id}$ are scaled by K_0 that is $K_{\rm id}$ in the limit $\tilde{U} \to 0$. Since $K_{\rm id}/K_0$ corresponds to the normalized viscosity increment (see Sect. 2.1), its values are quoted from Squires and Brady [7].

When $\phi = 0.1$ (Fig. 4.4), the values of K (symbols) are smaller than or equal to those of $K_{\rm id}$ (a solid curve) for all values of $\tilde{U}$. For small $\tilde{U}$, K is smaller than $K_{\rm id}$. The absolute value of the difference in the friction coefficients $|K - K_{\rm id}|$ decreases as $\tilde{U}$ becomes large and almost disappears for $\tilde{U} \ge 5$. Note that this difference is caused by the effect of the hard-sphere interactions between the colloidal particles. The effect of the interactions for small $\tilde{U}$ is also shown in Fig. 4.2.

In the case of $\phi = 0.4$ (Fig. 4.5), the relation $K < K_{\rm id}$ is obtained for small $\tilde{U}$, similarly to the results of $\phi = 0.1$. However, $K > K_{\rm id}$ is obtained for large $\tilde{U}$ (Fig. 4.5). In the $5 < \tilde{U} < 50$ range, in particular, $K > K_{\rm id}$ is obtained for all a/b. The relation $K > K_{\rm id}$ is also shown in Fig. 4.2, for large ϕ and large $\tilde{U}$. At $\tilde{U} = 100$, $K \approx K_{\rm id}$ is obtained for all a/b. Additionally, Fig. 4.5 shows stronger dependence on a/b than that in Fig. 4.4.

4.3.3 Density fields around probe particle

To see the appearance of the density field, I plot $\rho(\mathbf{r},\infty)$ and $\rho_{\rm id}(\mathbf{r},\infty)$ for $\tilde{U} = 0.1$ (Fig. 4.6) and 10 (Fig. 4.7). These figures show that the density fields depend on $\tilde{U}$ and ϕ. In the figures, darker areas represent higher density areas. The white areas

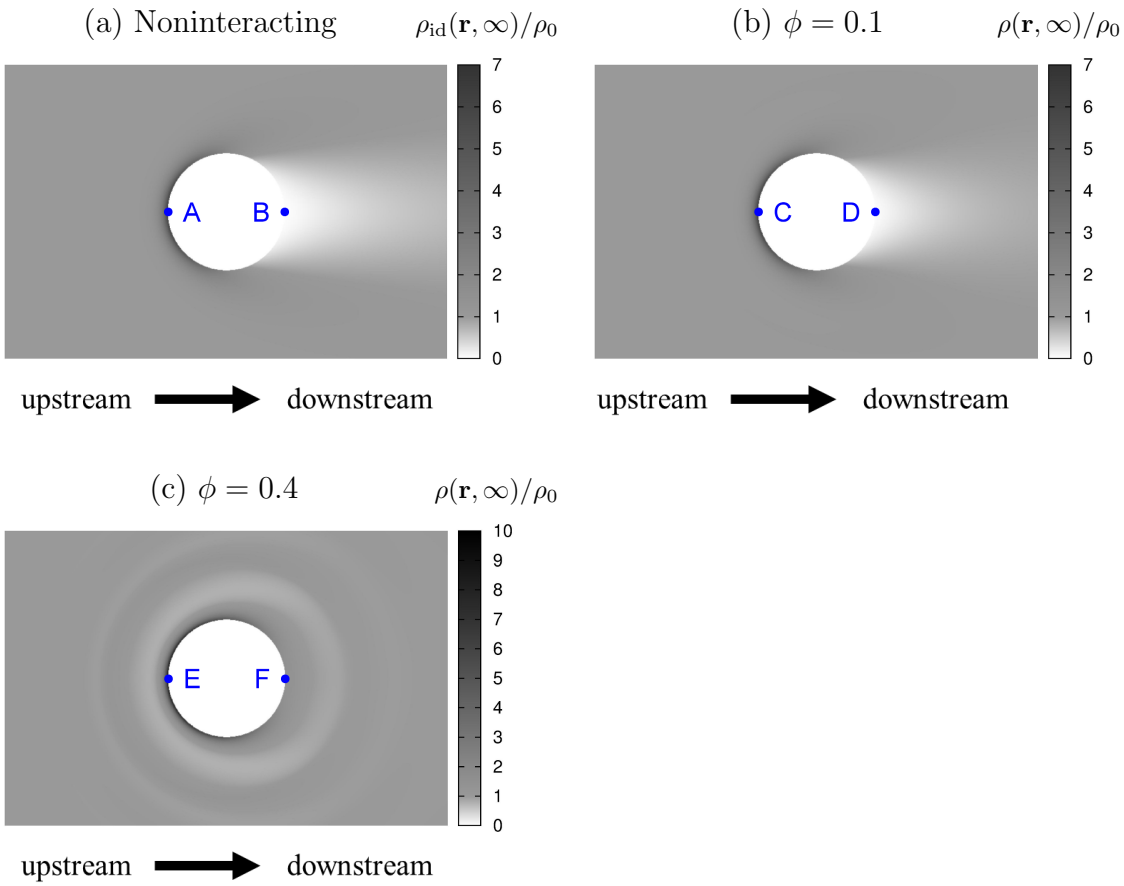

Figure 4.7: Identical to Fig. 4.6, but for $\tilde{U} = 10$. (a) $\rho_{\rm id}(\mathbf{r},\infty)$. (b) $\rho(\mathbf{r},\infty)$ for $\phi = 0.1$. (c) $\rho(\mathbf{r},\infty)$ for $\phi = 0.4$. At points A and B, $\rho_{\rm id}(\mathbf{r},\infty)/\rho_0$ are 6.44 and 0.02, respectively. At the other points, $\rho(\mathbf{r},\infty)/\rho_0$ are 6.53 (C), 0.04 (D), 9.15 (E), and 1.45 (F).

in the figures are the region which the colloidal particles cannot enter because of the excluded volume of the probe particle. The values of the density fields are higher on the upstream side of the probe particle (the left side of the white area) than that on the downstream side.

When $\tilde{U} = 0.1$ (Fig. 4.6), the plots show that the colloidal particles gather around the probe particle because of the hard-sphere interactions between the colloidal particles. For the noninteracting colloidal particles [Fig. 4.6(a)], $\rho_{\rm id}(\mathbf{r}, \infty) > \rho_0$ on the upstream side of the probe particle, while $\rho_{\rm id}(\mathbf{r}, \infty) < \rho_0$ on the downstream side. In contrast, $\rho(\mathbf{r}, \infty)$ for the interacting colloidal particles satisfies $\rho(\mathbf{r}, \infty) > \rho_0$ on the downstream side as well as on the upstream side. The values of $\rho(\mathbf{r}, \infty)$ near the probe particle are larger than those of $\rho_{\rm id}(\mathbf{r}, \infty)$. The difference in the density fields $\rho(\mathbf{r}, \infty) - \rho_{\rm id}(\mathbf{r}, \infty)$ is larger on the downstream side than that on the upstream side; in Fig. 4.6, the difference between the points A and C is 0.33 and that between the points B and D is 0.34.

In contrast to the case of $\tilde{U} = 0.1$, the results of $\tilde{U} = 10$ (Fig. 4.7) show that the effect of the interactions is modified by the rapid flux. When $\phi = 0.1$, the appearance of $\rho(\mathbf{r}, \infty)$ is similar to that of $\rho_{\rm id}(\mathbf{r}, \infty)$ [see Figs. 4.7(a) and (b)]. However, for a large volume fraction ($\phi = 0.4$), the values of $\rho(\mathbf{r}, \infty)$ near the probe particle are larger than those of $\rho_{\rm id}(\mathbf{r}, \infty)$ [see Figs. 4.7(a) and (c)]. The density difference $\rho(\mathbf{r}, \infty) - \rho_{\rm id}(\mathbf{r}, \infty)$ is larger on the upstream side than that on the downstream side; in Figs. 4.7(a) and (c), the difference between the points A and E is 2.71 and that between the points B and F is 1.43.

4.3.4 Density difference between upstream and downstream sides

To study the correlation between the density fields and the forces, I plot the density difference $\Delta\rho - \Delta\rho_{\rm id}$ and the force difference $\tilde{F} - \tilde{F}_{\rm id}$ against ϕ (Fig. 4.8). Here, $\Delta\rho = \rho(\mathbf{r}_A, \infty) - \rho(\mathbf{r}_B, \infty)$ and $\Delta\rho_{\rm id} = \rho_{\rm id}(\mathbf{r}_A, \infty) - \rho_{\rm id}(\mathbf{r}_B, \infty)$, where $\mathbf{r}_A$ and $\mathbf{r}_B$ are the measurement points on the upstream side and downstream side of the probe particle, respectively [Fig. 4.8(c)]. The ϕ-dependence of $\Delta\rho - \Delta\rho_{\rm id}$ is correlated with the nonmonotonic ϕ-dependence of $\tilde{F} - \tilde{F}_{\rm id}$ except for the results of $a/b = 3$ [see Figs. 4.8(a) and (b)]. Note that $\tilde{F} - \tilde{F}_{\rm id}$ for $a/b = 3$ does not have the minimum value. Except for $a/b = 3$, both $\Delta\rho - \Delta\rho_{\rm id}$ and $\tilde{F} - \tilde{F}_{\rm id}$ decrease and increase for small and large values of ϕ, respectively. The increase begins at $\phi = 0.25$–0.3, which depends on the size ratio a/b.

The correlation between $\Delta\rho - \Delta\rho_{\rm id}$ and $\tilde{F} - \tilde{F}_{\rm id}$ is explained by Eqs. (4.16) and (4.17). These equations show that the forces are caused by the anisotropy of the density field around the probe particle. The anisotropy is represented by the density difference between the upstream and downstream sides of the probe particle. Thus, $\Delta\rho$ and $\Delta\rho_{\rm id}$ are correlated with $\tilde{F}$ and $\tilde{F}_{\rm id}$, respectively, so that $\Delta\rho - \Delta\rho_{\rm id}$ is correlated with $\tilde{F} - \tilde{F}_{\rm id}$.

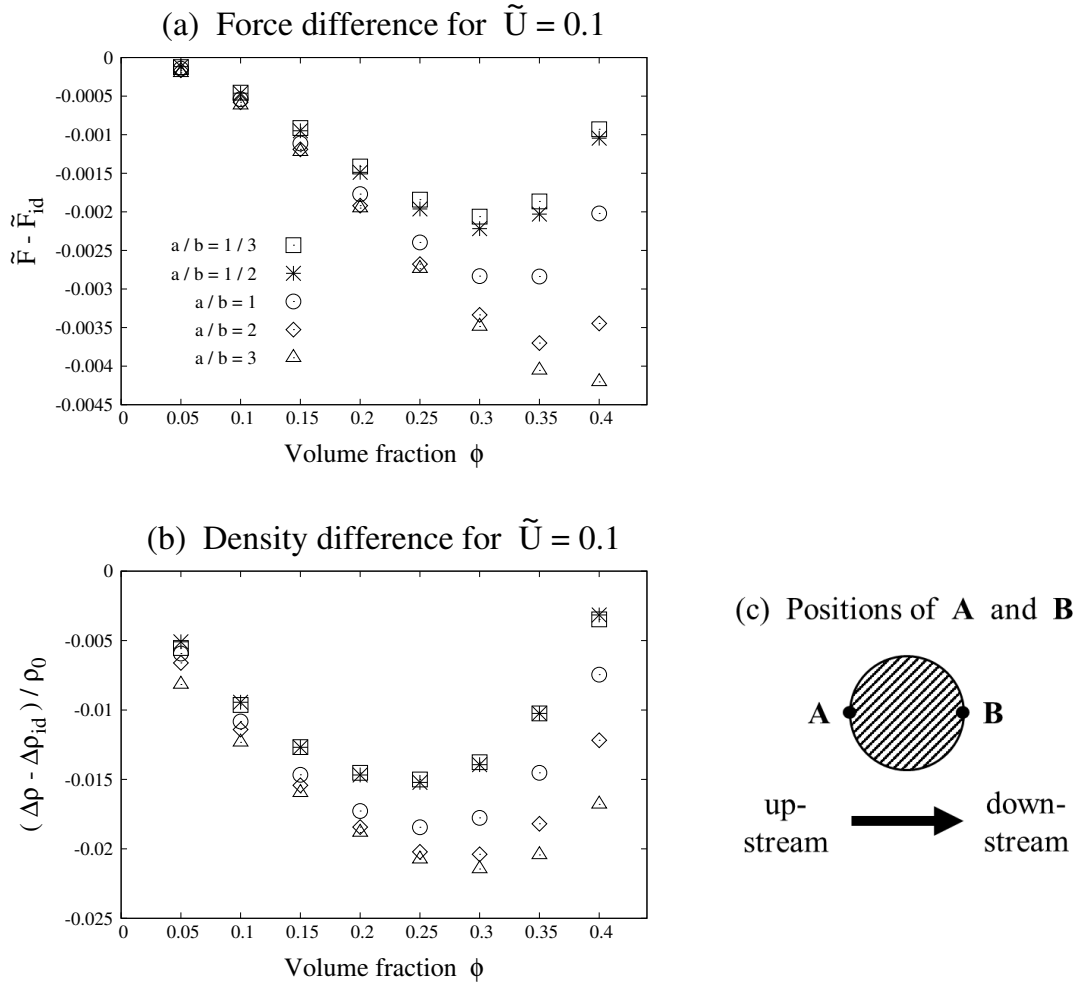

Figure 4.8: (a) ϕ-dependence of difference between $\mathbf{F}$ and $\mathbf{F}_{\rm id}$ for $\tilde{U} = 0.1$ and various a/b. The definitions of $\tilde{F}$, $\tilde{F}_{\rm id}$, and $\tilde{U}$ are identical to those in Fig. 4.2. Five types of symbols represent the results of different a/b values (see the legend). (b) ϕ-dependence of density difference $\Delta\rho$ between upstream and downstream sides of probe particle for $\tilde{U} = 0.1$ and various a/b. $\Delta\rho = \rho(\mathbf{r}_{\rm A}, \infty) - \rho(\mathbf{r}_{\rm B}, \infty)$, where $\rho(\mathbf{r}_{\rm A}, \infty)$ and $\rho(\mathbf{r}_{\rm B}, \infty)$ are the density fields at positions A and B, respectively, for the interacting colloidal particles at steady states. $\Delta\rho_{\rm id}$ is defined by $\Delta\rho_{\rm id} = \rho_{\rm id}(\mathbf{r}_{\rm A}, \infty) - \rho_{\rm id}(\mathbf{r}_{\rm B}, \infty)$, where $\rho_{\rm id}(\mathbf{r}_{\rm A}, \infty)$ and $\rho_{\rm id}(\mathbf{r}_{\rm B}, \infty)$ are the density fields at positions A and B, respectively, for the noninteracting colloidal particles at steady states. (c) Positions of A and B in symmetric plane of probe particle. A striped circle represents the region that the colloidal particles cannot enter because of the excluded volume of the probe particle. The direction of $\mathbf{U}$ is rightward. The cylindrical coordinates of A and B are given by $(r, z) = (\Delta r, -a - b)$ and $(\Delta r, a + b)$, respectively, where the origin is placed at the center of the probe particle. These points are placed on the data points neighboring the position $r = 0$ on the r-axis.

4.4 Discussion

To consider the ϕ-dependence of the density difference $\Delta\rho$, I discuss the effects of the interactions between the colloidal particles on the density field. When a colloidal particle approaches the fixed probe particle, it is pushed toward the probe particle by the other colloidal particles through the hard-sphere interaction. This leads to the increment in the average number density of the colloidal particles in the vicinity of the probe particle, which is called the depletion effect [44]. The depletion effect is shown in Fig. 4.6(b). As ϕ increases, the depletion effect becomes significant because of the increment in the collision between the colloidal particles.

The important factors of determining $\rho(\mathbf{r}, \infty)$ are the depletion effect and the advection. The depletion effect causes the increment in $\rho(\mathbf{r}, \infty)$ in the vicinity of the probe particle, while the advection causes the increment in $\rho(\mathbf{r}, \infty)$ on the upstream side and the decrement on the downstream side. In contrast to the case of the interacting colloidal particles, $\rho_{\mathrm{id}}(\mathbf{r}, \infty)$ for the noninteracting colloidal particles is not under the influence of the depletion effect, because a noninteracting colloidal particle is not pushed by the other colloidal particles. Therefore, the important factor of determining $\rho_{\mathrm{id}}(\mathbf{r}, \infty)$ is only the advection. The relation between $\Delta\rho$ and $\Delta\rho_{\mathrm{id}}$ is determined from the competition between the depletion effect and advection.

The relation $\Delta\rho - \Delta\rho_{\mathrm{id}} < 0$ shown in Fig. 4.8(b) is obtained when the depletion effect dominates over the advection. Here, I consider the virtual temporal development: starting from $\rho_{\mathrm{id}}(\mathbf{r}, \infty)$, the density field of the interacting colloidal particles grows to $\rho(\mathbf{r}, \infty)$. First, the number density of the colloidal particles is higher on the upstream side than on the downstream side due to the advection. Then, the number density in the vicinity of the probe particle increases due to the depletion effect; the increment in the number density is greater on the downstream side than on the upstream side [see Figs. 4.6(a) and (b)]. This leads to the relation $\Delta\rho - \Delta\rho_{\mathrm{id}} < 0$. I consider that the great increment on the downstream side is caused by the low density due to the advection, because a colloidal particle approaches the probe particle easily on the low density side without the disturbance due to the other colloidal particles.

In Fig. 4.8(b), although $\Delta\rho - \Delta\rho_{\mathrm{id}}$ becomes small as ϕ increases to $\phi = 0.25$–0.3, it becomes large once more as ϕ increases further. To discuss this nonmonotonic ϕ-dependence of $\Delta\rho - \Delta\rho_{\mathrm{id}}$, I consider another virtual temporal development: starting from $\rho(\mathbf{r}, \infty)$ at $\phi = 0.25$–0.3, the density field of the interacting colloidal particles grows to $\rho(\mathbf{r}, \infty)$ for $\phi > 0.3$. First, the number density of the colloidal particles is higher on the upstream side than on the downstream side due to the advection, but it is also sufficiently high on both sides due to the depletion effect at $\phi = 0.25$–0.3. Then, the number density in the vicinity of the probe particle increases further due to the depletion effect for $\phi > 0.3$; the increment in the number density is less on the downstream side than on the upstream side. This leads to the increment of $\Delta\rho - \Delta\rho_{\mathrm{id}}$ as ϕ increases from $\phi = 0.25$–0.3. I consider that the little increment on the downstream side is caused by the advection and the high density due to the depletion effect; a colloidal particle on this side approaches the probe particle under the disturbance due to the advection and the other colloidal

particles. In contrast to the downstream side, the advection assists a colloidal particle on the upstream side to approach the probe particle.

The relation $\tilde{F} > \tilde{F}_{\rm id}$ shown in Fig. 4.3 is obtained when the advection dominates over the depletion effect. Here, I consider the virtual temporal development: starting from $\rho_{\rm id}(\mathbf{r}, \infty)$, the density field of the interacting colloidal particles grows to $\rho(\mathbf{r}, \infty)$. First, the number density of the colloidal particles is much higher on the upstream side than on the downstream side due to the advection of the large $\tilde{U}$. Then, the number density in the vicinity of the probe particle increases due to the depletion effect; the increment in the number density is less on the downstream side than on the upstream side [see Figs. 4.7(a), (b), and (c)]. This enhances the anisotropy of $\rho(\mathbf{r}, \infty)$ around the probe particle so that the relation $\tilde{F} > \tilde{F}_{\rm id}$ is obtained. I consider that the little increment on the downstream side is caused by the advection of the large $\tilde{U}$, because a colloidal particle on the downstream side approaches the probe particle under the significant disturbance due to the advection.

The a/b-dependence of the friction coefficient K shown in Fig. 4.5 is stronger than that shown in Fig. 4.4. This means that ϕ has a great influence on the a/b-dependence of K. I consider that this great influence is caused by the enhancement of the interaction between the colloidal particles due to the increment in ϕ. The interaction between the colloidal particles is enhanced by the large ϕ because the interparticle distances become short as ϕ increases. Since the origin of the a/b-dependence is the interaction between the colloidal particles, the increment in ϕ leads to the strong a/b-dependence of K.

4.5 Summary

Having calculated the force exerted by colloidal particles on the probe particle via numerical calculations using the TDDFT, I have examined the effects of interactions between colloidal particles. For small values of the flux velocity, the force decreases due to the effect of hard-sphere interactions between the colloidal particles. In contrast, for large values of the velocity and the volume fraction, the force increases due to the effect of the interactions. Because of the effect of the interactions, the density field of the colloidal particles increases in the vicinity of the probe particle, which is called the depletion effect. The effects of the interactions are determined from the competition between the depletion effect and the advection.

In this study using the TDDFT, I have assumed that the solvent velocity is constant in the whole system. Since the flux of the solvent is disturbed by the probe and colloidal particles, the solvent velocity field is actually nonuniform in the vicinity of the probe particle. In the next step, I examine modification of the results obtained in the present chapter by the nonuniform solvent velocity. In Chap. 5, I explain the method of combining the DFT with the two-fluid model and derive the equations of motion for the colloidal particles and for the solvent. In Chap. 6, I apply this method to a system of a soft-core probe particle and examine the modification of the effects of the interactions by the nonuniform solvent velocity.

Chapter 5

Combination of density functional theory with two-fluid model

5.1 Introduction

In Chap. 4, I have examined effects of interactions between colloidal particles by calculating the force exerted by the colloidal particles on the probe particle. The solvent velocity has been assumed to be constant in the whole system, while the solvent velocity should be nonuniform because of the disturbance by the probe and colloidal particles. In this chapter, to examine the modification of the effects of the interactions by the nonuniform solvent velocity, I apply the two-fluid model to the system of active microrheology in a colloidal suspension. The application of the two-fluid model gives equations of motion for colloidal particles and for a solvent (see Chap. 3). By solving the equations of the two-fluid model numerically, I obtain the volume fraction field of colloidal particles and the solvent velocity field simultaneously.

Furthermore, to calculate effects of interactions between colloidal particles, I combine the density functional theory (DFT) with the two-fluid model. By applying the DFT to a many-particle system, I obtain the free-energy functional which includes the term of interactions between particles. In this chapter, combining the DFT with the two-fluid model, I derive the equations of motion for colloidal particles and for the solvent including the term of interactions between colloidal particles. Additionally, I expand the equations in the volume fraction of the colloidal particles. When the volume fraction is small, the neglect of high-order terms reduces the cost of the numerical calculations.

5.2 Application of density functional theory to two-fluid model

In the same way as Chap. 4, I consider a probe particle fixed at the origin in a colloidal suspension that flows at a constant velocity $\mathbf{U}$ far from the probe particle (Fig. 5.1). The colloidal particles are hard spheres with the volume v,

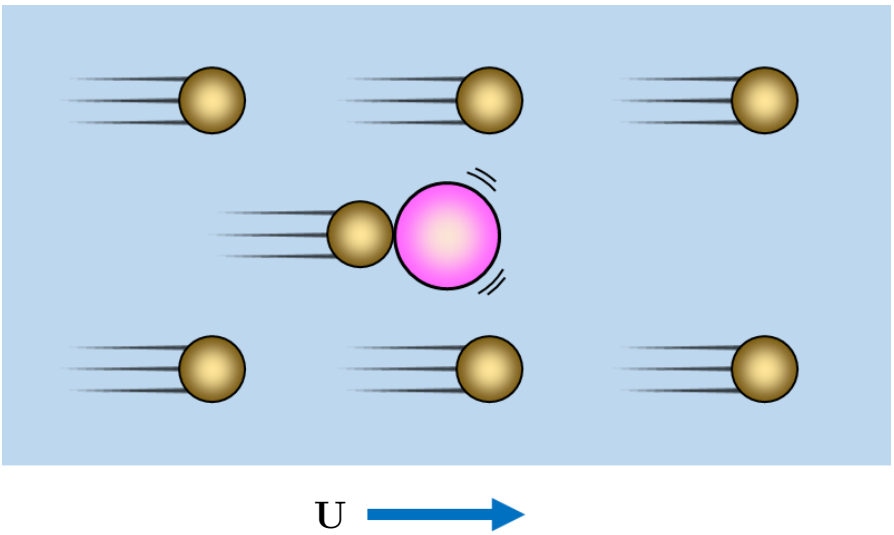

Figure 5.1: Model system for active microrheology in colloidal suspension. A probe particle is fixed spatially in a colloidal suspension. The colloidal suspension flows at a constant velocity $\mathbf{U}$ far from the probe particle. The colloidal particles are hard spheres with the volume v. The interaction between the probe and colloidal particles is given by a potential $V(\mathbf{r})$.

which interact with each other. The interaction between the probe and colloidal particles is given by a potential $V(\mathbf{r})$. In this system, the flux of the solvent is disturbed by the probe and by the colloidal particles around the probe particle; thus, the solvent velocity field is nonuniform in the vicinity of the probe particle.

For simplicity, I assume that the solvent velocity is disturbed only by the colloidal particles around the probe particle. Here, I consider effects of the colloidal particles on the solvent velocity field but neglect effects of the probe particle on it. Note that both of these effects on the solvent velocity field have been neglected in Chap. 4. Although the neglect of the effect of the probe particle may seem to be a poor approximation, I consider that there are cases where the effect of the colloidal particles is the object of study. The discussion about this assumption is described in Sect. 5.4.

5.2.1 Equations of two-fluid model

To consider the nonuniform solvent velocity disturbed by colloidal particles, I employ the two-fluid model (see Chap. 3). Regarding the colloidal particles and the solvent as two types of fluids, I apply the two-fluid model to the colloidal suspension. For the two-fluid model, at steady states, the incompressibility condition [Eq. (3.2)] is given by

$$0 = \nabla \cdot [\phi(\mathbf{r})\mathbf{v}_c(\mathbf{r}) + (1 - \phi(\mathbf{r}))\mathbf{v}_s(\mathbf{r})], \tag{5.1}$$

where $\phi(\mathbf{r})$ is the volume-fraction field of the colloidal particles and $\mathbf{v}_c(\mathbf{r})$ and $\mathbf{v}_s(\mathbf{r})$ are the velocity fields of the colloidal particles and the solvent, respectively.

I assume that the volume-fraction field of the solvent is given by $1-\phi(\mathbf{r})$. At steady states, the volume-fraction field satisfies the continuity equation [Eq. (3.1)],

$$0 = \nabla \cdot (\phi(\mathbf{r})\mathbf{v}_c(\mathbf{r})). \tag{5.2}$$

From the two-fluid model, at steady states, the equation of motion for the colloidal particles [Eq. (3.11)] is given by

$$\mathbf{0} = \Gamma(\phi(\mathbf{r}))(\mathbf{v}_c(\mathbf{r}) - \mathbf{v}_s(\mathbf{r})) + \phi(\mathbf{r})\nabla\frac{\delta F[\phi(\mathbf{r})]}{\delta\phi(\mathbf{r})} + \phi(\mathbf{r})\nabla p(\mathbf{r}). \tag{5.3}$$

Here, $\Gamma(\phi(\mathbf{r}))$ is the friction coefficient between the colloidal particles and the solvent, $F[\phi(\mathbf{r})]$ is the free-energy functional of the colloidal suspension, and $p(\mathbf{r})$ is the pressure field of the colloidal suspension. Note that the term of $F[\phi(\mathbf{r})]$ is expressed by the functional derivative. The definitions of the variables are the same as those in Sec. 3, where the derivation of Eq. (5.3) has been explained in detail. In Eq. (5.3), the effect of the interaction potential $V(\mathbf{r})$ is included in the second term on the right-hand side. Additionally, the effect of the interaction between colloidal particles is also included in this term.

The equation of morion for the solvent [Eq. (3.12)] at steady states is given by

$$\begin{aligned}\mathbf{0} = {} & \Gamma(\phi(\mathbf{r}))(\mathbf{v}_s(\mathbf{r}) - \mathbf{v}_c(\mathbf{r})) + (1-\phi(\mathbf{r}))\nabla p(\mathbf{r}) \\ & - \mu\nabla^2\mathbf{v}_s(\mathbf{r}) - (\lambda+\mu)\nabla(\nabla\cdot\mathbf{v}_s(\mathbf{r})),\end{aligned} \tag{5.4}$$

where μ and λ are the shear viscosity and volume viscosity of the solvent, respectively. In Eq. (5.4), the terms of $-\mu\nabla^2\mathbf{v}_s$ and $-(\lambda+\mu)\nabla(\nabla\cdot\mathbf{v}_s)$ represent the shear-viscosity and volume-viscosity terms, respectively. From the sum of Eqs. (5.3) and (5.4), the equation of the pressure field is given by

$$\nabla p(\mathbf{r}) = \mu\nabla^2\mathbf{v}_s(\mathbf{r}) + (\lambda+\mu)\nabla(\nabla\cdot\mathbf{v}_s(\mathbf{r})) - \phi(\mathbf{r})\nabla\frac{\delta F[\phi(\mathbf{r})]}{\delta\phi(\mathbf{r})}. \tag{5.5}$$

I impose the boundary condition that $\mathbf{v}_s(\mathbf{r})$ equals the constant flux velocity $\mathbf{U}$ far from the probe particle, which is expressed by

$$\mathbf{v}_s(\mathbf{r}) = \mathbf{U}, \quad \text{as} \quad |\mathbf{r}| \to \infty. \tag{5.6}$$

5.2.2 Friction coefficient between colloidal particles and solvent

The friction coefficient $\Gamma(\phi(\mathbf{r}))$ is defined by the energy dissipation W_f due to relative motion between the colloidal particles and the solvent,

$$W_f = \int \Gamma(\phi(\mathbf{r}))(\mathbf{v}_c(\mathbf{r}) - \mathbf{v}_s(\mathbf{r}))^2 \mathrm{d}\mathbf{r}. \tag{5.7}$$

To obtain W_f, I consider the friction force $\mathbf{f}(\mathbf{r})$ exerted by the solvent on the colloidal particles at a position $\mathbf{r}$. From the Stokes–Einstein relation, $\mathbf{f}(\mathbf{r})$ is given by

$$\mathbf{f}(\mathbf{r}) = -\frac{k_\mathrm{B}T}{D}(\mathbf{v}_c(\mathbf{r}) - \mathbf{v}_s(\mathbf{r})), \tag{5.8}$$

where D is the diffusion coefficient of the colloidal particles. I assume that all colloidal particles at a position $\mathbf{r}$ are subject to the friction force $\mathbf{f}(\mathbf{r})$ given by Eq. (5.8).

The energy dissipation W_f is obtained from the integration of the energy dissipation per colloidal particle $w_f(\mathbf{r})$ at a position $\mathbf{r}$. Being subject to the friction force $\mathbf{f}(\mathbf{r})$, a colloidal particle is moved through the vector $\mathbf{v}_c(\mathbf{r}) - \mathbf{v}_s(\mathbf{r})$ per unit time. Therefore, the one-particle energy dissipation $w_f(\mathbf{r})$ is given by

$$w_f(\mathbf{r}) = \frac{k_{\mathrm{B}}T}{D}(\mathbf{v}_c(\mathbf{r}) - \mathbf{v}_s(\mathbf{r}))^2. \tag{5.9}$$

At a position $\mathbf{r}$, the local number of the colloidal particles per unit volume is given by $\phi(\mathbf{r})/v$, where v is the volume of a colloidal particle. The whole energy dissipation W_f is given by

$$W_f = \frac{1}{v}\int w_f(\mathbf{r})\phi(\mathbf{r})\mathrm{d}\mathbf{r} = \frac{k_{\mathrm{B}}T}{Dv}\int \phi(\mathbf{r})(\mathbf{v}_c(\mathbf{r}) - \mathbf{v}_s(\mathbf{r}))^2\mathrm{d}\mathbf{r}. \tag{5.10}$$

Equations (5.7) and (5.10) give the friction coefficient $\Gamma(\phi(\mathbf{r}))$,

$$\Gamma(\phi(\mathbf{r})) = \frac{k_{\mathrm{B}}T}{Dv}\phi(\mathbf{r}). \tag{5.11}$$

From Eqs. (5.2) and (5.11), the divergence of Eq. (5.3) is given by

$$0 = \nabla\cdot\left(-\frac{k_{\mathrm{B}}T}{Dv}\phi(\mathbf{r})\mathbf{v}_s(\mathbf{r}) + \phi(\mathbf{r})\nabla\frac{\delta F[\phi(\mathbf{r})]}{\delta\phi(\mathbf{r})} + \phi(\mathbf{r})\nabla p(\mathbf{r})\right). \tag{5.12}$$

5.2.3 Application of density functional theory

To consider effects of the hard-sphere interactions between the colloidal particles, I employ the free-energy functional derived from the density functional theory (DFT). I substitute the free-energy functional of the DFT for $F[\phi(\mathbf{r})]$ in the equation of the two-fluid model [Eq. (5.12)]. Although the DFT gives the free energy of the colloidal particles, it does not give the free energy of the solvent. I neglect the free energy related to the solvent and consider the free energy of the colloidal particles only.

The free-energy functional of the DFT is given by [18, 21, 39]

$$\begin{aligned}\beta F[\phi(\mathbf{r})] = \beta F_{\mathrm{ideal}}[\phi(\mathbf{r})] &- \frac{c_1}{v}\int \Delta\phi(\mathbf{r})\mathrm{d}\mathbf{r} \\ &- \frac{1}{2v^2}\int c_2(\mathbf{r}_1 - \mathbf{r}_2)\Delta\phi(\mathbf{r}_1)\Delta\phi(\mathbf{r}_2)\mathrm{d}\mathbf{r}_1\mathrm{d}\mathbf{r}_2 + \mathrm{const},\end{aligned} \tag{5.13}$$

where

$$\Delta\phi(\mathbf{r}) = \phi(\mathbf{r}) - \phi_0. \tag{5.14}$$

Here, c_1 and $c_2(\mathbf{r})$ are one- and two-particle direct correlation functions, respectively, and ϕ_0 is the homogeneous volume fraction far from the probe particle. In

Eq. (5.13), $F_{\rm ideal}[\phi(\mathbf{r})]$ is the free-energy functional for ideal gas, which is given by [40]

$$\beta F_{\rm ideal}[\phi(\mathbf{r})] = \frac{1}{v}\int \phi(\mathbf{r})\left(\ln\phi(\mathbf{r}) + \beta V(\mathbf{r}) + \ln\frac{\Lambda^3}{v} - 1\right)\mathrm{d}\mathbf{r}, \tag{5.15}$$

where $V(\mathbf{r})$ is the interaction between the probe and colloidal particles and Λ is the thermal de Broglie wave length. Note that Eqs. (5.13) and (5.15) are obtained from the replacement of $\rho(\mathbf{r},t)$ in Eqs. (4.8) and (4.6) with $\phi(\mathbf{r})/v$.

Using the free-energy functional given by Eq. (5.13), I obtain the equations of the two-fluid model including the term of the interactions between the colloidal particles. From Eqs. (5.12) and (5.13), the divergence of the equation for the colloidal particles is given by

$$\begin{aligned} 0 = \nabla\cdot\Bigg(&\nabla\phi(\mathbf{r}) + \beta\phi(\mathbf{r})\nabla V(\mathbf{r}) - \frac{1}{v}\phi(\mathbf{r})\nabla\int c_2(\mathbf{r}-\mathbf{r}')\Delta\phi(\mathbf{r}')\mathrm{d}\mathbf{r}' \\ &- \frac{1}{D}\phi(\mathbf{r})\mathbf{v}_s(\mathbf{r}) + \beta v\phi(\mathbf{r})\nabla p(\mathbf{r})\Bigg). \end{aligned} \tag{5.16}$$

In the same way as Eq. (5.16), the equation of the pressure field [Eq. (5.5)] is given by

$$\begin{aligned} \nabla p(\mathbf{r}) = {}&\mu\nabla^2\mathbf{v}_s(\mathbf{r}) + (\lambda+\mu)\nabla(\nabla\cdot\mathbf{v}_s(\mathbf{r})) - \frac{k_{\rm B}T}{v}\nabla\phi(\mathbf{r}) \\ &- \frac{1}{v}\phi(\mathbf{r})\nabla V(\mathbf{r}) + \frac{k_{\rm B}T}{v^2}\phi(\mathbf{r})\nabla\int c_2(\mathbf{r}-\mathbf{r}')\Delta\phi(\mathbf{r}')\mathrm{d}\mathbf{r}'. \end{aligned} \tag{5.17}$$

By solving Eqs. (5.16), (5.17), and (5.1) simultaneously, $\phi(\mathbf{r})$, $\mathbf{v}_s(\mathbf{r})$, and $p(\mathbf{r})$ are obtained.

5.2.4 Approximate incompressibility condition

For simplicity, instead of the incompressibility condition given by Eq. (5.1), I employ the approximate incompressibility condition [Eq. (3.13)],

$$0 = \nabla\cdot\mathbf{v}_s(\mathbf{r}). \tag{5.18}$$

The approximate incompressibility condition [Eq. (5.18)] is accurate in the dilute limit. When the incompressibility condition is given by Eq. (5.18), the colloidal particles are not subject to the solvent pressure. The equation of motion for the colloidal particles [Eq. (3.16)] is given by

$$\mathbf{0} = \Gamma(\phi(\mathbf{r}))(\mathbf{v}_c(\mathbf{r}) - \mathbf{v}_s(\mathbf{r})) + \frac{\delta F[\phi(\mathbf{r})]}{\delta\phi(\mathbf{r})}, \tag{5.19}$$

and the equation for the solvent [Eq. (3.17)] is given by

$$\mathbf{0} = \Gamma(\phi(\mathbf{r}))(\mathbf{v}_s(\mathbf{r}) - \mathbf{v}_c(\mathbf{r})) + \nabla p(\mathbf{r}) - \mu\nabla^2\mathbf{v}_s(\mathbf{r}). \tag{5.20}$$

The derivation of Eqs. (5.19) and (5.20) is described in Sect. 3.2.6.

For the approximate incompressibility condition [Eq. (5.18)], from Eqs. (5.2), (5.11), and (5.13), the divergence of Eq. (5.19) is given by

$$0 = \nabla \cdot \Bigg(\nabla\phi(\mathbf{r}) + \beta\phi(\mathbf{r})\nabla V(\mathbf{r}) - \frac{1}{D}\phi(\mathbf{r})\mathbf{v}_s(\mathbf{r}) - \frac{1}{v}\phi(\mathbf{r})\nabla \int c_2(\mathbf{r}-\mathbf{r}')\Delta\phi(\mathbf{r}')\mathrm{d}\mathbf{r}' \Bigg). \tag{5.21}$$

From the sum of Eqs. (5.19) and (5.20), the equation of the pressure field is given by

$$\nabla p(\mathbf{r}) = \mu\nabla^2\mathbf{v}_s(\mathbf{r}) - \frac{k_\mathrm{B}T}{v}\nabla\phi(\mathbf{r}) - \frac{1}{v}\phi(\mathbf{r})\nabla V(\mathbf{r}) + \frac{k_\mathrm{B}T}{v^2}\phi(\mathbf{r})\nabla \int c_2(\mathbf{r}-\mathbf{r}')\Delta\phi(\mathbf{r}')\mathrm{d}\mathbf{r}'. \tag{5.22}$$

These equations are simpler than Eqs. (5.16) and (5.17). The approximate incompressibility condition [Eq. (5.18)] reduces the calculation cost of obtaining $\phi(\mathbf{r})$, $\mathbf{v}_s(\mathbf{r})$, and $p(\mathbf{r})$.

5.2.5 Noninteracting colloidal particles

To examine effects of the interactions between the colloidal particles, I also calculate the volume-fraction field of noninteracting colloidal particles $\phi_\mathrm{id}(\mathbf{r})$ at steady states. Note that the noninteracting colloidal particles do not interact with each other, but a noninteracting colloidal particle interacts with the probe particle and the solvent. In the case of the noninteracting colloidal particles, the term of $c_2(\mathbf{r})$ is removed from the free-energy functional [Eq. (5.13)]. For the incompressibility condition given by Eq. (5.1), the equations to be solved are given by

$$0 = \nabla \cdot \Bigg[\nabla\phi_\mathrm{id}(\mathbf{r}) + \beta\phi_\mathrm{id}(\mathbf{r})\nabla V(\mathbf{r}) - \frac{1}{D}\phi_\mathrm{id}(\mathbf{r})\mathbf{v}_\mathrm{id}(\mathbf{r}) + \beta v\phi_\mathrm{id}(\mathbf{r})\nabla p(\mathbf{r}) \Bigg], \tag{5.23}$$

$$\nabla p_\mathrm{id}(\mathbf{r}) = \mu\nabla^2\mathbf{v}_\mathrm{id}(\mathbf{r}) + (\lambda+\mu)\nabla(\nabla\cdot\mathbf{v}_\mathrm{id}(\mathbf{r})) - \frac{k_\mathrm{B}T}{v}\nabla\phi_\mathrm{id}(\mathbf{r}) - \frac{1}{v}\phi_\mathrm{id}(\mathbf{r})\nabla V(\mathbf{r}), \tag{5.24}$$

where $\mathbf{v}_\mathrm{id}(\mathbf{r})$ and $p_\mathrm{id}(\mathbf{r})$ are the solvent velocity field and the pressure field of the colloidal suspension for the case of the noninteracting colloidal particles, respectively. In the same way, for the approximate incompressibility condition [Eq. (5.22)], the equations to be solved are given by

$$0 = \nabla \cdot \Bigg[\nabla\phi_\mathrm{id}(\mathbf{r}) + \beta\phi_\mathrm{id}(\mathbf{r})\nabla V(\mathbf{r}) - \frac{1}{D}\phi_\mathrm{id}(\mathbf{r})\mathbf{v}_\mathrm{id}(\mathbf{r}) \Bigg], \tag{5.25}$$

$$\nabla p_{\mathrm{id}}(\mathbf{r}) = \mu\nabla^2\mathbf{v}_{\mathrm{id}}(\mathbf{r}) - \frac{k_{\mathrm{B}}T}{v}\nabla\phi_{\mathrm{id}}(\mathbf{r}) - \frac{1}{v}\phi_{\mathrm{id}}(\mathbf{r})\nabla V(\mathbf{r}). \tag{5.26}$$

I determine the effects of the interactions from the difference between $\phi_{\mathrm{id}}(\mathbf{r})$ and $\phi(\mathbf{r})$ of the interacting colloidal particles.

5.3 Expansion in volume fraction

To solve the equations represented in the preceding section, I expand $\phi(\mathbf{r})$, $\mathbf{v}_s(\mathbf{r})$, and $p(\mathbf{r})$ in the homogeneous volume fraction ϕ_0,

$$\phi(\mathbf{r}) = 0 + \phi^{(1)}(\mathbf{r})\phi_0 + \phi^{(2)}(\mathbf{r})\phi_0^2 + \cdots, \tag{5.27}$$

$$\mathbf{v}_s(\mathbf{r}) = \mathbf{v}_s^{(0)}(\mathbf{r}) + \mathbf{v}_s^{(1)}(\mathbf{r})\phi_0 + \mathbf{v}_s^{(2)}(\mathbf{r})\phi_0^2 + \cdots, \tag{5.28}$$

$$p(\mathbf{r}) = p^{(0)}(\mathbf{r}) + p^{(1)}(\mathbf{r})\phi_0 + p^{(2)}(\mathbf{r})\phi_0^2 + \cdots. \tag{5.29}$$

Here, $\phi^{(n)}(\mathbf{r})$, $\mathbf{v}_s^{(n)}(\mathbf{r})$, and $p^{(n)}(\mathbf{r})$ are the n-th-order coefficients of $\phi(\mathbf{r})$, $\mathbf{v}_s(\mathbf{r})$, and $p(\mathbf{r})$, respectively, and the zeroth-order term of $\phi(\mathbf{r})$ is obviously zero. From Eqs. (5.27), (5.28), and (5.29), the equations of the two fluid model are described as the series in ϕ_0. Then, I neglect the third- and higher-order terms of ϕ_0 in the equations. This approximation is accurate only when the homogeneous volume fraction ϕ_0 is sufficiently small.

5.3.1 Equations for the zeroth order

Expressing the equations of the two-fluid model [Eqs. (5.1), (5.16), and (5.17)] as the series in ϕ_0, I extract the equations of the zeroth-order terms from them. From the incompressibility condition [Eq. (5.1)], the zeroth-order term is extracted,

$$0 = \nabla \cdot \mathbf{v}_s^{(0)}(\mathbf{r}). \tag{5.30}$$

Similarly, the zeroth-order term of Eq. (5.17) is given by

$$\begin{aligned}\nabla p^{(0)}(\mathbf{r}) &= \mu\nabla^2\mathbf{v}_s^{(0)}(\mathbf{r}) + (\lambda+\mu)\nabla(\nabla\cdot\mathbf{v}_s^{(0)}(\mathbf{r})) \\ &= \mu\nabla^2\mathbf{v}_s^{(0)}(\mathbf{r}),\end{aligned} \tag{5.31}$$

where Eq. (5.30) is used. From Eq. (5.31) and the boundary condition for $\mathbf{v}_s(\mathbf{r})$ [Eq. (5.6)], $\mathbf{v}_s^{(0)}(\mathbf{r})$ and $p(\mathbf{r})$ are given by

$$\mathbf{v}_s^{(0)}(\mathbf{r}) = \mathbf{U} \quad \text{and} \quad p^{(0)}(\mathbf{r}) = \text{const.} \tag{5.32}$$

Note that the zeroth-order term of Eq. (5.16) equals zero.

5.3.2 Equations for the first order

In the same way, I extract the first-order terms of ϕ_0 from the equations of the two-fluid model [Eqs. (5.1), (5.16), and (5.17)]. The first-order term of Eq. (5.16) is given by

$$0 = \nabla \cdot \left(\nabla \phi^{(1)}(\mathbf{r}) + \beta \phi^{(1)}(\mathbf{r}) \nabla V(\mathbf{r}) - \frac{1}{D} \phi^{(1)}(\mathbf{r}) \mathbf{U} \right), \tag{5.33}$$

where Eq. (5.32) is used. Since Eq. (5.33) does not include $\mathbf{v}_s^{(1)}(\mathbf{r})$ and $p^{(1)}(\mathbf{r})$, $\phi^{(1)}(\mathbf{r})$ is obtained by solving this equation. From the incompressibility condition [Eq. (5.1)] and the equation of the pressure field [Eq. (5.17)], the first-order terms of these equations are given by

$$0 = \nabla \cdot (\mathbf{v}_s^{(1)}(\mathbf{r}) - \phi^{(1)}(\mathbf{r}) \mathbf{U}), \tag{5.34}$$

$$\begin{aligned} \nabla p^{(1)}(\mathbf{r}) = {} & \mu \nabla^2 \mathbf{v}_s^{(1)}(\mathbf{r}) + (\lambda + \mu) \nabla (\nabla \cdot \mathbf{v}_s^{(1)}(\mathbf{r})) \\ & - \frac{k_\mathrm{B} T}{v} \nabla \phi^{(1)}(\mathbf{r}) - \frac{1}{v} \phi^{(1)}(\mathbf{r}) \nabla V(\mathbf{r}). \end{aligned} \tag{5.35}$$

By use of $\phi^{(1)}(\mathbf{r})$ obtained from Eq. (5.33), $\mathbf{v}_s^{(1)}(\mathbf{r})$ and $p^{(1)}(\mathbf{r})$ are obtained by solving Eqs. (5.34) and (5.35).

5.3.3 Equations for the second order

Furthermore, I extract the second-order terms of ϕ_0 from the equations of the two-fluid model [Eqs. (5.1), (5.16), and (5.17)]. The second-order term of Eq. (5.16) is given by

$$\begin{aligned} 0 = \nabla \cdot \Bigg\{ & \nabla \phi^{(2)}(\mathbf{r}) + \beta \phi^{(2)}(\mathbf{r}) \nabla V(\mathbf{r}) - \frac{1}{D} (\phi^{(2)}(\mathbf{r}) \mathbf{U} + \phi^{(1)}(\mathbf{r}) \mathbf{v}_s^{(1)}(\mathbf{r})) \\ & + \beta v \phi^{(1)}(\mathbf{r}) \nabla p^{(1)}(\mathbf{r}) - \frac{1}{v} \phi^{(1)}(\mathbf{r}) \nabla \int c_2(\mathbf{r} - \mathbf{r}') \Delta \phi^{(1)}(\mathbf{r}') \mathrm{d}\mathbf{r}' \Bigg\}. \end{aligned} \tag{5.36}$$

By use of $\phi^{(1)}(\mathbf{r})$, $\mathbf{v}_s^{(1)}(\mathbf{r})$, and $p^{(1)}(\mathbf{r})$ obtained from Eqs. (5.33), (5.34), and (5.35), $\phi^{(2)}(\mathbf{r})$ is obtained by solving Eq. (5.36). From the incompressibility condition [Eq. (5.1)] and the equation of the pressure field [Eq. (5.17)], the second-order terms of these equations are given by

$$0 = \nabla \cdot (\mathbf{v}_s^{(2)}(\mathbf{r}) - \phi^{(1)}(\mathbf{r}) \mathbf{v}_s^{(1)}(\mathbf{r}) - \phi^{(2)}(\mathbf{r}) \mathbf{U}), \tag{5.37}$$

$$\begin{aligned} \nabla p^{(2)}(\mathbf{r}) = {} & \mu \nabla^2 \mathbf{v}_s^{(2)}(\mathbf{r}) + (\lambda + \mu) \nabla (\nabla \cdot \mathbf{v}_s^{(2)}(\mathbf{r})) - \frac{k_\mathrm{B} T}{v} \nabla \phi^{(2)}(\mathbf{r}) \\ & - \frac{1}{v} \phi^{(2)}(\mathbf{r}) \nabla V(\mathbf{r}) - \frac{k_\mathrm{B} T}{v^2} \phi^{(1)}(\mathbf{r}) \nabla \int c_2(\mathbf{r} - \mathbf{r}') \Delta \phi^{(1)}(\mathbf{r}') \mathrm{d}\mathbf{r}'. \end{aligned} \tag{5.38}$$

Note that $\phi^{(2)}(\mathbf{r})$, $\mathbf{v}_s^{(2)}(\mathbf{r})$, and $p^{(2)}(\mathbf{r})$ are under effects of the interactions between the colloidal particles because Eqs. (5.36) and (5.38) include the term of $c_2(\mathbf{r})$.

5.3.4 Equations for approximate incompressibility condition

For the approximate incompressibility condition [Eq. (5.18)], I also express the equations of the two-fluid model [Eq. (5.18), (5.21), and (5.22)] as the series in ϕ_0. From the equations expressed as the series in ϕ_0, I extract the equations of the zeroth-, first-, and second-order terms of ϕ_0. The zeroth-order terms are the same as those for the incompressibility condition given by Eq. (5.1); Eqs. (5.30) and (5.31) are obtained from Eqs. (5.18) and (5.22), respectively, and the zeroth-order term of Eq. (5.21) equals zero.

I extract the first-order terms of ϕ_0 from the equations of the two-fluid model [Eq. (5.18), (5.21), and (5.22)]. The first-order term of Eq. (5.21) corresponds to Eq. (5.33). Therefore, even for the approximate incompressibility condition, $\phi^{(1)}(\mathbf{r})$ is obtained as the solution to Eq. (5.33). From the approximate incompressibility condition [Eq. (5.18)] and the equation of the pressure field [Eq. (5.22)], the first-order terms of these equations are given by

$$0 = \nabla \cdot \mathbf{v}_s^{(1)}(\mathbf{r}), \tag{5.39}$$

$$\nabla p^{(1)}(\mathbf{r}) = \mu \nabla^2 \mathbf{v}_s^{(1)}(\mathbf{r}) - \frac{k_\mathrm{B}T}{v} \nabla \phi^{(1)}(\mathbf{r}) - \frac{1}{v} \phi^{(1)}(\mathbf{r}) \nabla V(\mathbf{r}). \tag{5.40}$$

By use of $\phi^{(1)}(\mathbf{r})$ obtained from Eq. (5.33), $\mathbf{v}_s^{(1)}(\mathbf{r})$ and $p^{(1)}(\mathbf{r})$ are obtained by solving Eqs. (5.39) and (5.40).

I extract the second-order terms of ϕ_0 from the equations of the two-fluid model [Eq. (5.18), (5.21), and (5.22)]. The second term of Eq. (5.21) is given by

$$\begin{aligned} 0 = \nabla \cdot \Bigg\{ & \nabla \phi^{(2)}(\mathbf{r}) + \beta \phi^{(2)}(\mathbf{r}) \nabla V(\mathbf{r}) - \frac{1}{D} \phi^{(2)}(\mathbf{r}) \mathbf{U} \\ & - \frac{1}{D} \phi^{(1)}(\mathbf{r}) \mathbf{v}_s^{(1)}(\mathbf{r}) - \frac{1}{v} \phi^{(1)}(\mathbf{r}) \nabla \int c_2(\mathbf{r} - \mathbf{r}') \Delta \phi^{(1)}(\mathbf{r}') \mathrm{d}\mathbf{r}' \Bigg\}. \end{aligned} \tag{5.41}$$

In contrast to Eq. (5.36), $p^{(1)}(\mathbf{r})$ is not necessary to obtain $\phi^{(2)}(\mathbf{r})$ from Eq. (5.41). From the approximate incompressibility condition [Eq. (5.18)] and the equation of the pressure field [Eq. (5.22)], the second-order terms of these equations are given by

$$0 = \nabla \cdot \mathbf{v}_s^{(2)}(\mathbf{r}), \tag{5.42}$$

$$\begin{aligned} \nabla p^{(2)}(\mathbf{r}) = {} & \mu \nabla^2 \mathbf{v}_s^{(2)}(\mathbf{r}) - \frac{k_\mathrm{B}T}{v} \nabla \phi^{(2)}(\mathbf{r}) - \frac{1}{v} \phi^{(2)}(\mathbf{r}) \nabla V(\mathbf{r}) \\ & - \frac{k_\mathrm{B}T}{v^2} \phi^{(1)}(\mathbf{r}) \nabla \int c_2(\mathbf{r} - \mathbf{r}') \Delta \phi^{(1)}(\mathbf{r}') \mathrm{d}\mathbf{r}'. \end{aligned} \tag{5.43}$$

$\phi^{(2)}(\mathbf{r})$, $\mathbf{v}_s^{(2)}(\mathbf{r})$, and $p^{(2)}(\mathbf{r})$ are under the effects of the interactions between the colloidal particles.

5.3.5 Equations for noninteracting colloidal particles

In the same way, for the case of the noninteracting colloidal particles, I expand $\phi_{\rm id}(\mathbf{r})$, $\mathbf{v}_{\rm id}(\mathbf{r})$, and $p_{\rm id}(\mathbf{r})$ in the homogeneous volume fraction ϕ_0,

$$\phi_{\rm id}(\mathbf{r}) = 0 + \phi_{\rm id}^{(1)}(\mathbf{r})\phi_0 + \phi_{\rm id}^{(2)}(\mathbf{r})\phi_0^2 + \cdots , \tag{5.44}$$

$$\mathbf{v}_{\rm id}(\mathbf{r}) = \mathbf{v}_{\rm id}^{(0)}(\mathbf{r}) + \mathbf{v}_{\rm id}^{(1)}(\mathbf{r})\phi_0 + \mathbf{v}_{\rm id}^{(2)}(\mathbf{r})\phi_0^2 + \cdots , \tag{5.45}$$

$$p_{\rm id}(\mathbf{r}) = p_{\rm id}^{(0)}(\mathbf{r}) + p_{\rm id}^{(1)}(\mathbf{r})\phi_0 + p_{\rm id}^{(2)}(\mathbf{r})\phi_0^2 + \cdots . \tag{5.46}$$

The equations to the second-order of ϕ_0 are obtained by removing the term of $c_2(\mathbf{r})$ from the equations for the interacting colloidal particles. The equations for the zeroth and first order are the same as those for the interacting colloidal particles because these equations do not include the term of $c_2(\mathbf{r})$. Therefore, $\mathbf{v}_{\rm id}^{(0)}(\mathbf{r})$ and $p_{\rm id}^{(0)}(\mathbf{r})$ are obtained in the same way as Eq. (5.32),

$$\mathbf{v}_{\rm id}^{(0)}(\mathbf{r}) = \mathbf{U} \quad \text{and} \quad p_{\rm id}^{(0)}(\mathbf{r}) = \text{const.} \tag{5.47}$$

In addition, the equations for the second order are given in the following:

- the divergence of the equation for the colloidal particles when the incompressibility condition is given by Eq. (5.1)

$$\begin{aligned} 0 = \nabla \cdot \Bigg(& \nabla\phi_{\rm id}^{(2)}(\mathbf{r}) + \beta\phi_{\rm id}^{(2)}(\mathbf{r})\nabla V(\mathbf{r}) - \frac{1}{D}\phi_{\rm id}^{(2)}(\mathbf{r})\mathbf{U} \\ & - \frac{1}{D}\phi_{\rm id}^{(1)}(\mathbf{r})\mathbf{v}_{\rm id}^{(1)}(\mathbf{r}) + \beta v\phi_{\rm id}^{(1)}(\mathbf{r})\nabla p_{\rm id}^{(1)}(\mathbf{r}) \Bigg); \end{aligned} \tag{5.48}$$

- the equation of the pressure field for the incompressibility condition given by Eq. (5.1)

$$\begin{aligned} \nabla p_{\rm id}^{(2)}(\mathbf{r}) = {} & \mu\nabla^2\mathbf{v}_{\rm id}^{(2)}(\mathbf{r}) + (\lambda+\mu)\nabla(\nabla\cdot\mathbf{v}_{\rm id}^{(2)}(\mathbf{r})) \\ & - \frac{k_{\rm B}T}{v}\nabla\phi_{\rm id}^{(2)}(\mathbf{r}) - \frac{1}{v}\phi_{\rm id}^{(2)}(\mathbf{r})\nabla V(\mathbf{r}); \end{aligned} \tag{5.49}$$

- the divergence of the equation for the colloidal particles when the incompressibility condition is approximated [Eq. (5.18)]

$$\begin{aligned} 0 = \nabla \cdot \Bigg\{ & \nabla\phi_{\rm id}^{(2)}(\mathbf{r}) + \beta\phi_{\rm id}^{(2)}(\mathbf{r})\nabla V(\mathbf{r}) \\ & - \frac{1}{D}(\phi_{\rm id}^{(2)}(\mathbf{r})\mathbf{U} + \phi_{\rm id}^{(1)}(\mathbf{r})\mathbf{v}_{\rm id}^{(1)}(\mathbf{r})) \Bigg\}; \end{aligned} \tag{5.50}$$

- the equation of the pressure field for the approximate incompressibility condition [Eq. (5.18)]

$$\nabla p_{\rm id}^{(2)}(\mathbf{r}) = \mu\nabla^2\mathbf{v}_{\rm id}^{(2)}(\mathbf{r}) - \frac{k_{\rm B}T}{v}\nabla\phi_{\rm id}^{(2)}(\mathbf{r}) - \frac{1}{v}\phi_{\rm id}^{(2)}(\mathbf{r})\nabla V(\mathbf{r}). \tag{5.51}$$

5.4 Discussion

For simplicity, I have considered the effect of the colloidal particles on $\mathbf{v}_s(\mathbf{r})$ but have neglected the effect of the probe particle on it. If the effect of the probe particle is considered, since the zeroth-order term of $\mathbf{v}_s(\mathbf{r})$ corresponds to the solvent velocity field at $\phi_0 = 0$, it is obviously given by the Stokes flow around the probe particle. The colloidal particles have an effect on the the first- and higher-order terms of $\mathbf{v}_s(\mathbf{r})$. Therefore, even in the case that the effect of the probe particle is considered, the effect of the colloidal particles is studied by obtaining the first- or higher-order terms of $\mathbf{v}_s(\mathbf{r})$. However, in order to obtain the effect of the colloidal particles accurately, it should be examined in consideration of the effect of the probe particle.

I consider that there are two method of calculating the effect of the probe particle on $\mathbf{v}_s(\mathbf{r})$. One is the boundary condition for calculating $\mathbf{v}_s(\mathbf{r})$ and $p(\mathbf{r})$, which gives values of them on the surface of the probe particle. Here, the boundary condition is imposed on the equations of $\mathbf{v}_s(\mathbf{r})$ and $p(\mathbf{r})$ derived in the preceding sections. The other method is the calculation of the friction between the solvent and the probe particle in the same way as that between the solvent and the colloidal particles. In this method, the term of the friction against the probe particle is added to the equation of motion for the solvent.

Chapter 6

Application to system of soft-core probe particle

Solving the equations derived in Chap. 5 numerically, I obtain the volume fraction field of colloidal particles and the solvent velocity field. By using the obtained volume fraction field, I calculate the force exerted by the colloidal particles on the probe particle and determine effects of interactions between the colloidal particles on the force. In this chapter, the nonuniform solvent velocity field is considered in the numerical calculations using the two-fluid model in contrast to Chap. 4. Here, I examine the modification of the effects of the interactions by the nonuniform solvent velocity field.

6.1 Model and Method

A probe particle is fixed at the origin in a colloidal suspension that flows at a constant velocity $\mathbf{U}$ far from the probe particle (Fig. 6.1). The probe particle is subject to the force $\mathbf{F}$ exerted by the colloidal particles. Similarly to the system considered in Chap. 4, the interaction between the colloidal particles is given by the hard sphere with the diameter $2b$. However, in contrast to Chap. 4, I consider that the interaction between the probe and colloidal particles is given by the soft-core potential $V(\mathbf{r})$ for simplicity of numerical calculations,

$$V(\mathbf{r}) = \epsilon\left(\frac{|\mathbf{r}|}{\sigma}\right)^{-12}, \tag{6.1}$$

where ϵ and σ are fitting parameters for energy and length, respectively, and the origin of the vector $\mathbf{r}$ is placed at the center of the probe particle. The discussion about the soft-core probe particle is described in Sect. 6.3. I assume that the solvent velocity is disturbed only by the colloidal particles in the same way as Chap. 5.

6.1.1 Equations of two-fluid model

Regarding the colloidal particles and solvent as two types of fluids, I employ the two-fluid model combined with the density functional theory (see Sect. 5.2.1).

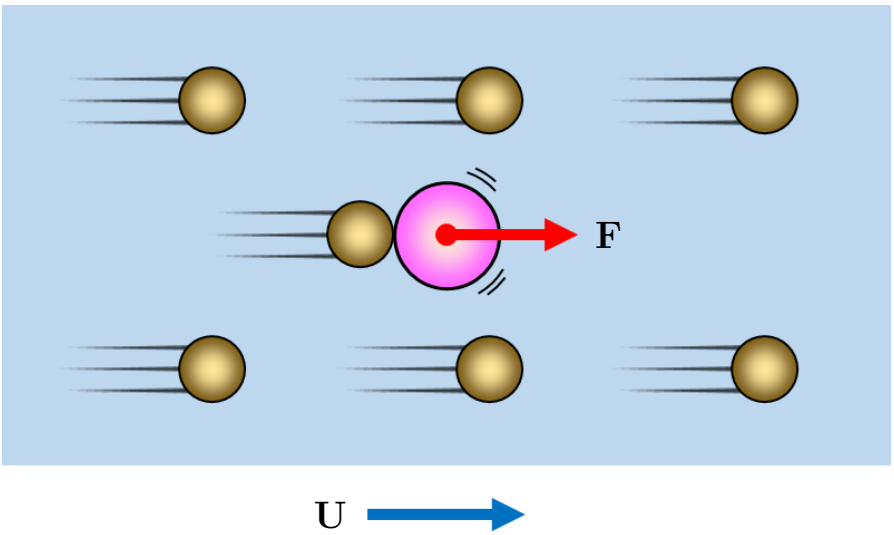

Figure 6.1: Model system for active microrheology in colloidal suspension. A probe particle is fixed spatially in a colloidal suspension. The colloidal suspension flows at a constant velocity $\mathbf{U}$ far from the probe particle. The probe particle is subject to the force $\mathbf{F}$ exerted by the colloidal particles. The colloidal particles are hard spheres with the radius b. The interaction between the probe particle and colloidal particles is given by Eq. (6.1).

When the incompressibility condition is given by Eq. (5.1), Eqs. (5.1),(5.16), and (5.17) give the volume-fraction field of the colloidal particles $\phi(\mathbf{r})$, the solvent velocity field $\mathbf{v}_s(\mathbf{r})$, and the pressure field of the colloidal suspension $p(\mathbf{r})$. I obtain $\phi(\mathbf{r})$, $\mathbf{v}_s(\mathbf{r})$, $p(\mathbf{r})$ numerically and calculate the force $\mathbf{F}$ from the obtained $\phi(\mathbf{r})$. I also calculate $\phi(\mathbf{r})$, $\mathbf{v}_s(\mathbf{r})$, and $p(\mathbf{r})$ for the approximate incompressibility condition given by Eq. (5.18). Here, $\phi(\mathbf{r})$, $\mathbf{v}_s(\mathbf{r})$, and $p(\mathbf{r})$ are obtained from Eqs. (5.18), (5.21), and (5.22).

To examine effects of interactions between the colloidal particles, I also calculate $\phi_{\rm id}(\mathbf{r})$, $\mathbf{v}_{\rm id}(\mathbf{r})$, and $p_{\rm id}(\mathbf{r})$ for the noninteracting colloidal particles. The noninteracting colloidal particles do not interact with each other, but a noninteracting colloidal particle interacts with the probe particle and solvent. In the same way as Chap. 4, I determine the effects of the interactions from the difference between the obtained $\mathbf{F}$ for the interacting colloidal particles and that for the noninteracting colloidal particles. When the incompressibility condition is given by Eq. (5.1), $\phi_{\rm id}(\mathbf{r})$, $\mathbf{v}_{\rm id}(\mathbf{r})$, and $p_{\rm id}(\mathbf{r})$ are obtained from Eqs. (5.1), (5.23), and (5.24). For the approximate incompressibility condition [Eq. (5.18)], $\phi_{\rm id}(\mathbf{r})$, $\mathbf{v}_{\rm id}(\mathbf{r})$, and $p_{\rm id}(\mathbf{r})$ are obtained from Eqs. (5.18), (5.25), and (5.26).

6.1.2 Force exerted by colloidal particles on probe particle

For the soft-core probe particle, by using the volume-fraction fields $\phi(\mathbf{r})$ and $\phi_{\rm id}(\mathbf{r})$, the forces exerted by the colloidal particles are obtained from

$$\mathbf{F} = \frac{1}{v}\int \phi(\mathbf{r})\nabla V(\mathbf{r})\mathrm{d}\mathbf{r}, \tag{6.2}$$

$$\mathbf{F}_{\rm id} = \frac{1}{v}\int \phi_{\rm id}(\mathbf{r})\nabla V(\mathbf{r})\mathrm{d}\mathbf{r}. \tag{6.3}$$

Here, $\mathbf{F}_{\rm id}$ is the force exerted by the noninteracting colloidal particles and v is the volume of a colloidal particle. Equations (6.2) and (6.3) show that the forces are generated by the anisotropies of the volume-fraction fields around the probe particle. As the anisotropy of $\phi(\mathbf{r})$ differs from that of $\phi_{\rm id}(\mathbf{r})$, the value of $\mathbf{F}$ differs from that of $\mathbf{F}_{\rm id}$. From the difference between $\mathbf{F}$ and $\mathbf{F}_{\rm id}$, I determine the effects of the interactions between the colloidal particles.

6.1.3 Assumption of small volume fraction

In the same way as Sect. 5.3, I expand $\phi(\mathbf{r})$, $\mathbf{v}_s(\mathbf{r})$, and $p(\mathbf{r})$ in the homogeneous volume fraction ϕ_0 [see Eqs. (5.27), (5.28), and (5.29)]. For the case of the noninteracting colloidal particles, $\phi_{\rm id}$, $\mathbf{v}_s(\mathbf{r})$, and $p_{\rm id}(\mathbf{r})$ are also expanded in ϕ_0. To examine effects of the interactions for small volume fractions, I neglect the third- and higher-order terms of ϕ_0 in the equations. I calculate the forces $\mathbf{F}$ and $\mathbf{F}_{\rm id}$ by using the first- and second-order terms in the volume-fraction fields,

$$\mathbf{F} = \frac{\phi_0}{v}\int (\phi^{(1)}(\mathbf{r}) + \phi_0\phi^{(2)}(\mathbf{r}))\nabla V(\mathbf{r})\mathrm{d}\mathbf{r}, \tag{6.4}$$

$$\mathbf{F}_{\rm id} = \frac{\phi_0}{v}\int (\phi_{\rm id}^{(1)}(\mathbf{r}) + \phi_0\phi_{\rm id}^{(2)}(\mathbf{r}))\nabla V(\mathbf{r})\mathrm{d}\mathbf{r}. \tag{6.5}$$

To calculate the forces, I obtain the first- and second-order terms in the volume-fraction fields by solving the equations derived in Sect. 5.3 numerically.

6.1.4 Numerical calculation

When the incompressibility condition is given by Eq. (5.1), $\phi^{(1)}(\mathbf{r})$ and $\phi^{(2)}(\mathbf{r})$ are obtained from Eqs. (5.33), (5.34), (5.35), and (5.36). First, I obtain $\phi^{(1)}(\mathbf{r})$ numerically by solving Eq. (5.33). Next, by use of the obtained $\phi^{(1)}(\mathbf{r})$, $\mathbf{v}_s^{(1)}(\mathbf{r})$ and $p^{(1)}(\mathbf{r})$ are calculated from Eqs. (5.34) and (5.35). Finally, using the obtained $\phi^{(1)}(\mathbf{r})$, $\mathbf{v}_s^{(1)}(\mathbf{r})$, and $p^{(1)}(\mathbf{r})$, I calculate $\phi^{(2)}(\mathbf{r})$ by solving Eq. (5.36). In the same way, for the approximate incompressibility condition [Eq. (5.18)], $\phi^{(1)}(\mathbf{r})$ and $\phi^{(2)}(\mathbf{r})$ are obtained from Eqs. (5.33), (5.39), (5.40), and (5.41). For the case of the noninteracting colloidal particles, I also obtain $\phi_{\rm id}^{(1)}(\mathbf{r})$ and $\phi_{\rm id}^{(2)}(\mathbf{r})$ numerically in the same way as the interacting colloidal particles.

To obtain $\mathbf{v}_s^{(1)}(\mathbf{r})$ for the incompressibility condition given by Eq. (5.1), I consider the rotation of Eq. (5.35),

$$\begin{aligned}\mathbf{0} &= \mu\nabla\times\nabla^2\mathbf{v}_s^{(1)}(\mathbf{r}) - \frac{1}{v}\nabla\times(\phi^{(1)}(\mathbf{r})\nabla V(\mathbf{r})) \\ &= \mu\nabla^2\boldsymbol{\omega}(\mathbf{r}) - \frac{1}{v}\nabla\times(\phi^{(1)}(\mathbf{r})\nabla V(\mathbf{r})),\end{aligned} \tag{6.6}$$

$$\boldsymbol{\omega}(\mathbf{r}) \equiv \nabla\times\mathbf{v}_s^{(1)}(\mathbf{r}), \tag{6.7}$$

where $\boldsymbol{\omega}(\mathbf{r})$ is the solvent vorticity field. I obtain $\boldsymbol{\omega}(\mathbf{r})$ numerically by solving Eq. (6.6) via the Gauss–Seidel method [41, 45]. Then, $\mathbf{v}_s^{(1)}(\mathbf{r})$ is determined from the obtained $\boldsymbol{\omega}(\mathbf{r})$ and the incompressibility condition in the first order [Eq. (5.34)]. $p^{(1)}(\mathbf{r})$ is determined from the numerical integration of Eq. (5.35). For the approximate incompressibility condition [Eq. (5.18)] or the noninteracting colloidal particles, $\mathbf{v}_s^{(1)}(\mathbf{r})$ and $p^{(1)}(\mathbf{r})$ or $\mathbf{v}_{\mathrm{id}}^{(1)}(\mathbf{r})$ and $p_{\mathrm{id}}^{(1)}(\mathbf{r})$ are obtained in the same way. The details of these numerical calculations are described in Append. D.2.

In order to obtain $\phi^{(1)}(\mathbf{r})$ and $\phi^{(2)}(\mathbf{r})$ for the incompressibility condition given by Eq. (5.1), I solve Eqs. (5.33) and (5.36), respectively, via the iterative calculation. The spatial derivatives are calculated via the finite difference method in the axially-symmetric cylindrical coordinate system (r, z). In the same way as Chap. 4, I calculate the convolution integral in Eq. (5.36) by using the fast Fourier transform [41] on the z-axis and the discrete Hankel transform on the r-axis. Note that the convolution integral in Eq. (5.36) does not require iterative updating because it is determined by $\phi^{(1)}(\mathbf{r})$ obtained from Eq. (5.33). For the approximate incompressibility condition [Eq. (5.18)] or the noninteracting colloidal particles, $\phi^{(1)}(\mathbf{r})$ and $\phi^{(2)}(\mathbf{r})$ or $\phi_{\mathrm{id}}^{(1)}(\mathbf{r})$ and $\phi_{\mathrm{id}}^{(2)}(\mathbf{r})$ are obtained in the same way. The details of these numerical calculation are described in Append. D.1.

The parameters of the present system are the reduced probe-particle size $\tilde{\sigma}$, the reduced velocity $\tilde{U}$, and the homogeneous volume fraction ϕ_0. $\tilde{\sigma}$ and $\tilde{U}$ are defined by

$$\tilde{\sigma} \equiv \beta\epsilon\left(\frac{\sigma}{2b}\right)^{12}, \tag{6.8}$$

$$\tilde{U} \equiv \frac{2b}{D}|\mathbf{U}|. \tag{6.9}$$

$\tilde{U}$ is related to the $\mathbf{U}$-terms of the equations in the nondimensional forms and $\tilde{\sigma}$ is related to the $V(\mathbf{r})$-terms in the nondimensional equations. In addition, ϕ_0 is related to $c_2(\mathbf{r})$ as well as to the boundary condition of $\phi^{(1)}(\mathbf{r})$ and $\phi_{\mathrm{id}}^{(1)}(\mathbf{r})$ far from the probe particle.

In the numerical calculation, the data points are placed on the z-axis at the constant interval of $b/50$. The data points on the r-axis are placed on the zeros of the order-zero Bessel function of the first kind $J_0(r)$ to ensure the orthogonality of the discrete Hankel transform (see Append. C.1), so that the average value

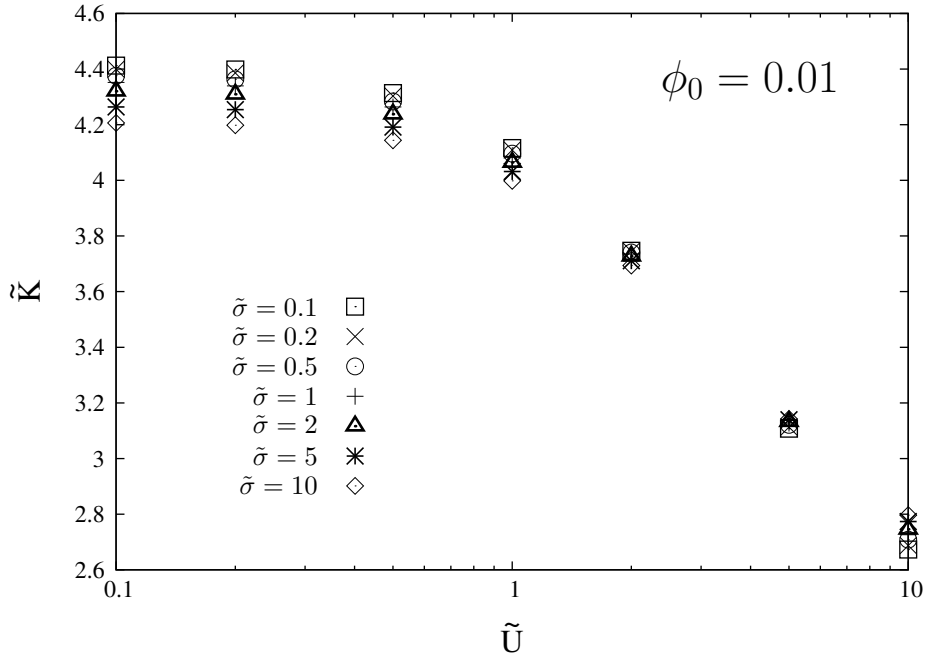

Figure 6.2: $\tilde{U}$-dependence of calculated friction coefficient for volume fraction $\phi_0 = 0.01$ and various reduced probe-particle size $\tilde{\sigma}$. The reduced friction coefficient $\tilde{K}$ is defined by Eq. (6.10) for interacting colloidal particles. The reduced flux velocity $\tilde{U}$ is defined by Eq. (6.9). Each symbol represents a different value of $\tilde{\sigma}$, where $\tilde{\sigma}$ is defined by Eq. (6.8). In obtaining these results, the incompressibility condition given by Eq. (5.1) is employed.

of the intervals equals that on the z-axis. The numerical calculation ranges are $0 < r/b \leq 16$ and $-20.48 \leq z/b \leq 20.48$, where the origin is placed at the center of the probe particle. I employ the $c_2(\mathbf{r})$ obtained numerically from the Ornstein–Zernike relation [Eq. (4.20)] and the HNC approximation [Eq. (4.21)].

To obtain $\mathbf{v}_s^{(1)}(\mathbf{r})$ and $\mathbf{v}_{\rm id}^{(1)}(\mathbf{r})$ numerically, I impose boundary conditions at the edges of the numerical calculation ranges. On the edges of the z-axis, I impose the boundary condition that the z-components of $\mathbf{v}_s^{(1)}(\mathbf{r})$ and $\mathbf{v}_{\rm id}^{(1)}(\mathbf{r})$ equal zero. On the edge of the r-axis, I impose the boundary condition that the r-components of $\mathbf{v}_s^{(1)}(\mathbf{r})$ and $\mathbf{v}_{\rm id}^{(1)}(\mathbf{r})$ equal zero. I have confirmed that the calculated results remain almost unchanged when I impose another condition that the z-components of $\mathbf{v}_s^{(1)}(\mathbf{r})$ and $\mathbf{v}_{\rm id}^{(1)}(\mathbf{r})$ equal zero at the edge of r-axis. In addition, to solve Eq. (6.6), I impose the boundary condition that $\boldsymbol{\omega}(\mathbf{r})$ equals zero at the edges of the numerical calculation ranges.

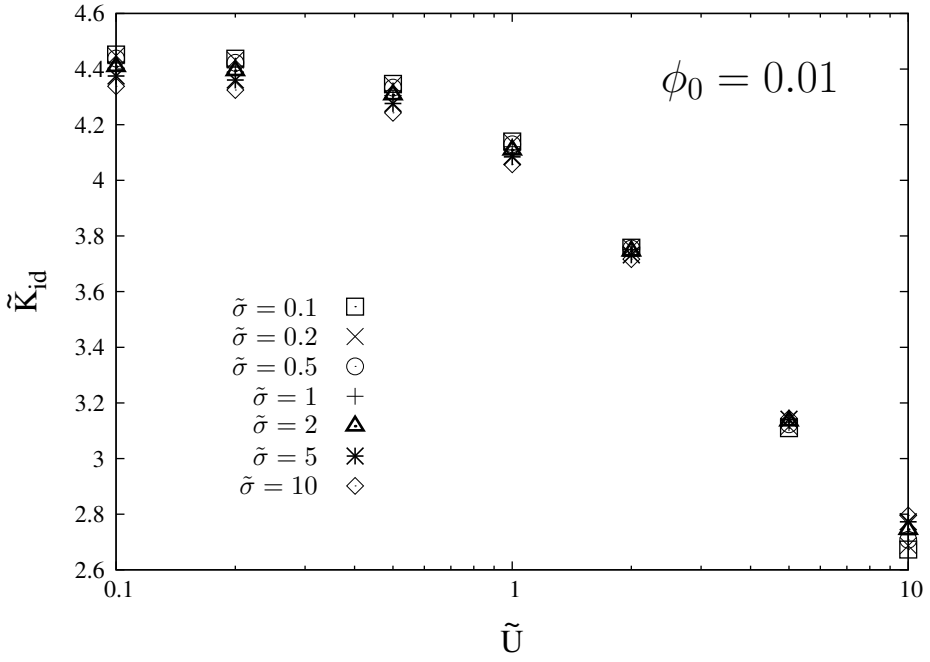

Figure 6.3: Identical to Fig. 6.2 but for noninteracting colloidal particles.

6.2 Results

6.2.1 Velocity dependence of friction coefficient

To examine the $\tilde{U}$-dependence of $\mathbf{F}$ and $\mathbf{F}_{\rm id}$, I define the reduced friction coefficients $\tilde{K}$ and $\tilde{K}_{\rm id}$ by

$$\tilde{K} \equiv \frac{\beta D}{\phi_0}\frac{|\mathbf{F}|}{|\mathbf{U}|} \quad \text{and} \quad \tilde{K}_{\rm id} \equiv \frac{\beta D}{\phi_0}\frac{|\mathbf{F}_{\rm id}|}{|\mathbf{U}|}. \tag{6.10}$$

Note that $\tilde{K}$ and $\tilde{K}_{\rm id}$ are defined not only in the linear region, where the force is proportional to $\tilde{U}$, but also in the nonlinear region for large $\tilde{U}$. I plot the calculated $\tilde{K}$ and $\tilde{K}_{\rm id}$ for $\phi_0 = 0.01$ (Figs. 6.2 and 6.3). In Figs. 6.2 and 6.3, $\tilde{K}$ and $\tilde{K}_{\rm id}$ decrease with increasing $\tilde{U}$ similarly to Figs. 4.4 and 4.5. In contrast to the results in Chap. 4, $\tilde{K}_{\rm id}$ depends on the reduced probe-particle size $\tilde{\sigma}$ (Fig. 6.3) because the reduced flux velocity $\tilde{U}$ is defined by the diameter of a colloidal particle $2b$ [Eq. (6.9)].

The comparison between Figs. 6.2 and 6.3 shows that the values of $\tilde{K}$ are smaller than or equal to those of $K_{\rm id}$. For small $\tilde{U}$, $\tilde{K}$ is slightly smaller than $\tilde{K}_{\rm id}$. The absolute value of the difference between $\tilde{K}$ and $\tilde{K}_{\rm id}$ decreases with increasing $\tilde{U}$. $|\tilde{K} - \tilde{K}_{\rm id}|$ increases with $\tilde{\sigma}$. Note that the difference between K and $K_{\rm id}$ is caused by the effect of the hard-sphere interactions between the colloidal particles.

Next, I plot the $\tilde{U}$-dependence of $\tilde{K}$ and $\tilde{K}_{\rm id}$ for $\phi_0 = 0.05$ (Figs. 6.4 and 6.5). The comparison between Figs. 6.4 and 6.5 shows that the values of $\tilde{K}$ are smaller than or equal to those of $K_{\rm id}$, similarly to the results for $\phi_0 = 0.01$. For small values of $\tilde{U}$, the absolute values of the difference between $\tilde{K}$ and $\tilde{K}_{\rm id}$ are larger than those

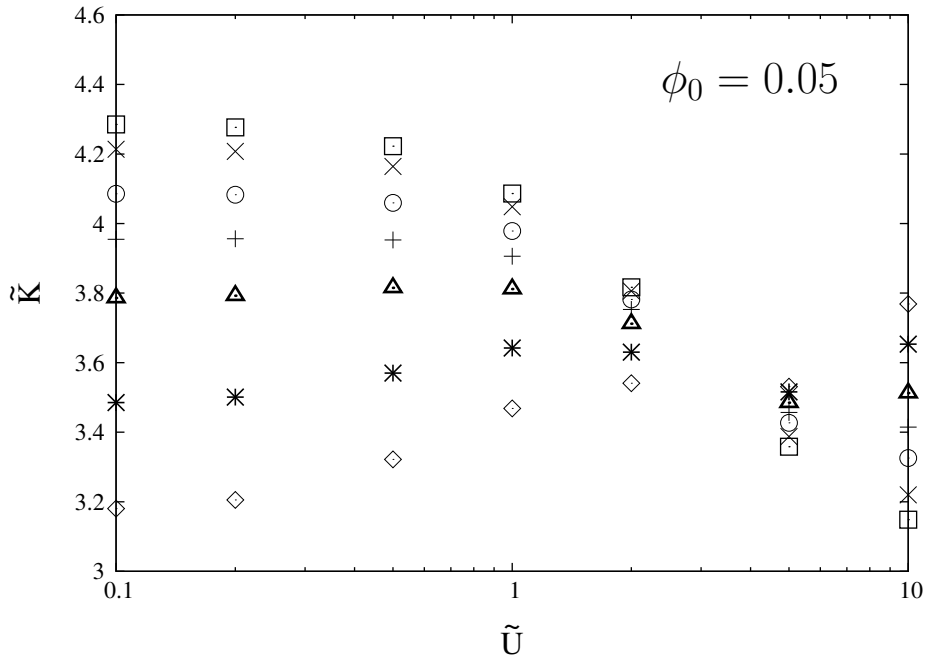

Figure 6.4: Identical to Fig. 6.2 but for volume fraction $\phi_0 = 0.05$.

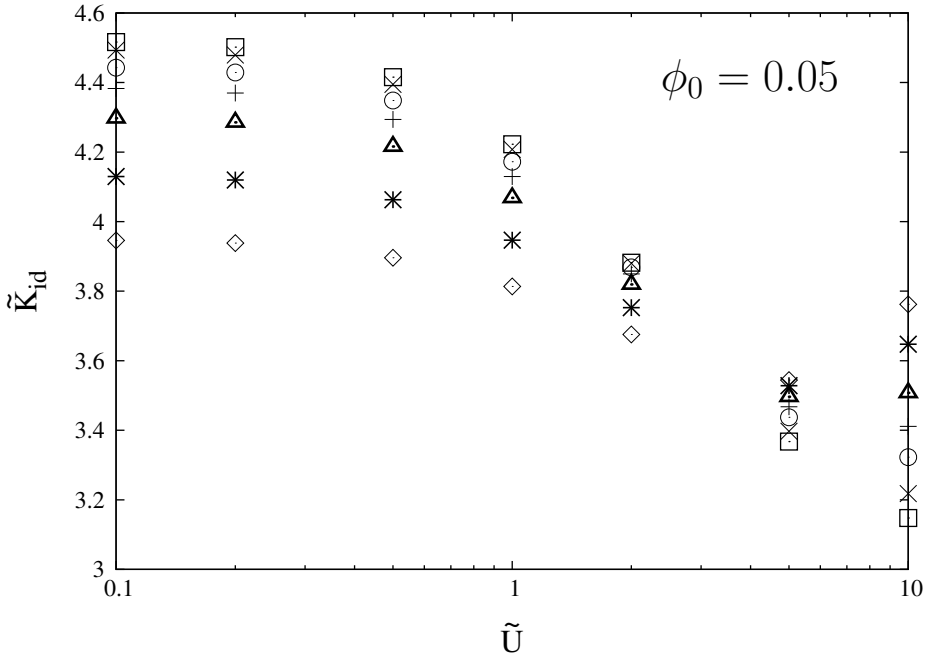

Figure 6.5: Identical to Fig. 6.4 but for noninteracting colloidal particles.

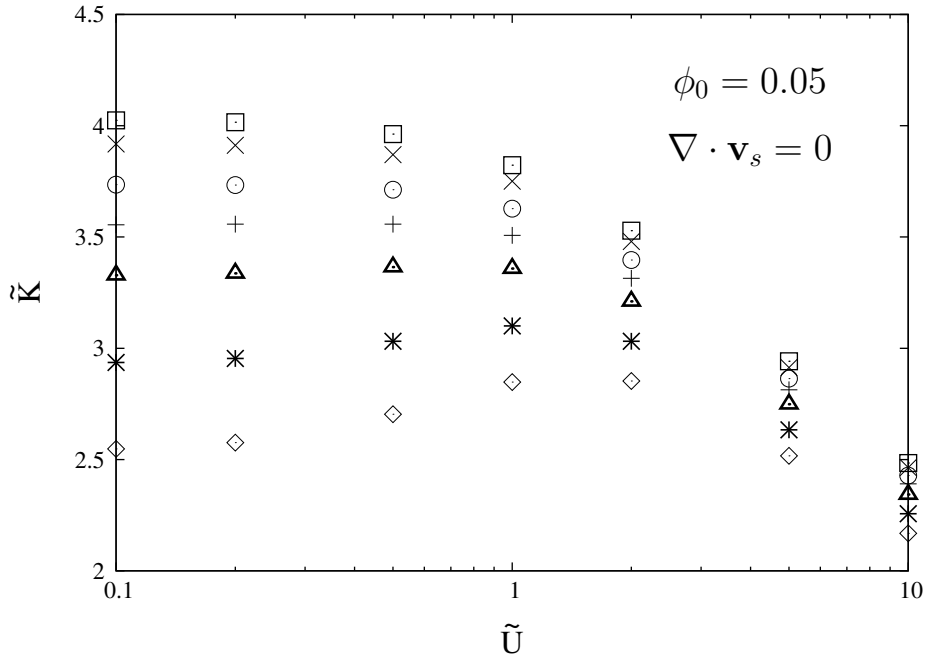

Figure 6.6: $\tilde{U}$-dependence of calculated friction coefficient for approximate incompressibility condition given by Eq. 5.18. These results are obtained for $\phi_0 = 0.05$. Each symbol represents the same value of $\tilde{\sigma}$ as that in Fig. 6.2. The definitions of $\tilde{K}$, $\tilde{K}_{\rm id}$, $\tilde{U}$, and $\tilde{\sigma}$ are the same as those in Fig. 6.2.

in Figs. 6.2 and 6.3. This means that the effect of the interactions between the colloidal particles is enhanced due to the increment in ϕ_0. In addition, Figs. 6.4 and 6.5 show stronger dependence on $\tilde{\sigma}$ than Figs. 6.2 and 6.3.

In Figs. 6.4 and 6.5, the values of $\tilde{K}$ and $\tilde{K}_{\rm id}$ at $\tilde{U} = 10$ are significantly larger than those in Figs. 6.2 and 6.3; particularly, $\tilde{K}$ and $\tilde{K}_{\rm id}$ for $\tilde{\sigma} = 5$ and 10 increase for the $5 < \tilde{U} < 10$ range. The large values at $\tilde{U} = 10$ are caused by the strong flow of the solvent into the probe particle. Since there are few colloidal particles in the vicinity of the center of the probe particle, the solvent flows into the probe particle, which leads to the strong flow. This strong flow is an artificial factor originating from the assumption that the solvent does not interact with the probe particle. To examine the effects of the interactions in the absence of this artificial factor, I calculate $\tilde{K}$ and $\tilde{K}_{\rm id}$ for the approximate incompressibility condition given by Eq. (5.18).

6.2.2 Results for approximate incompressibility condition

For the case of the approximate incompressibility condition [Eq. (5.18)], I plot the $\tilde{U}$-dependence of $\tilde{K}$ and $\tilde{K}_{\rm id}$ for $\phi_0 = 0.05$ (Figs. 6.6 and 6.7). In contrast to Figs. 6.4 and 6.5, the values of $\tilde{K}$ and $\tilde{K}_{\rm id}$ in Figs. 6.6 and 6.7 decrease for the $5 < \tilde{U} < 10$ range. This means that the results for the approximate incompressibility condition are not under the effect of the artificial factor, or the strong flow into the probe particle. In fact, the solvent velocity field obtained from Eq. (5.18) does not

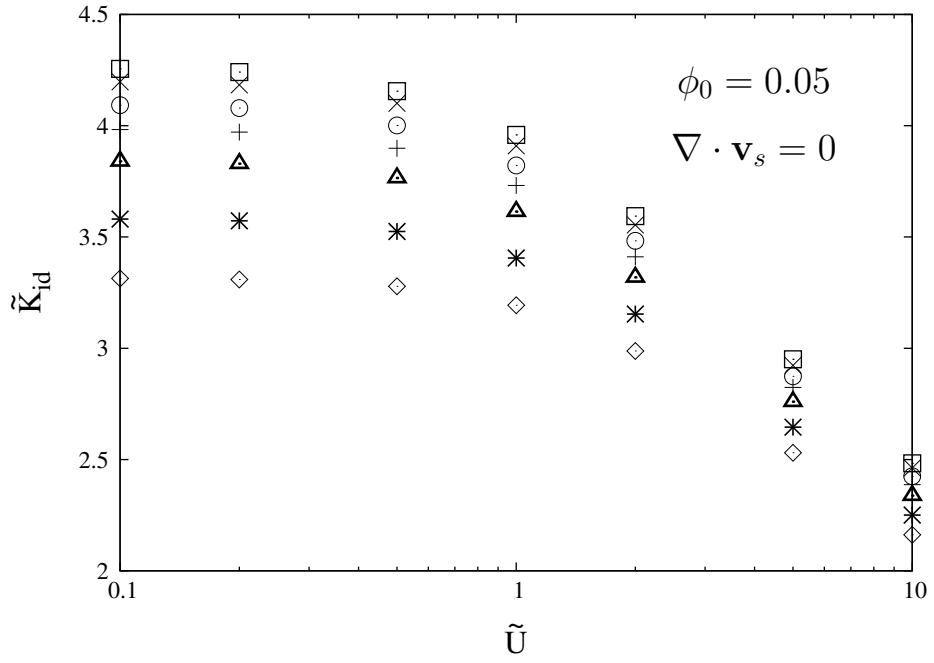

Figure 6.7: Identical to Fig. 6.6 but for noninteracting colloidal particles.

include the strong flow into the probe particle, which is represented in Sect. 6.2.4.

The comparison between Figs. 6.6 and 6.7 shows that $\tilde{K}$ is smaller than or equal to $\tilde{K}_{\rm id}$ as in the case of the incompressibility condition given by Eq. (5.1) (see Figs. 6.4 and 6.5). Note that the difference between $\tilde{K}$ and $\tilde{K}_{\rm id}$ is caused by the effect of the interactions between the colloidal particles. In Figs. 6.6 and 6.7, the $\tilde{U}$-dependence of $\tilde{K} - \tilde{K}_{\rm id}$ is qualitatively the same as that in Figs. 6.4 and 6.5 Thus, by using the approximate incompressibility condition [Eq. (5.18)], the effect of the interactions is examined in the absence of the artificial factor. In the following sections, to see the appearance of the volume fraction field and the solvent velocity field, I plot the results for the approximate incompressibility condition.

6.2.3 Density fields around probe particle

For the case of the approximate incompressibility condition, I plot the calculated $\phi^{(1)}(\mathbf{r})$ for $\tilde{U} = 0.1$ [Fig. 6.8(a)] and 10 [Fig. 6.8(b)]. Note that $\phi^{(1)}(\mathbf{r})$ is in agreement with $\phi^{(1)}_{\rm id}(\mathbf{r})$ because it is not under the effects of the interactions between the colloidal particles. In these figures, a darker area represents a larger volume-fraction area. The center of the probe particle is placed on the center of each figure and colloidal particles cannot enter the white area because of the soft-core potential given by Eq. (6.1). For $\tilde{U} = 0.1$ [Fig. 6.8(a)], under the influence of the flux, the $\phi^{(1)}(\mathbf{r})$ value is slightly larger on the upstream side of the probe particle (the left side of the white area) than that on the downstream side. In contrast, $\phi^{(1)}(\mathbf{r})$ for $\tilde{U} = 10$ is obviously larger on the upstream side than on the downstream side due to the rapid flux.

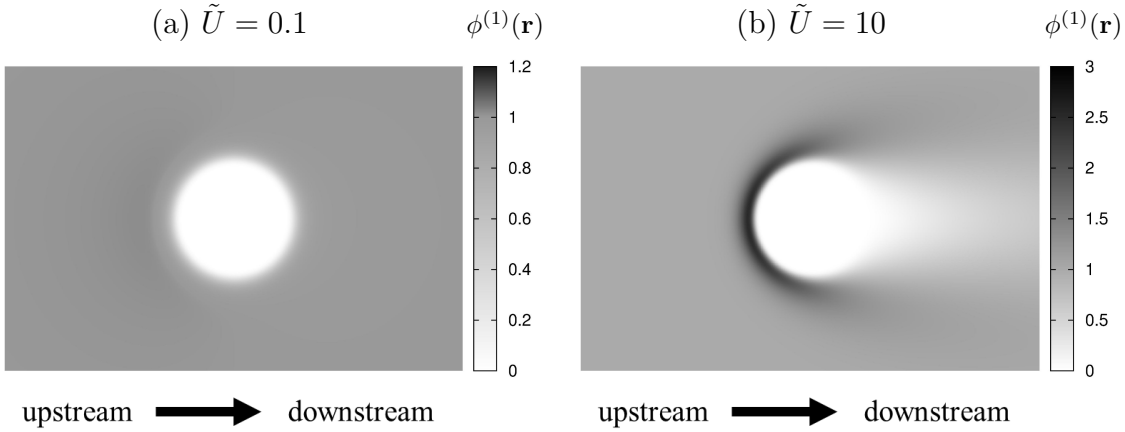

Figure 6.8: Calculated volume-fraction fields in first order of ϕ_0 for approximate incompressibility condition in symmetric plane of probe particle. (a) $\phi^{(1)}(\mathbf{r})$ obtained from Eq. (5.33) for $\tilde{U} = 0.1$. (b) $\phi^{(1)}(\mathbf{r})$ for $\tilde{U} = 10$. A darker area corresponds to a larger volume-fraction area. The center of the probe particle is placed on the center of each figure. The reduced probe-particle size is given by $\tilde{\sigma} = 1$, where $\tilde{\sigma}$ is defined by Eq. (6.8). The direction of $\mathbf{U}$ is rightward.

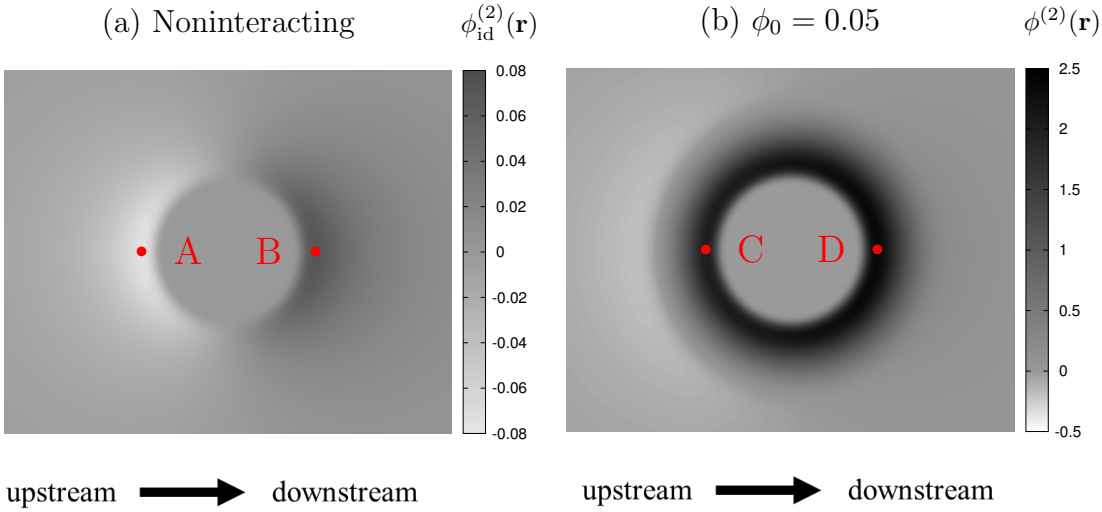

Figure 6.9: Calculated volume-fraction fields in second order of ϕ_0 for $\tilde{U} = 0.1$ and approximate incompressibility condition in symmetric plane of probe particle. (a) $\phi^{(2)}_{\mathrm{id}}(\mathbf{r})$ obtained from Eq. (5.50) for noninteracting colloidal particles. (b) $\phi^{(2)}(\mathbf{r})$ obtained from Eq. (5.41) for interacting colloidal particles and $\phi_0 = 0.05$. A darker area corresponds to a larger volume-fraction area. The center of the probe particle is placed on the center of each figure. The reduced probe-particle size is given by $\tilde{\sigma} = 1$. The direction of $\mathbf{U}$ is rightward. At points A and B, the values of $\phi^{(2)}_{\mathrm{id}}(\mathbf{r})$ are -0.079 and 0.073, respectively, where the cylindrical coordinates of A and B are given by $(r, z) = (\Delta r, -1.16(\beta\epsilon)^{-12}\sigma)$ and $(\Delta r, 1.17(\beta\epsilon)^{-12}\sigma)$, respectively. At points C and D, $\phi^{(2)}_{\mathrm{id}}(\mathbf{r})$ is 2.00 and 2.38, respectively, where the coordinates of C and D are $(\Delta r, -1.14(\beta\epsilon)^{-12}\sigma)$ and $(\Delta r, 1.16(\beta\epsilon)^{-12}\sigma)$, respectively. Here, ϵ and σ are defined by Eq. (6.1) and the origin is placed on the center of the probe particle. These points are placed on the data points neighboring the position $r = 0$, where the values of $\phi^{(2)}_{\mathrm{id}}(\mathbf{r})$ and $\phi^{(2)}(\mathbf{r})$ are top or bottom.

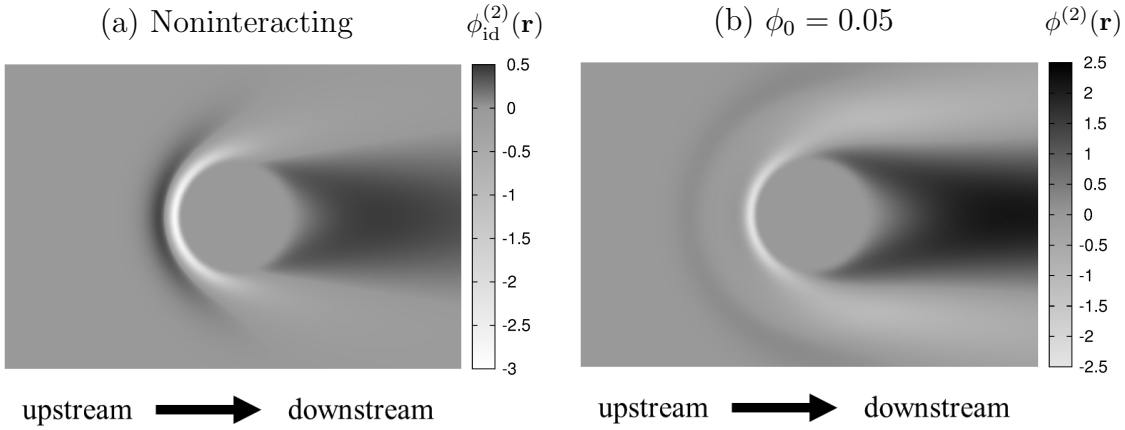

Figure 6.10: Identical to Fig. 6.9 but for $\tilde{U} = 10$. (a) $\phi_{\rm id}^{(2)}(\mathbf{r})$ obtained from Eq. (5.50) for noninteracting colloidal particles. (b) $\phi^{(2)}(\mathbf{r})$ obtained from Eq. (5.41) for interacting colloidal particles and $\phi_0 = 0.05$.

Next, I plot the calculated $\phi_{\rm id}^{(2)}(\mathbf{r})$ and $\phi^{(2)}(\mathbf{r})$ for $\tilde{U} = 0.1$ (Fig. 6.9). In Fig. 6.9(a), $\phi_{\rm id}^{(2)}(\mathbf{r})$ for the noninteracting colloidal particles is smaller on the upstream side than that on the downstream side. This is caused by the solvent velocity field $\mathbf{v}_s^{(1)}(\mathbf{r})$ in the first order of ϕ_0 (see Sect. 6.2.4). In contrast, Fig. 6.9(b) shows that the value of $\phi^{(2)}(\mathbf{r})$ is larger in the vicinity of the probe particle than that of $\phi_{\rm id}^{(2)}(\mathbf{r})$. Note that the difference between Figs. 6.9(a) and (b) is caused by the effect of the interactions between the colloidal particles.

I also plot $\phi_{\rm id}^{(2)}(\mathbf{r})$ and $\phi^{(2)}(\mathbf{r})$ for $\tilde{U} = 10$ (Fig. 6.10). These figures show that the effect of the interactions is modified by the rapid flux. In Fig. 6.10, $\phi_{\rm id}^{(2)}(\mathbf{r})$ and $\phi^{(2)}(\mathbf{r})$ are smaller on the upstream side than on the downstream side. The difference between $\phi_{\rm id}^{(2)}(\mathbf{r})$ and $\phi^{(2)}(\mathbf{r})$ is smaller than that in Fig. 6.9.

6.2.4 Velocity fields of solvent

In the case of the approximate incompressibility condition [Eq. (5.18)], I plot the calculated $\mathbf{v}_s^{(1)}(\mathbf{r})$ for $\tilde{U} = 0.1$ (Fig. 6.11) and $\tilde{U} = 10$ (Fig. 6.12). In these figures, the magnitude and direction of $\mathbf{v}_s^{(1)}(\mathbf{r})$ are represented by colored arrows, where red and blue arrows correspond to large and small values of $|\mathbf{v}_s^{(1)}(\mathbf{r})|$, respectively. The dashed circle satisfies $|\mathbf{r}| = (\beta\epsilon)^{-12}\sigma$ and represents the probe-particle size roughly. These figures show that $\mathbf{v}_s^{(1)}(\mathbf{r})$ is directed to the opposite direction of $\mathbf{U}$ in the vicinity of the probe particle.

In Figs. 6.11 and 6.12, $\mathbf{v}_s^{(1)}(\mathbf{r})$ forms the flux opposite to the direction of $\mathbf{U}$ in the vicinity of the probe particle. On the upstream side (the left side of the dashed circle), $\mathbf{v}_s^{(1)}(\mathbf{r})$ gets away from the probe particle along the r-axis of the cylindrical coordinates. In contrast to the upstream side, $\mathbf{v}_s^{(1)}(\mathbf{r})$ on the downstream side gets close to the probe particle along the r-axis. Therefore, the total solvent velocity field $\mathbf{v}_s(\mathbf{r}) \approx \mathbf{U} + \phi_0\mathbf{v}_s^{(1)}(\mathbf{r})$ includes the flow around the probe particle. The comparison between Figs. 6.11 and 6.12 shows that $\mathbf{v}_s^{(1)}(\mathbf{r})$ for $\tilde{U} = 0.1$ is

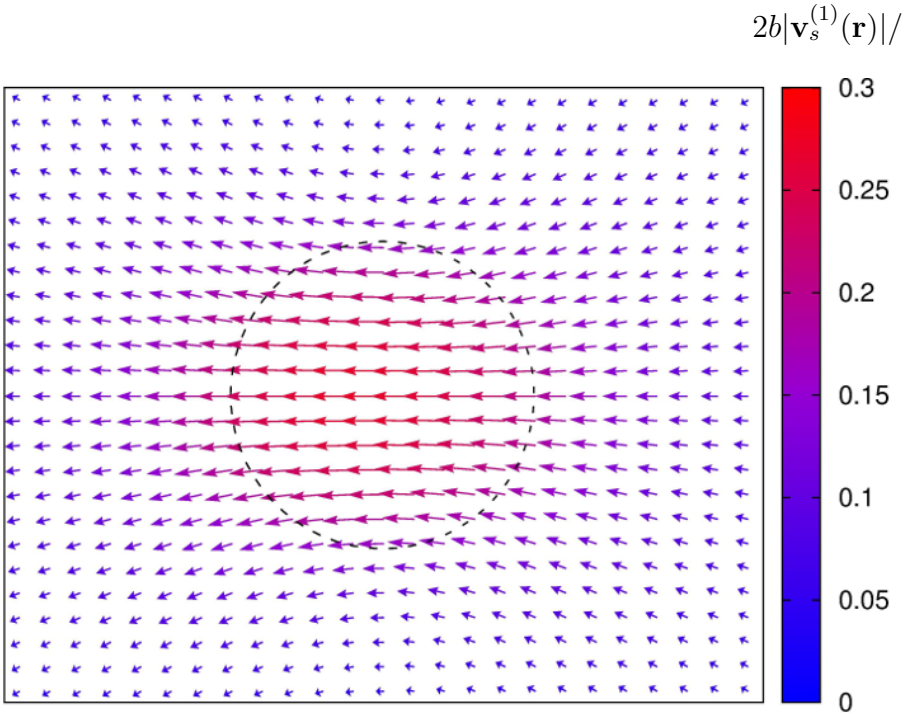

Figure 6.11: Calculated solvent velocity field in first order of ϕ_0 for approximate incompressibility condition and $\tilde{U} = 0.1$ in symmetric plane of probe particle. The length and direction of the arrows represent the magnitude and direction of $\mathbf{v}_s^{(1)}(\mathbf{r})$, respectively, where longer arrows correspond to higher velocity. Additionally, the color of the arrows represents absolute values of $\mathbf{v}_s^{(1)}(\mathbf{r})$, where red and blue arrows correspond to large and small values of $|\mathbf{v}_s^{(1)}(\mathbf{r})|$, respectively. Here, $|\mathbf{v}_s^{(1)}(\mathbf{r})|$ is nondimensionalized in the same way as Eq. (6.9). The reduced probe-particle size is given by $\tilde{\sigma} = 1$. The dashed circle satisfies $|\mathbf{r}| = (\beta\epsilon)^{-12}\sigma$ and represents the probe-particle size roughly. The direction of $\mathbf{U}$ is rightward.

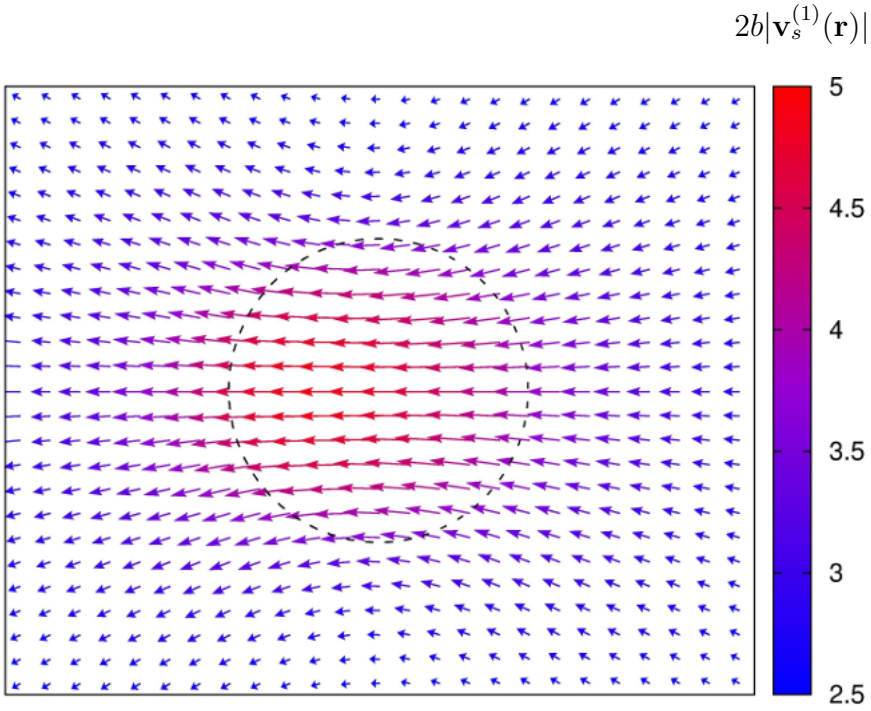

Figure 6.12: Identical to Fig. 6.11 but for $\tilde{U} = 10$.

qualitatively similar to that for $\tilde{U} = 10$. However, the absolute value $|\mathbf{v}_s^{(1)}(\mathbf{r})|$ for $\tilde{U} = 10$ are obviously larger than that for $\tilde{U} = 0.1$.

6.3 Discussion

Figure 6.9 shows that the colloidal particles gather around the probe particle because of the interactions between the colloidal particles in the same manner as the results in Chap. 4. In Fig. 6.9, $\phi^{(2)}(\mathbf{r}_C) - \phi^{(2)}(\mathbf{r}_D)$ is smaller than $\phi_{\rm id}^{(2)}(\mathbf{r}_A) - \phi_{\rm id}^{(2)}(\mathbf{r}_B)$, where $\mathbf{r}_A$, $\mathbf{r}_B$, $\mathbf{r}_C$, and $\mathbf{r}_D$ are the measurement points plotted in the figure. In contrast to $\phi^{(2)}(\mathbf{r})$ and $\phi_{\rm id}^{(2)}(\mathbf{r})$, $\phi^{(1)}(\mathbf{r})$ is larger on the upstream side than on the downstream side (see Fig. 6.8). Therefore, the total volume-fraction field $\phi(\mathbf{r}) \approx \phi_0\phi^{(1)}(\mathbf{r}) + \phi_0^2\phi^{(2)}(\mathbf{r})$ is more isotropic than that for the noninteracting colloidal particles because $\phi^{(1)}(\mathbf{r}) = \phi_{\rm id}^{(1)}(\mathbf{r})$. Since the forces $\mathbf{F}$ and $\mathbf{F}_{\rm id}$ are generated by the anisotropy of the volume-fraction field [see Eqs. (6.2) and (6.3)], the reduced friction coefficient $\tilde{K}$ is smaller than $\tilde{K}_{\rm id}$ for $\tilde{U} = 0.1$. Thus, the force exerted by colloidal particles decreases due to the effect of the hard-sphere interactions between the colloidal particles in the same manner as the results in Chap. 4.

In Figs. 6.9(a) and 6.10(a), $\phi_{\rm id}^{(2)}(\mathbf{r}) < 0$ on the upstream side and $\phi_{\rm id}^{(2)}(\mathbf{r}) > 0$ on the downstream side. These results are explained by the solvent velocity field $\mathbf{v}_s^{(1)}(\mathbf{r})$ in the first order of ϕ_0 [Figs. 6.11 and 6.12]. The total velocity field $\mathbf{v}_s(\mathbf{r}) \approx \mathbf{U} + \phi_0\mathbf{v}_s^{(1)}(\mathbf{r})$ includes the flow around the probe particle. The colloidal particles are transported from the upstream side to the downstream side by the flow around the probe particle, which leads to $\phi_{\rm id}^{(2)}(\mathbf{r}) < 0$ on the upstream side and $\phi_{\rm id}^{(2)}(\mathbf{r}) > 0$

on the downstream side. For $\tilde{U} = 0.1$, however, the effect of $\mathbf{v}_s^{(1)}(\mathbf{r})$ is weaker than the effect of the interactions between the colloidal particles, so that $\phi^{(2)}(\mathbf{r}) > 0$ is satisfied even on the upstream side [see Fig. 6.9(b)]. In contrast, the effect of $\mathbf{v}_s^{(1)}(\mathbf{r})$ is enhanced by large $\tilde{U}$ so that the effect of the interactions is almost not reflected in Fig. 6.10(b).

From Figs. 6.11 and 6.12, the total solvent velocity field $\mathbf{v}_s(\mathbf{r}) \approx \mathbf{U} + \phi_0 \mathbf{v}_s^{(1)}(\mathbf{r})$ includes the flow around the probe particle. Since the solvent velocity is assumed to be disturbed only by the colloidal particles, $\mathbf{v}_s^{(1)}(\mathbf{r})$ is determined from $\phi^{(1)}(\mathbf{r})$. Under the influence of the uniform flux, $\phi^{(1)}(\mathbf{r})$ is simply larger on the upstream side of the probe particle than on the down stream side (see Fig. 6.8). To avoid the overlap of the solvent and a large number of the colloidal particles on the upstream side, $\mathbf{v}_s^{(1)}(\mathbf{r})$ forms the flux opposite to the direction of $\mathbf{U}$ in the vicinity of the probe particle (see Figs. 6.11 and 6.12). The solvent flows around the colloidal particles on the upstream side, so that $\mathbf{v}_s^{(1)}(\mathbf{r})$ on the upstream side gets away from the probe particle and that on the downstream side gets close to the probe particle.

In the present study, I have neglected the effect of the probe particle on the solvent velocity. However, for the accurate examination of the effects of the interactions between the colloidal particles, it is necessary to consider the effect of the probe particle on the solvent velocity. As described in Sect. 5.4, I consider that there are two methods of considering this effect: the boundary condition which gives values of $\mathbf{v}_s^{(1)}(\mathbf{r})$ and $p^{(1)}(\mathbf{r})$ on the surface of the probe particle and the calculation of the friction between the solvent and the probe particle. To employ these methods, it is necessary to give the interaction between the solvent and the probe particle.

In a case where the interaction between the solvent and the probe particle is given by a repulsive potential such as a hard-sphere potential, I speculate that the interaction enhances the flow around the probe particle. In this case, the solvent velocity field in the zeroth order of ϕ_0 is given by the Stokes flow around the probe particle, which has an effect on the volume-fraction field. Here, the probe particle is subject to the force exerted by the solvent, which is obtained from the solvent velocity field. The force exerted by the solvent is modified by the interactions between the colloidal particles, which should be observed only in the second- and higher-order terms of ϕ_0 because these interactions have an effect on the solvent velocity field in the second and higher order of ϕ_0.

In the present study, I have considered the soft-core probe particle, in contrast to the hard-sphere probe particle considered in Chap. 4. The soft-core probe particle simplifies the numerical calculations. In the case of the soft-core probe particle, the volume-fraction field of the colloidal particles is a spatially continuous function even in the vicinity of the probe particle. Since the solvent velocity field is assumed to be under only the effect of the colloidal particles, it is also a spatially continuous function in the whole system. If the probe particle is a hard-sphere, the volume fraction field is discontinuous across the surface of the probe particle so that the solvent velocity field is also a discontinuous function, which causes the force dependent on the gradient of the solvent velocity. By employing the

TDDFT, I have confirmed that the results in Chap. 4 are qualitatively unchanged when the soft-core probe particle is adopted. Thus, I speculate that the effects of the interactions obtained in this chapter are qualitatively the same as those on the hard-sphere probe particle.

6.4 Summary

Having solved the equations of the two-fluid model numerically, I have obtained the force exerted by the colloidal particles on the probe particle and the nonuniform solvent velocity field disturbed only by the colloidal particles. By combining the DFT with the two-fluid model, I have examined the modification of the effect of the interactions between the colloidal particles by the nonuniform solvent velocity field. As a result, for small values of the volume fraction, the force exerted by the colloidal particles decreases due to the effect of the hard-sphere interactions between the colloidal particles. This effect of the interactions is similar to that obtained by the numerical calculations using the TDDFT (see Chap. 4). This indicates that for the small volume fractions, the effect of the interactions on the force is almost unmodified by the nonuniform solvent velocity filed.

Chapter 7

Conclusion

In this thesis, I have examined effects of interactions between colloidal particles on the force exerted by the colloidal particles on a probe particle in a system of active microrheology. I have considered a spatially fixed probe particle and a flowing colloidal suspension comprised of hard-sphere colloidal particles and a solvent. To calculate the force exerted by the the colloidal particles on the probe particle, I have employed two theoretical methods: the time-dependent density functional theory (TDDFT) and the combination of the density functional theory (DFT) with the two-fluid model. By obtaining the force numerically via the two methods, I have examined the effects of the interactions between the colloidal particles on the force.

First, by calculating the force via numerical calculations using the TDDFT, I have examined the effects of the hard-sphere interactions between the colloidal particles. As a result, for small values of the flux velocity, the force decreases due to the effect of the interactions. In contrast, for large values of the flux velocity and the volume fraction, the force increases due to the effect of the interactions. These effects are caused by the increment in the number of the colloidal particles in the vicinity of the probe particle . In the numerical calculations, I have assumed that the probe particle is a hard sphere and the solvent velocity is constant in the whole system without the disturbance due to the probe and colloidal particles.

Next, by solving the equations of the two-fluid model numerically, I have obtained the nonuniform solvent velocity field disturbed by the colloidal particles. Having calculated the force exerted by the colloidal particles on the probe particle, I have examined the modification of the effect of the interactions on the force by the nonuniform solvent velocity field. To examine the modification of the effect of the interactions for small volume fractions, I have employed the approximation accurate to the second order of the homogeneous volume fraction far from the probe particle. As a result, for small volume fraction, the force decreases due to the effect of the hard-sphere interactions between the colloidal particles. The obtained solvent velocity fields include the flow around the probe particle. In the numerical calculations, for simplicity, I have assumed that the probe particle is a soft-core particle and the solvent velocity is disturbed only by the colloidal particles.

By comparing the results obtained from the two theoretical methods, I have examined the modification of the effect of the interactions by the nonuniform

solvent velocity field. The solvent velocity field has been assumed to be uniform in the whole system in the study using the TDDFT, while it has been assumed to be disturbed by the colloidal particles in the study using the DFT and the two-fluid model. For small volume fractions, both of two types of the results show that the force decreases due to the hard-sphere interactions between the colloidal particles. This indicates that for small volume fractions, the effect of the interactions on the force is almost unmodified by the nonuniform solvent velocity field disturbed by the colloidal particles.

Acknowledgments

I am grateful to Professor Akira Yoshimori (Niigata University) for guiding my study with detailed advice and comments. I am also indebted to Professor Jun Matsui for his comments and assistance in numerical calculations. In addition, I would like to thank Professor Hiizu Nakanishi and Professor Jun-ichi Fukuda for their detailed comments on my study.

I am indebted to Professor Daisuke Mizuno and Professor Ryo Akiyama for their valuable advice and comments on my study. I also wish to acknowledge valuable discussions with Professor Tsuyoshi Yamaguchi (Nagoya University), Professor Takashi Taniguchi (Kyoto University), and Professor Ryoichi Yamamoto (Kyoto University).

Finally, I thank the members of the condensed matter theory groups in Kyushu University and Niigata University. In addition, I am grateful to my parents for their invaluable support of my life.

Appendix A

Force exerted by colloidal particles on probe particle through hard-sphere interaction

Here, I derive the equation of the force exerted by colloidal particles on a probe particle through the hard-sphere interaction [Eqs. (2.5), (4.16), and (4.17)]. I consider a probe particle fixed at the origin and a colloidal suspension flowing at a constant velocity $\mathbf{U}$ (Fig. 4.1). In this system, interaction between the probe and colloidal particles is given by the hard-sphere potential [Eqs. (2.1) and (4.11)]. This system does not correspond to the system studied by Squires and Brady (Fig. 2.1) [7], where a probe particle is pulled at a constant velocity through a stationary colloidal suspension. However, when the density field of the colloidal particles is given, the force is determined from the same equation in both systems (Figs. 2.1 and 4.1).

A.1 Derivation of equation of force

The probe particle is subject to the force $\mathbf{F}$ exerted by the colloidal particles. Since the probe particle interacts with the colloidal particles through the hard-sphere potential [Eqs. (2.1) and (4.11)], the force $\mathbf{F}$ is generated from the collision between the probe and colloidal particles. Therefore, the force $\mathbf{F}$ is exerted by the colloidal particles located on the spherical surface satisfying $|\mathbf{r}| = a + b$, where a and b are the radii of the probe and colloidal particles, respectively, and the origin of the vector $\mathbf{r}$ is located at the center of the probe particle. Here, I consider the force $\mathrm{d}\mathbf{F}(\mathbf{r}')$ exerted by the colloidal particles located on a micro-area element $\mathrm{d}S$ at the position $\mathbf{r}'$ satisfying $|\mathbf{r}'| = a + b$ (see Fig. A.1).

The force $\mathrm{d}\mathbf{F}(\mathbf{r}')$ is given by

$$\mathrm{d}\mathbf{F}(\mathbf{r}') = \mathbf{F}_1 \mathrm{d}N(\mathbf{r}'), \tag{A.1}$$

where $\mathbf{F}_1$ is the force generated from the collision of one colloidal particle with the probe particle and $\mathrm{d}N(\mathbf{r}')$ is the number of the colliding colloidal particles through the micro area $\mathrm{d}S$ per unit time. Since all particles are hard spheres, the collision

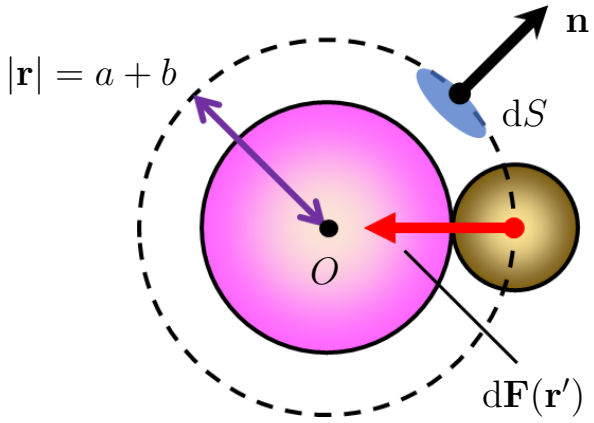

Figure A.1: Force $\mathrm{d}\mathbf{F}(\mathbf{r}')$ exerted by colloidal particles located on micro area $\mathrm{d}S$ at position $\mathbf{r}'$. $\mathrm{d}S$ is a micro-area element of the spherical surface satisfying $|\mathbf{r}| = a + b$, where a and b are the radii of the probe and colloidal particles, respectively, and the origin of the vector $\mathbf{r}$ is located at the center of the probe particle. $\mathbf{n}$ is the normal vector of the micro area $\mathrm{d}S$.

between the probe and colloidal particles is perfectly elastic. From the change of the momentum of the colliding colloidal particle, $\mathbf{F}_1$ is given by

$$\mathbf{F}_1 = -2mv_n\mathbf{n}, \tag{A.2}$$

where m is mass of a colloidal particle, $\mathbf{n}$ is the normal vector of the micro area $\mathrm{d}S$, and v_n is the component of the velocity of the colliding colloidal particles parallel to $\mathbf{n}$. Note that the direction of v_n is opposite to $\mathbf{n}$ so that the colliding colloidal particles satisfy $v_n > 0$ and the particles satisfying $v_n < 0$ get away from the probe particle. When the density field of the colloidal particles is given by $\rho(\mathbf{r})$, $\mathrm{d}N(\mathbf{r}')$ is given by

$$\mathrm{d}N(\mathbf{r}') = v_n\rho(\mathbf{r}')\mathrm{d}S, \tag{A.3}$$

where it is assumed that all particles at the position $\mathbf{r}'$ move at the same velocity. From Eqs. (A.1), (A.2), and (A.3), the force $\mathrm{d}\mathbf{F}(\mathbf{r}')$ is given by

$$\mathrm{d}\mathbf{F}(\mathbf{r}') = -2mv_n^2\rho(\mathbf{r}')\mathbf{n}\mathrm{d}S. \tag{A.4}$$

To obtain the equation of the force $\mathbf{F}$, I determine v_n from the Maxwell–Boltzmann distribution. Here, I assume that the velocity distribution of the colloidal particles is given by the Maxwell–Boltzmann distribution on the spherical surface satisfying $|\mathbf{r}| = a + b$. Under this assumption, the mean square of v_n is given by

$$\langle v_n^2 \rangle = \frac{1}{Z_1}\int_0^\infty v_n^2 \exp\left[-\frac{m}{2k_\mathrm{B}T}v_n^2\right]\mathrm{d}v_n, \tag{A.5}$$

where Z_1 is the partition function of the one-dimensional Maxwell–Boltzmann distribution defined by

$$Z_1 \equiv \int_{-\infty}^{\infty} \exp\left[-\frac{m}{2k_{\rm B}T}v_n^2\right] {\rm d}v_n = \left(\frac{2\pi k_{\rm B}T}{m}\right)^{1/2}. \tag{A.6}$$

Note that the integration range in Eq. (A.5) is $0 \leq v_n \leq \infty$ because the colloidal particles satisfying $v_n < 0$ do not collide with the probe particle. From Eqs. (A.5) and (A.6), the mean square of v_n is given by

$$\begin{aligned}\langle v_n^2 \rangle &= \frac{1}{2Z_1}\int_{-\infty}^{\infty} v_n^2 \exp\left[-\frac{m}{2k_{\rm B}T}v_n^2\right] {\rm d}v_n \\ &= -k_{\rm B}T\frac{\partial}{\partial m}\ln Z_1 \\ &= \frac{k_{\rm B}T}{2m}.\end{aligned} \tag{A.7}$$

By use of Eqs. (A.4) and (A.7), the force $\mathbf{F}$ is obtained from the surface integral of ${\rm d}\mathbf{F}(\mathbf{r}')$,

$$\mathbf{F} = -k_{\rm B}T \oint_{|\mathbf{r}|'=a+b} \rho(\mathbf{r}')\mathbf{n}{\rm d}S, \tag{A.8}$$

which corresponds to Eqs. (2.5), (4.16), and (4.17).

A.2 Validity of Maxwell–Boltzmann distribution

To obtain the equation of the force $\mathbf{F}$ [Eq. (A.8)], I have assumed that the velocity distribution of the colloidal particles is given by the Maxwell–Boltzmann distribution. This assumption is valid for the velocity distribution at equilibrium states, while that at nonequilibrium steady states should be different from the Maxwell–Boltzmann distribution because of the flux velocity $\mathbf{U}$. Particularly, when the flux velocity $\mathbf{U}$ is large, the velocity distribution of the colloidal particles should be different from the Maxwell–Boltzmann distribution significantly. In this section, I estimate the validity of the assumption of the Maxwell–Boltzmann distribution. For the estimation, I compare the root-mean-square velocity given by the Maxwell–Boltzmann distribution with the flux velocity in the experimental study by Wilson *et al.* [4] (see Sect. 2.2).

Referring to the experimental study [4], I estimate the root-mean-square velocity of the colloidal particles given by the Maxwell–Boltzmann distribution. Here, I calculate the root-mean-square of one component of the velocity because the flux velocity has an influence only on the component of the velocity parallel to it. From

the Maxwell–Boltzmann distribution, the mean-square velocity is given by

$$\begin{aligned}\langle v_z^2 \rangle &= \frac{1}{Z_1} \int_{-\infty}^{\infty} v_z^2 \exp\left[-\frac{m}{2k_\mathrm{B}T} v_z^2 \right] \mathrm{d}v_z \\ &= -2k_\mathrm{B}T \frac{\partial}{\partial m} \ln Z_1 \\ &= \frac{k_\mathrm{B}T}{m}, \end{aligned} \tag{A.9}$$

where v_z is the component of the velocity parallel to the flux. To estimate the root-mean-square of v_z in the experimental study [4], I employ the radius of a colloidal particle $b \approx 900$ nm and the temperature $T \approx 300$ K (see Sect. 2.2). Additionally, employing the mass density of the PMMA colloidal particles $\rho_m = 1.18$ g/cm^3 at room temperature, I estimate the mass of a colloidal particle,

$$m = \frac{4}{3} \pi b^3 \rho_m \approx 3.60 \times 10^{-12} \text{ kg}. \tag{A.10}$$

From Eqs. (A.9) and (A.10), I obtain the root-mean-square of v_z given by the Maxwell–Boltzmann distribution,

$$\sqrt{\langle v_z^2 \rangle} = \left(\frac{k_\mathrm{B}T}{m} \right)^{1/2} \approx 3.39 \times 10^{-5} \text{ m/s}. \tag{A.11}$$

In the same way, I also estimate the absolute value of the flux velocity $|\mathbf{U}|$ in the experimental study [4]. In this experimental study, $|\mathbf{U}|$ is nondimensionalized by Eq. (2.34). From Eq. (2.34) and the Stokes–Einstein relation, $|\mathbf{U}|$ is given by

$$|\mathbf{U}| = \frac{k_\mathrm{B}T}{12\pi\eta_0 a^2} \mathrm{Pe}, \tag{A.12}$$

where η_0 is the viscosity of the solvent and Pe is the Péclet number defined by Eq. (2.34). Referring to the experimental study [4], I employ the solvent viscosity $\eta_0 = 2.56$ mPa $\cdot$ s and the radius of the probe particle $a \approx 1$ μm (see Sect. 2.2). Eventually, $|\mathbf{U}|$ is given by

$$|\mathbf{U}| \approx \mathrm{Pe} \times 4.29 \times 10^{-8} \text{ m/s}. \tag{A.13}$$

By using Eqs. (A.11) and (A.13), I estimate the validity of the assumption that the velocity distribution of the colloidal particles is given by the Maxwell–Boltzmann distribution. Since the calculation range of the flux velocity is $0.1 \leq \mathrm{Pe} \leq 100$ in the numerical calculation of Chap. 4, I estimate the validity for $\mathrm{Pe} = 0.1$ and 100. From Eq. (A.13), $|\mathbf{U}| \approx 4.29 \times 10^{-9}$ m/s for $\mathrm{Pe} = 0.1$, which is much smaller than the value of Eq. (A.11). This means that for $\mathrm{Pe} = 0.1$, the velocity distribution of the colloidal particles is considered to be close to the Maxwell–Boltzmann distribution. In contrast, $|\mathbf{U}| \approx 4.29 \times 10^{-6}$ m/s for $\mathrm{Pe} = 100$, which is about 13% of the value of Eq. (A.11). This means that for $\mathrm{Pe} = 100$, the root-mean-square of v_z under the flux may be different from that given by the Maxwell–Boltzmann distribution by about 13%.

Appendix B

Free energy derived from density functional theory

Here, I derive the equation of the free energy of many-particle systems from the density functional theory (DFT). The DFT gives the free energy defined as the functional of the density field of particles. In my study, the derived equation of the free-energy functional is applied to the equation of the time-dependent density functional theory (Sect. 4.2.2) and to the equations of motion of the two-fluid model (Sect. 5.2).

B.1 Density field at nonequilibrium states

In many-particle systems at nonequilibrium states, the density field $\rho(\mathbf{r})$ represents the number density of particles at a position $\mathbf{r}$. I assume that the density field $\rho(\mathbf{r})$ is independent of time t. At an equilibrium state, the density field corresponds to the equilibrium one $\rho_{\rm eq}(\mathbf{r})$, which is defined by

$$\rho_{\rm eq}(\mathbf{r}) = \left\langle \sum_{i=1}^{N} \delta(\mathbf{r} - \mathbf{r}_i) \right\rangle. \tag{B.1}$$

Here, N is the number of particles in the system, $\mathbf{r}_i$ is the position of the i-th particle, and $\langle \cdots \rangle$ represents the average in the grand canonical ensemble.

In the framework of the DFT, the density field $\rho(\mathbf{r})$ is treated as an extensive variable. By using the intensive variable $\psi(\mathbf{r})$ paired with $\rho(\mathbf{r})$, the thermodynamic potential $\hat{\Omega}[\psi(\mathbf{r})]$ is defined by

$$e^{-\beta\hat{\Omega}[\psi(\mathbf{r})]} = \sum_{N=1}^{\infty} \frac{e^{N\beta\mu}}{N!h^{3N}} \int \prod_{i=1}^{N} \mathrm{d}\mathbf{r}_i \mathrm{d}\mathbf{p}_i \exp\left[-\beta\left(H_N + \int \psi(\mathbf{r})\hat{\rho}(\mathbf{r})\mathrm{d}\mathbf{r}\right)\right], \tag{B.2}$$

$$\hat{\rho}(\mathbf{r}) = \sum_{i=1}^{N} \delta(\mathbf{r} - \mathbf{r}_i). \tag{B.3}$$

Here, $\beta = 1/k_{\mathrm{B}}T$, h is the Planck's constant, μ is the chemical potential, and H_N is the Hamiltonian of the system comprised of N particles. By using the grand potential, $\hat{\Omega}[\psi(\mathbf{r})]$ is also expressed by

$$\hat{\Omega}[\psi(\mathbf{r})] = \Omega - k_{\mathrm{B}}T \ln\left\langle \exp\left[-\beta \int \psi(\mathbf{r})\hat{\rho}(\mathbf{r})\mathrm{d}\mathbf{r}\right]\right\rangle, \tag{B.4}$$

where Ω is the grand potential and $\langle \cdots \rangle$ represents the average in the grand canonical ensemble. The intensive variable $\psi(\mathbf{r})$ corresponds to the external field, but note that it is the virtual physical quantity to define $\hat{\Omega}[\psi(\mathbf{r})]$ [18].

The density field $\rho(\mathbf{r})$ is defined by the average in the grand canonical ensemble with the intensive variable $\psi(\mathbf{r})$,

$$\rho(\mathbf{r}) = \langle\, \hat{\rho}(\mathbf{r}) \,\rangle_{\psi(\mathbf{r})} = \left\langle \sum_{i=1}^{N} \delta(\mathbf{r} - \mathbf{r}_i) \right\rangle_{\psi(\mathbf{r})}, \tag{B.5}$$

where $\langle \cdots \rangle_{\psi(\mathbf{r})}$ represents the average in the grand canonical ensemble with $\psi(\mathbf{r})$. From Eq. (B.4), $\rho(\mathbf{r})$ is also expressed by the functional derivative of $\hat{\Omega}[\psi(\mathbf{r})]$,

$$\rho(\mathbf{r}) = \frac{\delta\hat{\Omega}[\psi(\mathbf{r})]}{\delta\psi(\mathbf{r})}. \tag{B.6}$$

At an equilibrium state, $\psi(\mathbf{r})$ equals zero in the whole system so that Eq. (B.5) corresponds to Eq. (B.1).

B.2 Free-energy functional

The free-energy functional of $\rho(\mathbf{r})$ is obtained from the Legendre transformation. Through the Legendre transformation, I transform $\hat{\Omega}[\psi(\mathbf{r})]$ into the functional of $\rho(\mathbf{r})$,

$$\Omega[\rho(\mathbf{r})] = \hat{\Omega}[\psi(\mathbf{r})] - \int \psi(\mathbf{r})\rho(\mathbf{r})\mathrm{d}\mathbf{r}. \tag{B.7}$$

In the same way, to obtain the free-energy functional of $\rho(\mathbf{r})$, I transform $\Omega[\rho(\mathbf{r})]$ into

$$F[\rho(\mathbf{r})] = \Omega[\rho(\mathbf{r})] + \mu N, \tag{B.8}$$

where μ is the chemical potential and N is the number of particles in the system.

When the particles interact with each other, $F[\rho(\mathbf{r})]$ is determined from the difference between $F[\rho(\mathbf{r})]$ and the free-energy functional for ideal gas $F_{\mathrm{ideal}}[\rho(\mathbf{r})]$. Here, I define the difference in the free energy as

$$\Psi[\rho(\mathbf{r})] = F_{\mathrm{ideal}}[\rho(\mathbf{r})] - F[\rho(\mathbf{r})]. \tag{B.9}$$

If $\rho(\mathbf{r})$ is close to $\rho_{\rm eq}(\mathbf{r})$, $\Psi[\rho(\mathbf{r})]$ is expanded in the difference between $\rho(\mathbf{r})$ and $\rho_{\rm eq}(\mathbf{r})$ [18],

$$\Psi[\rho(\mathbf{r})] = \Psi[\rho_{\rm eq}(\mathbf{r})] + k_{\rm B}Tc_1 \int \Delta\rho(\mathbf{r})\mathrm{d}\mathbf{r} + k_{\rm B}T\sum_{n=2}^{\infty}\frac{1}{n!}\int c_n(\mathbf{r}_1,\cdots,\mathbf{r}_n)\Delta\rho(\mathbf{r}_1)\cdots\Delta\rho(\mathbf{r}_n)\mathrm{d}\mathbf{r}_1\cdots\mathrm{d}\mathbf{r}_n, \tag{B.10}$$

$$\Delta\rho(\mathbf{r}) = \rho(\mathbf{r}) - \rho_{\rm eq}(\mathbf{r}). \tag{B.11}$$

Here, $c_n(\mathbf{r}_1,\cdots,\mathbf{r}_n)$ is the n-particle direct correlation function defined at an equilibrium state,

$$c_n(\mathbf{r}_1,\cdots,\mathbf{r}_n) = \left.\frac{\beta\delta^n\Psi[\rho(\mathbf{r})]}{\delta\rho(\mathbf{r}_1)\cdots\delta\rho(\mathbf{r}_n)}\right|_{\rho(\mathbf{r})=\rho_{\rm eq}(\mathbf{r})}, \tag{B.12}$$

where c_1 is a constant. In Eq. (B.10), I neglect the three- and more-particle direct correlation functions; this approximation corresponds to the hypernetted-chain (HNC) approximation [40]. From Eq. (B.10) and the HNC approximation, the equation of $F[\rho(\mathbf{r})]$ is given by

$$\beta F[\rho(\mathbf{r})] = \beta F_{\rm ideal}[\rho(\mathbf{r})] - \beta\Psi[\rho_{\rm eq}(\mathbf{r})] - c_1\int\Delta\rho(\mathbf{r})\mathrm{d}\mathbf{r} - \frac{1}{2}\int c_2(\mathbf{r}_1-\mathbf{r}_2)\Delta\rho(\mathbf{r}_1)\Delta\rho(\mathbf{r}_2)\mathrm{d}\mathbf{r}_1\mathrm{d}\mathbf{r}_2. \tag{B.13}$$

The equation of $F_{\rm ideal}[\rho(\mathbf{r})]$ is obtained from Eq. (B.2) and the Legendre transformation. For ideal gas, the Hamiltonian H_N is expressed by

$$H_N = \sum_{i=1}^{N}\left(\frac{\mathbf{p}_i^2}{2m} + V(\mathbf{r}_i)\right), \tag{B.14}$$

where m is the mass of a particle, $\mathbf{p}_i$ is the momentum of the i-th particle, and $V(\mathbf{r})$ is the external field. From Eq. (B.2), the thermodynamic potential is given by

$$\hat{\Omega}_{\rm ideal}[\psi(\mathbf{r})] = -k_{\rm B}Te^{\beta\mu}\int\frac{1}{\Lambda^3}e^{-\beta(V(\mathbf{r})+\psi(\mathbf{r}))}\mathrm{d}\mathbf{r}, \tag{B.15}$$

where Λ is the thermal de Broglie wave length defined by

$$\Lambda = \left(\frac{h^2}{2\pi m k_{\rm B}T}\right)^{1/2}. \tag{B.16}$$

By using Eq. (B.6), $\rho(\mathbf{r})$ for ideal gas is given by

$$\rho(\mathbf{r}) = e^{-\beta(V(\mathbf{r})+\psi(\mathbf{r})-\mu)}. \tag{B.17}$$

In the same way as Eqs. (B.7) and (B.8), $\hat{\Omega}_{\rm ideal}[\psi(\mathbf{r})]$ is transformed into $F_{\rm ideal}[\rho(\mathbf{r})]$, which is expressed by

$$\beta F_{\rm ideal}[\rho(\mathbf{r})] = \int\rho(\mathbf{r})[\,\ln\rho(\mathbf{r}) + \beta V(\mathbf{r}) + \ln\Lambda^3 - 1\,]\mathrm{d}\mathbf{r}. \tag{B.18}$$

Appendix C

Numerical calculation of time-dependent density functional theory

Here, I explain the numerical method of solving Eqs. (4.12) and (4.13) in detail. In the numerical calculations, I solve these equations numerically in the cylindrical coordinate system with axial symmetry (r, z). I employ the iterative method to solve these equations under the condition that the time derivatives on the left-hand side equal zero. The spatial derivatives are calculated via the finite difference method. Furthermore, I calculate the convolution integral in Eq. (4.12) by use of the Fourier–Hankel transform.

C.1 Fourier–Hankel transform

The convolution integral in Eq. (4.12) is calculated via factorization using Fourier transform (FT). In the cylindrical coordinate system with axial symmetry (r, z), the FT is calculated through the combination of the one-dimensional FT with the Hankel transform (HT), such that

$$\Delta\tilde{\rho}(k_r, k_z, t) = \int_{-\infty}^{\infty} \mathrm{d}z \int_0^{\infty} 2\pi r \mathrm{d}r \Delta\rho(r, z, t) e^{ik_z z} J_0(k_r r). \tag{C.1}$$

Here, $\Delta\tilde{\rho}(k_r, k_z, t)$ is the Fourier–Hankel transform of $\Delta\rho(r, z, t)$, k_r and k_z are the r- and z-components of the wave number vector, respectively, and $J_0(k_r r)$ is the order-zero Bessel function of the first kind. From Eq. (C.1), the convolution integral in Eq. (4.12) is given by

$$\begin{aligned} &\int_{-\infty}^{\infty} \mathrm{d}z \int_0^{\infty} 2\pi r \mathrm{d}r \int c_2(\mathbf{r} - \mathbf{r}') \Delta\rho(\mathbf{r}', t) \mathrm{d}\mathbf{r}' e^{ik_z z} J_0(k_r r) \\ &= \tilde{c}_2(k_r, k_z) \Delta\tilde{\rho}(k_r, k_z, t), \end{aligned} \tag{C.2}$$

where $\tilde{c}_2(k_r, k_z)$ is the Fourier–Hankel transform of $c_2(\mathbf{r})$.

The Fourier–Hankel transform is numerically calculated via the fast FT (FFT) [41] and discrete HT on two-dimensional grids in the cylindrical coordinate system (r, z). Here, I place data points on the grid crossings. Note that the data points along the r-axis must be placed on the zeros of $J_0(r)$. This ensures $J_0(r)$-orthogonality for the functions defined by discrete points, instead of the continuous functions [42,43]. The orthogonality in the FFT requires regular intervals between two neighboring data points along the z-axis.

C.2 Finite difference methods

The spatial derivatives in Eqs. (4.12) and (4.13) are obtained via the finite difference methods in the cylindrical coordinate system with axial symmetry (r, z). I calculate the derivatives on the right-hand side of these equations via the central difference method. The derivatives obtained from the central difference method include the calculation error of $O[(\Delta r)^2]$ and $O[(\Delta z^2)]$, where Δr and Δz are intervals between two neighboring data points along the r-axis and z-axis, respectively. The advective term on the left-hand side is calculated via the backward difference method, in order to stabilize the finite difference calculation [41, 46]. The derivatives obtained from the backward difference method include the calculation error of $O(\Delta r)$ and $O(\Delta z)$.

C.3 Iterative calculation

I solve Eqs. (4.12) and (4.13) via iterative calculations under the condition that the time derivatives on the left-hand side equal zero. Here, Eq. (4.12) is iteratively calculated by use of the difference equation

$$\rho_{i+1}(\mathbf{r}) = \rho_i(\mathbf{r}) + h\nabla \cdot \mathbf{j}_i(\mathbf{r}), \tag{C.3}$$

$$\begin{aligned}\mathbf{j}_i(\mathbf{r}) = {} & D\nabla\rho_i(\mathbf{r}) - \mathbf{U}\rho_i(\mathbf{r}) + D\beta\rho_i(\mathbf{r})\nabla V(\mathbf{r}) \\ & - D\rho_i(\mathbf{r})\nabla \int c_2(\mathbf{r}-\mathbf{r}')\Delta\rho_{s\times[i/s]}(\mathbf{r}')\mathrm{d}\mathbf{r}' \quad (s \geq 1),\end{aligned} \tag{C.4}$$

$$\Delta\rho_{s\times[i/s]}(\mathbf{r}) = \rho_{s\times[i/s]}(\mathbf{r}) - \rho_0, \tag{C.5}$$

where h is the step value of the iterative calculation. In addition, $\rho_i(\mathbf{r})$ and $\mathbf{j}_i(\mathbf{r})$ are the density and current density fields at step $i = 1, 2, \cdots$, respectively. The Gauss symbol $[X]$ represents the integer part of a real number X, so that $\Delta\rho_{s\times[i/s]}(\mathbf{r})$ is updated at intervals of s steps. In the case of the noninteracting colloidal particles [Eq. (4.13)], $\mathbf{j}_i(\mathbf{r})$ is defined in the same manner. By using Eqs. (C.3) and (C.4), I calculate the density field at the next step iteratively until the divergence of $\mathbf{j}_i(\mathbf{r})$ becomes close to zero.

The update scheme given in Eq. (C.4) reduces the cost of the numerical calculation of $\rho(\mathbf{r}, \infty)$ because the convolution integral is calculated only once per s

steps. Excessively large values of s, however, yields $\rho_i(\mathbf{r})$ divergence. To avoid this divergence, s must take a suitable value depending on $\mathbf{U}$, $V(\mathbf{r})$, and $c_2(\mathbf{r})$. For example, in the range of $s \leq 100$, density fields at steady states have been stably obtained from numerical calculations for the hard-sphere system.

Appendix D

Numerical calculation of two-fluid model

Here, I explain the numerical method for solving the motion equations of the two-fluid model in detail. In the numerical calculations, I solve the equations numerically in the cylindrical coordinate system with axial symmetry (r, z). I employ the iterative method to obtain $\phi^{(1)}(\mathbf{r})$ and $\phi^{(2)}(\mathbf{r})$. In addition, I employ the Gauss-Seidel method [41,45] to obtain $\mathbf{v}_s^{(1)}(\mathbf{r})$ and $p^{(2)}(\mathbf{r})$. The space derivatives in the equations are calculated via the finite difference method.

D.1 Calculation of volume fraction field

To obtain $\phi^{(1)}(\mathbf{r})$ for the incompressibility condition given by Eq. (5.1), I solve Eq. (5.33) numerically via the iterative method. Here, Eq. (5.33) is iteratively calculated by use of the difference equation

$$\phi_{i+1}^{(1)}(\mathbf{r}) = \phi_i^{(1)}(\mathbf{r}) + h\nabla \cdot \mathbf{j}_i^{(1)}(\mathbf{r}), \tag{D.1}$$

$$\mathbf{j}_i^{(1)}(\mathbf{r}) = \nabla\phi_i^{(1)}(\mathbf{r}) + \beta\phi_i^{(1)}(\mathbf{r})\nabla V(\mathbf{r}) - \frac{1}{D}\phi_i^{(1)}(\mathbf{r})\mathbf{U}, \tag{D.2}$$

where h is the step value of the iterative calculation. In addition, $\phi_i^{(1)}(\mathbf{r})$ and $\mathbf{j}_i^{(1)}(\mathbf{r})$ are the volume fraction and current volume fraction fields at step $i = 1, 2, \cdots$, respectively. By using Eqs. (D.1) and (D.2), I calculate the volume fraction field at the next step iteratively until the divergence of $\mathbf{j}_i^{(1)}(\mathbf{r})$ becomes close to zero. Even for the approximate incompressibility condition [Eq. (5.18)] and for noninteracting colloidal particles, the volume fraction fields are obtained from the difference equations in the same form as Eqs. (D.1) and (D.2).

In the same way, $\phi^{(2)}(\mathbf{r})$ is obtained via the iterative method. For the incompressibility condition given by Eq. (5.1), I calculate Eq. (5.36) iteratively by using the difference equation

$$\phi_{i+1}^{(2)}(\mathbf{r}) = \phi_i^{(2)}(\mathbf{r}) + h\nabla \cdot \mathbf{j}_i^{(2)}(\mathbf{r}), \tag{D.3}$$

$$\mathbf{j}_i^{(2)}(\mathbf{r}) = \nabla\phi_i^{(2)}(\mathbf{r}) + \beta\phi_i^{(2)}(\mathbf{r})\nabla V(\mathbf{r}) - \frac{1}{D}(\phi_i^{(2)}(\mathbf{r})\mathbf{U} + \phi^{(1)}(\mathbf{r})\mathbf{v}_s^{(1)}(\mathbf{r})) + \beta v\phi^{(1)}(\mathbf{r})\nabla p^{(1)}(\mathbf{r}) - \frac{1}{v}\phi^{(1)}(\mathbf{r})\nabla\int c_2(\mathbf{r}-\mathbf{r}')\Delta\phi^{(1)}(\mathbf{r}')\mathrm{d}\mathbf{r}', \tag{D.4}$$

where $\mathbf{v}_s^{(1)}(\mathbf{r})$ and $p^{(1)}(\mathbf{r})$ are obtained from Eqs. (5.34) and (5.35). The convolution integral in Eq. (D.4) is calculated via the Fourier–Hankel transform (see Append. C.1). For the case of the approximate incompressibility condition [Eq. (5.18)], in the same manner as Eqs. (D.3) and (D.4), I solve Eq. (5.41) which does not include the term of the pressure field $p^{(1)}(\mathbf{r})$. In the case of the non-interacting colloidal particles, Eqs. (5.48) and (5.50) are the same as Eqs. (5.36) and (5.41) except for the absence of the term of the convolution integral, so that $\phi_{\mathrm{id}}^{(2)}(\mathbf{r})$ is obtained via the iterative calculation in the same manner.

In the numerical calculations of $\phi^{(1)}(\mathbf{r})$ and $\phi^{(2)}(\mathbf{r})$, the spatial derivatives are obtained via the finite difference methods in the cylindrical coordinate system with axial symmetry (r, z). I calculate the derivatives of the advective terms related to $\mathbf{U}$ or $\mathbf{v}_s^{(1)}(\mathbf{r})$ by use of the backward difference method, in order to stabilize the finite difference calculation [41, 46]. The derivatives obtained from the backward difference method include the calculation error of $O(\Delta r)$ and $O(\Delta z)$, where Δr and Δz are intervals between two neighboring data points along r-axis and z-axis, respectively. In contrast to the advective terms, the other terms are calculated via the central difference method. The derivatives obtained from the central difference method include the calculation error of $O[(\Delta r)^2]$ and $O[(\Delta z)^2]$.

D.2 Calculation of solvent velocity field

To calculate $\mathbf{v}_s^{(1)}(\mathbf{r})$ for the incompressibility condition given by Eq. (5.1), I solve Eq. (6.6) via the Gauss-Seidel method [41,45] and obtain the solvent vorticity field $\boldsymbol{\omega}(\mathbf{r})$ defined by Eq. (6.7). Here, from the incompressibility condition in the first order of ϕ_0 [Eq. (5.34)], the stream function $\psi(\mathbf{r})$ is defined by [47]

$$v_r'(\mathbf{r}) = \frac{1}{r}\frac{\partial\psi(\mathbf{r})}{\partial z} \quad \text{and} \quad v_z'(\mathbf{r}) = -\frac{1}{r}\frac{\partial\psi(\mathbf{r})}{\partial r}, \tag{D.5}$$

$$\mathbf{v}'(\mathbf{r}) \equiv \mathbf{v}_s^{(1)}(\mathbf{r}) - \phi^{(1)}(\mathbf{r})\mathbf{U}, \tag{D.6}$$

where $v_r'(\mathbf{r})$ and $v_z'(\mathbf{r})$ are the r- and z-components of $\mathbf{v}'(\mathbf{r})$, respectively. From the definition of $\boldsymbol{\omega}(\mathbf{r})$ [Eq. (6.7)], I derive the equation of $\psi(\mathbf{r})$

$$\left(\frac{\partial^2}{\partial r^2} - \frac{1}{r}\frac{\partial}{\partial r} + \frac{\partial^2}{\partial z^2}\right)\psi(\mathbf{r}) = r[\boldsymbol{\omega}(\mathbf{r}) - \nabla\times(\phi^{(1)}(\mathbf{r})\mathbf{U})]_\theta, \tag{D.7}$$

where θ is the angular axis of the cylindrical coordinate system. I obtain $\psi(\mathbf{r})$ numerically by solving Eq. (D.7) via the Gauss-Seidel method. Here, I calculate $\mathbf{v}_s^{(1)}(\mathbf{r})$ by using the obtained $\psi(\mathbf{r})$ and Eqs. (D.5) and (D.6).

Even for the approximate incompressibility condition [Eq. (5.18)], I obtain $\boldsymbol{\omega}(\mathbf{r})$ numerically by solving Eq. (6.6) via the Gauss-Seidel method. Here, from the approximate incompressibility condition in the first order of ϕ_0 [Eq. (5.39)], the stream function $\psi(\mathbf{r})$ is defined by

$$v_{s,r}^{(1)}(\mathbf{r}) = \frac{1}{r}\frac{\partial \psi(\mathbf{r})}{\partial z} \quad \text{and} \quad v_{s,z}^{(1)}(\mathbf{r}) = -\frac{1}{r}\frac{\partial \psi(\mathbf{r})}{\partial r}, \tag{D.8}$$

where $v_{s,r}^{(1)}(\mathbf{r})$ and $v_{s,z}^{(1)}(\mathbf{r})$ are the r- and z-components of $\mathbf{v}_s^{(1)}(\mathbf{r})$. From the definition of $\boldsymbol{\omega}(\mathbf{r})$ [Eq. (6.7)], I derive the equation of $\psi(\mathbf{r})$

$$\left(\frac{\partial^2}{\partial r^2} - \frac{1}{r}\frac{\partial}{\partial r} + \frac{\partial^2}{\partial z^2}\right)\psi(\mathbf{r}) = r\omega_\theta(\mathbf{r}), \tag{D.9}$$

where $\omega_\theta(\mathbf{r})$ is the θ-component of $\boldsymbol{\omega}(\mathbf{r})$. I solve Eq. (D.9) numerically via the Gauss-Seidel method.

In the numerical calculations, I place data points of $\boldsymbol{\omega}(\mathbf{r})$ and $\psi(\mathbf{r})$ at the positions separated from each data point of $\phi^{(1)}(\mathbf{r})$ by $\Delta r/2$ on the r-axis and by $\Delta z/2$ on the z-axis. Additionally, data points of $v_{s,r}^{(1)}(\mathbf{r})$ and $v_{s,z}^{(1)}(\mathbf{r})$ are placed at the positions separated from each data point of $\phi^{(1)}(\mathbf{r})$ by $\Delta r/2$ on the r-axis and by $\Delta z/2$ on the z-axis, respectively. The spatial derivatives are calculated via the central difference method. In order to solve Eq. (6.6) numerically, I impose the boundary condition that $\boldsymbol{\omega}(\mathbf{r})$ equals zero at the edges of the calculation range. For consistency with the boundary condition of $\boldsymbol{\omega}(\mathbf{r})$, the boundary condition must be imposed on either r-component or z-component of $\mathbf{v}_s^{(1)}(\mathbf{r})$ at the edges of the calculation range. I impose the boundary condition that the z-components of $\mathbf{v}_s^{(1)}(\mathbf{r})$ equal the z-component of $\mathbf{U}$ at the edges of the z-axis and that the r-components of $\mathbf{v}_s^{(1)}(\mathbf{r})$ equal zero at the edge of the r-axis.

References

[1] T. G. Mason. *Rheol. Acta*, 39:371, 2000.

[2] T A Waigh. *Rep. Prog. Phys.*, 68:685, 2005.

[3] A. Meyer, A. Marshall, B. G. Bush, and E. M. Furst. *J. Rheol.*, 50:77, 2006.

[4] L. G. Wilson, A. W. Harrison, A. B. Schofield, J. Arlt, and W. C. K. Poon. *J. Phys. Chem. B*, 113:3806, 2009.

[5] D. Mizuno, R. Bacabac, C. Tardin, D. Head, and C. F. Schmidt. *Phys. Rev. Lett.*, 102:168102, 2009.

[6] D. A. Head and D. Mizuno. *Phys. Rev. E*, 81:041910, 2010.

[7] T. M. Squires and J. F. Brady. *Phys. Fluids*, 17:073101, 2005.

[8] I. C. Carpen and J. F. Brady. *J. Rheol.*, 49:1483, 2005.

[9] A. S. Khair and J. F. Brady. *J. Fluid Mech.*, 557:73, 2006.

[10] A. S. Khair and J. F. Brady. *J. Rheol.*, 52:165, 2008.

[11] M. Inoue and A. Yoshimori. *J. Mol. Liq.*, 200, Part A:81, 2014.

[12] M. Inoue and A. Yoshimori. *J. Phys. Soc. Jpn.*, 86:074604, 2017.

[13] M. Doi and A. Onuki. *J. Phys. II France*, 2:1631, 1992.

[14] S. T. Milner. *Phys. Rev. Lett.*, 66:1477, 1991.

[15] S. T. Milner. *Phys. Rev. E*, 48:3674, 1993.

[16] L. D. Landau and E. M. Lifshitz. *Statistical Physics*. Butterworth Heinemann, Oxford, third edition, 1980. Chap. 12.

[17] M. Doi. *J. Chem. Phys.*, 79:5080, 1983.

[18] A. Yoshimori. *J. Theor. Comput. Chem.*, 03:117, 2004.

[19] A. Yoshimori. *Chem. Phys. Lett.*, 184:76, 1991.

[20] A. Yoshimori. *Stud. Phys. Theor. Chem.*, 83:297, 1995.

[21] A. Yoshimori, T. J. F. Day, and G. N. Patey. *J. Chem. Phys.*, 108:6378, 1998.

[22] A. Yoshimori, T. J. F. Day, and G. N. Patey. *J. Chem. Phys.*, 109:3222, 1998.

[23] S. Murata and A. Yoshimori. *J. Chem. Phys.*, 125:244501, 2006.

[24] B. Bagchi and A. Chandra. *Proc. Indian Acad. Sci. (Chem. Sci.)*, 100:353, 1988.

[25] A. Chandra and B. Bagchi. *Chem. Phys. Lett.*, 151:47, 1988.

[26] A. Chandra and B. Bagchi. *J. Chem. Phys.*, 91:1829, 1989.

[27] A. Yoshimori. *Phys. Rev. E*, 59:6535, 1999.

[28] A. Yoshimori. *J. Mol. Liq.*, 90:29, 2001.

[29] A. Yoshimori. *Phys. Rev. E*, 71:031203, 2005.

[30] T. Munakata. *J. Phys. Soc. Jpn.*, 45:749, 1978.

[31] K. Fuchizaki. and K. Kawasaki. *J. Phys. Soc. Jpn.*, 67:1505, 1998.

[32] U. M. B. Marconi. and P. Tarazona. *J. Chem. Phys.*, 110:8032, 1999.

[33] U. M. B. Marconi and P. Tarazona. *J. Phys.: Condens. Matter*, 12:A413, 2000.

[34] F. Penna and P. Tarazona. *J. Chem. Phys.*, 119:1766, 2003.

[35] F. Penna, J. Dzubiella, and P. Tarazona. *Phys. Rev. E*, 68:061407, 2003.

[36] J Dzubiella and C N Likos. *J. Phys.: Condens. Matter*, 15:L147, 2003.

[37] A. J. Archer and R. Evans. *J. Chem. Phys.*, 121:4246, 2004.

[38] A. J. Archer and M. Rauscher. *J. Phys. A: Math. Gen.*, 37:9325, 2004.

[39] J. Araki and T. Munakata. *Phys. Rev. E*, 52:2577, 1995.

[40] J.-P. Hansen and I. R. Mcdonald. *Theory of Simple Liquids*. Academic Press, London, third edition, 2006.

[41] W. H. Press, B. P. Flannery, S. A. Teukolsky, and W. T. Vetterling. *Numerical Recipes in C [Japanese version]*. Gijutsu-Hyohron Co., Ltd, Tokyo, 1993 [in Japanese].

[42] H. F. Johnson. *Comput. Phys. Commun.*, 43(2):181, 1987.

[43] Q. Wang, O. Ronneberger, and H. Burkhardt. Technical Report 1, IIF-LMB, Computer Science Department, University of Freiburg, 2008.

[44] H. N. W. Lekkerkerker and R. Tuinier. *Colloids and the Depletion Interaction*. Springer, Dordrecht, 2011.

[45] M. Yasuhara and H. Daiguji. *Suchi-ryutairikigaku*. University of Tokyo Press, Tokyo, 1992 [in Japanese].

[46] F. Mesinger and A. Arakawa. *Numerical methods used in atmospheric models, volume 1*. Global Atmospheric Research Program World Meteorological Organization, Geneva, 1976.

[47] T. Tatsumi. *Ryutairikigaku*. Baifukan Co., Ltd, Tokyo, 1982 [in Japanese].